

---

# NEUTRON STARS

## Lecture Notes

---

**Niccolò Bucciantini**

INAF - Osservatorio Astrofisico di Arcetri  
L.go Fermi 5, 50125 Firenze, Italy

*Spero che dopo aver letto questi  
appunti gli studenti non  
rimpiangano il giorno in cui  
decisero di fare Fisica, e non  
meledicano quello in cui io decisi  
di insegnarla.*





# CONTENTS

---

<b>1</b>	<b>Compact Stars</b>	<b>1</b>
1.1	History	1
1.1.1	Pulsar History	2
1.2	Pulsars are Neutron Stars	3
1.3	The NS zoo	5
1.3.1	Pulsars	5
1.3.2	Magnetars	6
1.3.3	INS and CCO	8
1.3.4	LMXB and HMXB	9
<b>2</b>	<b>The State of Matter in Neutron Stars</b>	<b>11</b>
2.1	Fermi-Dirac Distribution	11
2.1.1	Classical Boltzmann Distribution	11
2.1.2	Quantum mechanics and the Fermi-Dirac Distribution	14
2.1.3	Heuristic interpretation of the Fermi Momentum	17
2.1.4	Equation of State in the Fully Degenerate Case	17
2.2	Atmosphere	19
2.3	Degeneracy and Ionization	21
2.4	Gas - Liquid - Solid	22
2.4.1	Modeling melting OCP	23
2.5	Phase Diagram of Outer Crust	24
2.6	Neutronization and the Liquid Drop Model	24
2.7	Neutron Drip	27
2.8	Above Neutron Drip	28

2.8.1	Corrections	31
2.9	The Core	31
2.9.1	Higher densities	33
<b>3</b>	<b>Politropic models for Neutron Stars</b>	<b>35</b>
3.1	Lane-Emden Equation and the Classical Polytropic Model	35
3.1.1	Chandrasekhar Mass	36
3.2	TOV equations	37
3.2.1	Constant Density Model	38
3.2.2	Polytropic Model	39
3.3	Mass and Radius	39
3.3.1	Constraints on the Mass-Radius relation	42
3.3.2	Mass Limits and Rotation	42
<b>4</b>	<b>Pulsar Electrodynamics</b>	<b>45</b>
4.1	Spinning Dipole and the Lighthouse model	45
4.2	The Unipolar Inductor	48
4.3	The Aligned Rotator	49
4.3.1	The polar cap size	51
4.3.2	Outer Gaps	51
4.4	The Orthogonal Rotator	52
4.5	QED Pair Creation	55
4.6	Pair Creation in the Polar Cap	58
4.7	The Force Free Pulsar Equation	59
4.8	The Split Monopole Solution	63
4.8.1	Torque and Energy Losses	64
4.9	From the monopole to the dipole	65
<b>5</b>	<b>Pulsar Nebulae</b>	<b>67</b>
5.1	Observations	67
5.2	PWNe Models	68
5.2.1	Shock Jump Conditions	69
5.2.2	Nebular Flow	70
5.3	PWNe Evolution	72
5.3.1	The PWN	73
5.3.2	The Swept-up Shell	73
5.3.3	Self-Similar Solution	74
5.3.4	Interaction with the SNR	74
5.3.5	Late Time Evolution	75
5.4	PWNe Emission	75
5.4.1	Particles Losses	75
5.4.2	Particles Distribution	77
5.4.3	Synchrotron Spectrum	79
5.4.4	IC Emission	81
5.5	Cooling	83

# CHAPTER 1

---

## COMPACT STARS

---

In this chapter we will briefly introduce compact stars (White Dwarves and Neutron Stars) from an historical point of view. NSs show a vast and diverse phenomenology, ranging from the canonical PSRs, to extreme objects like Magnetars, from old isolated NSs to accreting systems. Here we present a brief review of the various classes in which they have been divided during the years. The divisions are mostly based on their observational properties, but the distinctions often hide a much more profound difference in the mechanisms responsible for their emission/evolution. At the moment a unifying picture able to relate all of them is still lacking.

### 1.1 History

On the 31st of January 1783 the british astronomer William Herschel discovered two companions (B/C) of the main sequence star 40 Eridani A. The 31st of January 1862 Alvan Graham Clark observed a previously unseen star close to Sirius, later identified as the companion predicted by Friedrich Bessel (who had observed the oscillatory motion of Sirius A). In 1910, Henry Norris Russell, Edward Charles Pickering and Williamina Fleming discovered that, despite being a dim star, 40 Eridani B was of spectral type A, or white. Five years later in 1915, Walter Adams announced that he had found the spectrum of Sirius B to be similar to that of Sirius A (spectral type A). In 1917, Adriaan van Maanen discovered the Van Maanen's Star, an isolated star, of spectral type F, but much fainter than similar main sequence stars.

The radius of Sirius B inferred from its luminosity and the mass derived from the binary dynamics, suggested this object to have a density  $10^5$  times higher than that of Sirius A. The high mass density was confirmed in 1925 by the american astronomer Walter Adams when he measured the gravitational redshift of Sirius B and found a value of  $21 \text{ km s}^{-1}$ . Willem Luyten appears to have been the first to use the term *White Dwarf (WD)* when he examined this class of stars in 1922.

In 1926, the astrophysicist Ralph Fowler used the new theory of quantum mechanics to show that these stars are supported by an electron gas in a degenerate state. The Fermi gas model was then used by the physicist E. C. Stoner in 1929 to calculate the relationship among the mass, radius, and density of WDs, assuming them to be homogeneous spheres. In a series of papers published between 1931 and 1935, Subrahmanyan Chandrasekhar solved the hydrostatic equation together with the non-relativistic Fermi gas equation of state, and also treated the case of a relativistic Fermi gas, showing the existence of a mass limit.

In 1952 the astrophysicist Leon Mestel demonstrated that the energy emitted by a WD is the surviving heat from a prior period of nuclear fusion. He showed that nuclear burning no longer occurs within a WD. It was recognized that WDs were the remnants of main sequence stars, in particular the degenerate remnants of their cores, that become exposed during the phase of Planetary Nebula.

In 1934, Walter Baade and Fritz Zwicky proposed the existence of the *Neutron Star (NS)*, only a year after the discovery of the neutron by Sir James Chadwick. In seeking an explanation for the origin of a supernova, they tentatively proposed that in supernova explosions ordinary stars are turned into stars that consist of extremely closely packed neutrons that they called NSs. Baade and Zwicky correctly proposed at that time that the release of the gravitational binding energy of the NS powers the supernova.

The first tentative calculations of the mass radius relationship for NSs was done by Zwicky in 1938 using a simple energy argument applied to a system behaving like a large nucleus. The first correct model of NSs in General Relativity (GR) was put forward in 1939 by R.C. Tolman, J.R. Oppenheimer and G.M. Volkoff (TOV), assuming it to be formed by free degenerate neutrons. As found by Chandrasekhar, a maximum mass was derived also for Neutron Stars, but found to be smaller than the limit for WDs. The small radii, making these objects virtually undetectable, and the lower maximum mass, creating an evolutionary gap (NSs could not originate from collapsing WDs being their maximum mass smaller) led to a stalemate in their study. Only in 1959 it was recognized by Cameron that neutrons inside a NS were too close to neglect their mutual strong attraction, and could not be described as a free fermion gas. New models were computed leading to a maximum mass higher than the Chandrasekhar limit for WDs.

However, little work was done on them until November 1967, when Franco Pacini pointed out that if the NSs were spinning and had large magnetic fields, then electromagnetic waves would be emitted. Unbeknown to him in 1967, Jocelyn Bell and Antony Hewish discovered regular radio pulses from CP 1919. This *pulsar* (PSR) was later interpreted as an isolated, rotating neutron star.

In 1971, Riccardo Giacconi, and collaborators discovered a 4.8 second pulsations in an X-ray source in the constellation Centaurus, Cen X-3. They interpreted this as resulting from a rotating hot NS. The energy source was supposed to be gravitational and results from a rain of gas falling onto the surface of the NS from a companion star.

Since then more than 2000 NSs have been discovered. The vast majority of them are Pulsars, but other classes are present with tens of members, including Magnetars (NSs with strong magnetic field whose emission is likely powered by the magnetic field decay), and Thermal Isolated Neutron Stars (NS with a weak magnetic field and a purely thermal spectrum).

### 1.1.1 Pulsar History

The first PSR was observed on November 28, 1967, by Jocelyn Bell Burnell and Antony Hewish. They observed radio pulses with a well defined period of 1.33 seconds that was shown, in the following days, to originate from the same location on the sky. The source was also keeping to sidereal time. Since the source of the pulses followed sidereal time, it could not be man-made radio frequency interference. In 1968 a PSR was discovered at the centre of the Crab Nebula, the remnant of a Supernova (SN) exploded in 1054 AD. This discovery confirmed an original idea by Franco Pacini, in 1967, that a rotating neutron star with a magnetic field would emit radiation, and that such energy could be pumped into a supernova remnant (SNR). Indeed, in 1968, Thomas Gold independently argued that this model could explain the pulsed radiation observed by Bell Burnell and Hewish. The discovery of the Crab pulsar, confirmed also the hypothesis of Walter Baade and Fritz Zwicky, in 1934, that a NS could be born in a SN.

Today the association of PSRs/NSs with SNe is well established. All young PSRs (age  $< 10^4$  yr) are found inside SNRs. There is an estimated number of  $10^4$  PSRs in the Galaxy (of which only  $\sim 2000$  are observed) with typical ages  $\sim 10^6$  yr, setting a typical birth rate  $\sim 1$  every 100 yr, similar to the Core-Collapse Supernova rate (1 every 30 yr). SNe are the ending phase in the life of a massive ( $M > 9M_{\odot}$ ) star. Given the mass luminosity relation,  $L \propto M^3$ , its typical lifetime is only a few tens of million years, much smaller than the galactic orbital period ( $\sim 3 \times 10^8$  yr). SNe are supposed to explode mainly in the spiral arms of the Galaxy, where the star forming regions are located. PSRs are also found mostly in spiral arms, Fig 1.1.

In 1982, Don Backer led a group which discovered a PSR with a rotation period of just 1.6 milliseconds, the

first *millisecond pulsar*. Millisecond pulsars have since been detected also in the radio, X-ray, and for a substantial fraction in gamma-ray. Millisecond pulsars, which can be timed with high precision, have a stability comparable to atomic-clock-based time standards when averaged over decades.

In 1974, Joseph Hooton Taylor and Russell Hulse discovered for the first time a *PSR in a binary system*, PSR B1913+16. This PSR orbits another NS with an orbital period of just 7.75 hours, and the two neutron stars are believed to be nearly equal in mass, about 1.4 solar masses. The minimum separation is about 1.1 solar radii, while the maximum is 4.8. The orbit is inclined at about 45 degrees with respect to the plane of the sky, and the orientation of periastron changes because of GR precession by about 4.2 degrees per year. Observations and timing of the pulsed emission showed that the orbit continually contracts, according to the predictions of General Relativity for emission of gravitational waves, providing the first evidence ever of their existence.

In 1992, A. Wolszczan discovered the *first extrasolar planets* around PSR B1257+12, by timing residuals. The pulsar was orbited by two planets, whose masses were initially estimated to be 3.4 and 2.8 times Earth's mass. The radii of their orbits are 0.36 and 0.47 AU respectively.

In 2003 radio astronomer Marta Burgay discovered PSR J0737-3039(A/B), the only known system containing two pulsars, thus a *double pulsar system*. The object is similar to PSR B1913+16. The orbital period of J0737-3039 is 2.4 hours, the shortest yet known, which enables the most precise tests of gravity, showing an excellent agreement between GR and observations. The energy loss due to gravitational waves shrinks the orbit ( $4 \times 10^7$  km in radius, with eccentricity 0.09) by 7 mm per day. Pulsar A has a period of 23 milliseconds, and a mass  $1.34M_{\odot}$ . Pulsar B has a period of 2.8 seconds, and a mass  $1.25M_{\odot}$ . The orbit is seen almost edge on, with eclipses when the magnetosphere of pulsar B, which is filled with absorbing plasma, blocks radiation from pulsar A. Due to relativistic spin precession, the pulses from Pulsar B are no longer detectable since March 2008, but are expected to reappear in 2035.

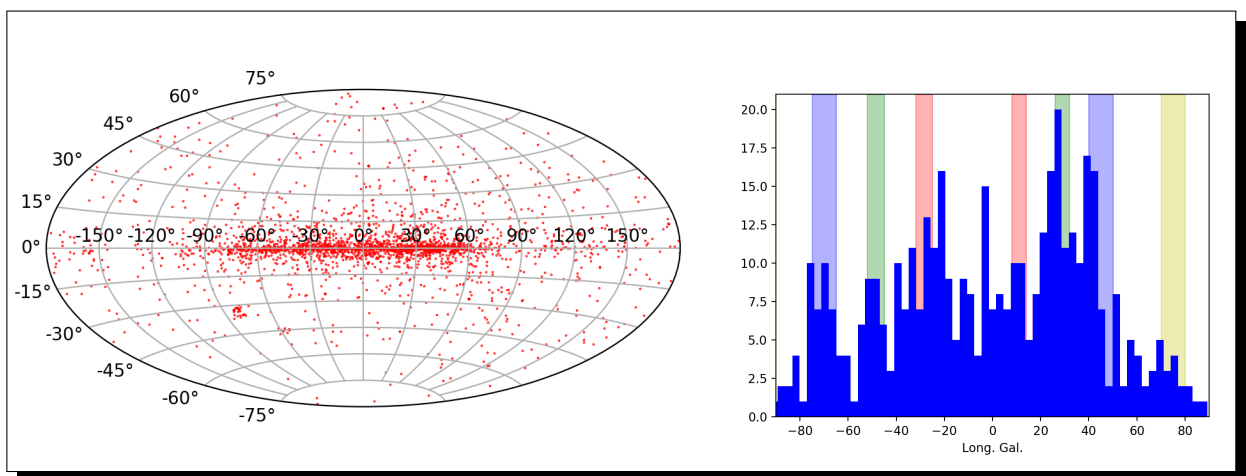


**Figure 1.1:** Left panel: distribution of pulsars on the sky in galactic coordinates. Right: distribution of young pulsars (spin-down age  $< 1$  Myr) at low galactic latitudes ( $-20^\circ < b < 20^\circ$ ), as a function of their galactic longitude. Shaded areas indicate the location of the galactic spiral arms (red is the Norma arm, green the Crux-Scutum, blue the Sagittarius-Carina, and yellow the Orion one)

## 1.2 Pulsars are Neutron Stars

It was immediately recognized, after the discovery of PSRs, that only NSs could be at the origin of the observed radio pulsed emission. PSRs are concentrated on the plane of the galaxy. This implies that they are a galactic population, analogous to regular stars, and similar objects. The two main characteristics of PSRs are the period  $P$  and the period derivative  $\dot{P}$  (which is always positive, indicating that the period increases with time). Fig. 1.2

shows the period and period derivative of known PSRs. It is immediately evident the existence of two populations: one characterized by periods ranging from  $P = 0.03$  s to a few s, and with typical period derivatives in the range  $\dot{P} = 10^{-17} - 10^{-13}$  s s $^{-1}$ ; the other with periods in the range  $P = 10^{-3} - 10^{-2}$  s, and period derivatives in the range  $\dot{P} = 10^{-21} - 10^{-19}$  s s $^{-1}$ . The first group is generally referred as the *regular or canonical pulsars*, the second as *millisecond or recycled pulsars*. While the origin of these two populations is different, the first being the outcome of Core-Collapse SNe of single progenitor, the second instead originating in binary systems after mass transfer episodes, their emission and the conditions of their magnetospheres are supposed to be governed by the same physics.

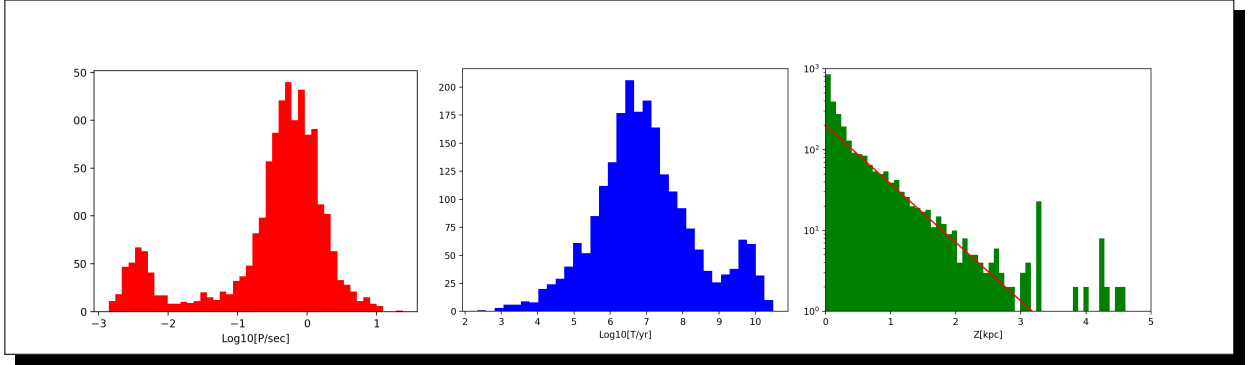


**Figure 1.2:** Left panel: distribution of pulsars spin period in seconds Middle panel: distribution of pulsar spin-down ages in years. Right panel: distribution of the pulsar height from the galactic plane in kpc. The red line represent an exponential distribution with scale-height equal to 650 pc.

The rapid periodicity, up to a few milliseconds, reduces greatly the possible choices. The origin must be a compact, stellar mass object, either a White Dwarf, a Neutron Star or a Black Hole. In astrophysics there are only three mechanisms that can give origin to periodic emission: *pulsation, orbital motion, and rotation*. Each of these has characteristic properties that allow one to identify it. Let us discuss them one by one:

- **Pulsation.** Stars are known to pulsate. A self gravitating gaseous sphere has a typical pulsating frequency that can be derived from a simple dimensional argument (for a more detailed derivation see ...). There is only one possible combination of a mass  $M$  a radius  $R$  and the gravitational constant  $G$  that has the dimension of time, and this is:

$$\tau = \sqrt{R^3/GM} = 1/\sqrt{G\rho} \quad (1.1)$$

where  $\rho$  is the average density. To get the typical observed periods, the ratio  $M/R^3$  should be in the range  $10^8 - 10^{13}$  g cm $^{-3}$ . This range is too high for WDs, whose typical masses are  $\sim M_\odot$  and typical radii are  $\sim 10^9$  cm, giving a density of the order of  $10^6$  g cm $^{-3}$ . It is too small for NSs, which have typical densities of the order of  $10^{14}$  g cm $^{-3}$ . BHs can oscillate only for very brief periods of the order of their light crossing time. Moreover, whatever the origin of the oscillation, it is unlikely that only one mode (i.e. the fundamental) will be excited. One would expect power also at higher harmonics, which is not observed.

- **Orbital motion.** A star orbiting a companion can give rise to a modulated signal. The period of the signal will be the Keplerian orbital period of the emitting star. It is well known that the orbital period increases with the distance between the two stars. The minimum possible period corresponds to a situation where the two stars are in contact with each other, and their separation is of the order of their radius. The minimum Keplerian orbital period is:

$$2R(4\pi^2)/\tau^2 = GM/R^2 \rightarrow \tau \simeq \sqrt{R^3/GM} = 1/\sqrt{G\rho} \quad (1.2)$$

analogous to what was found previously. For typical WD binaries the minimum Keplerian period is larger than the observed PSRs periods. For binary NSs the minimum Keplerian period is smaller, so, in principle,

with a suitable choice of separations one could reproduce the observations. The same holds for binary BHs or BH-NS systems. However close binary systems are known to be sources of gravitational waves (see section ...). The loss of energy, due to gravitational waves emission, leads to a contraction of the orbital distance, and to a secular decrease of the period (the orbital speed increases). This is the opposite of what is observed.

- **Rotation.** If an emitting spot is present on the surface of a rotating object, a periodic signal will be produced, with a period equal to the rotational one. The minimum rotation period of a self gravitating object is given by equating the centrifugal acceleration at the equator to the gravitational one:

$$R(4\pi^2)/\tau^2 = GM/R^2 \rightarrow \tau \simeq \sqrt{R^3/GM} = 1/\sqrt{G\rho}. \quad (1.3)$$

Again the same result. While nothing prevents a BH from rotating, it is impossible to attach anything to its surface. Based on the previous discussion the minimum rotation period of a WD is  $\sim 10$  s, too long. For NSs the the minimum rotation period is  $\sim 10^{-3}$  s. PSRs could be rotating NSs. Moreover, a rotating object that loses energy will spin down, and one would expect a secular increase of the period, compatible with what is observed.

From the above discussion it is evident that, among the possibilities discusses, only rotating NSs can explain the observed periods and period derivatives.

## 1.3 The NS zoo

NSs show a vast and diverse phenomenology, ranging from the canonical PSRs, to extreme objects like Magnetars, from old isolated NSs to accreting systems. Here we present a brief review of the various classes in which they have been divided during the years. The divisions are mostly based on their observational properties, but the distinctions often hide a much more profound difference in the mechanisms responsible for their emission/evolution. At the moment a unifying picture able to relate all of them is still lacking.

### 1.3.1 Pulsars

Having already discussed their theory, we will here only review briefly their observational properties. Rotational Powered Pulsars represent the bulk of the observed NSs, with periods that span the range from  $\sim 1$  ms up to 10 s. Looking at the  $P - \dot{P}$  diagram in Fig. 1.3 it is evident that Pulsars can be grouped in two main families: the **Canonical PSRs** and the **Millisecond PSRs** (MSPs). Canonical PSRs have periods ranging from  $P \sim 0.003$  s to a few seconds, with spin-down rates  $\dot{P} \sim 10^{-18} \div 10^{-11}$  and dipole magnetic fields  $\sim 10^{10} - 10^{14}$  G. They are born in the Core-Collapse supernova of a massive progenitor. Millisecond Pulsars are characterized by very short periods  $P \lesssim 10$  ms and weak dipole magnetic fields  $B \lesssim 10^{10}$  G. With a characteristic age  $\tau \gtrsim 1$  Gyr, MSPs are believed to be the final outcome of NSs undergoing mass accretion from a companion in a close binary systems. Initially born as a normal PSRs the NS spin down for tens of Myr until, if the geometry of the binary is favorable for mass transfer, it undergoes accretion that spins it up and buries its magnetic field.

Both canonical and millisecond PSRs have traditionally been detected thanks to their radio pulsations and are consequently generally referred as Radio-PSRs. At present we know more than 2500 Radio-PSRs. Some of them are visible also at other wavelengths, as pulsating optical, X-ray or  $\gamma$ -ray sources. We have detected more than 100 X-ray PSRs and almost 160  $\gamma$ -ray PSRs. Today we also know radio-quiet PSRs that have been discovered thanks to their pulsed high energy emission (typically  $\gamma$ -rays).

The pulse profile of PSRs differs depending on the energy one is looking at. The X-ray or  $\gamma$ -ray pulses are usually not in phase with radio pulses, and much broader, suggesting that they have origin in different regions of the magnetosphere: closer to the polar cap for the radio, in the outer magnetosphere for the  $\gamma$ -rays.

The spinning dipole model predicts that the spin down of RPPs should be typically smooth and predictable. This is observed on a secular timescale, even if none of the measured braking indexes agrees with the dipole expectation  $n = 3$ . However, in a few PSRs we observe glitches, i.e. sudden and unpredictable changes in spin down, during which the spin rate increases to return to its initial value on a timescale of days to weeks.

Sometimes PSRs can also undergo *pulse nulling*: an abrupt cessation of pulsed radio emission that can last even for  $\sim 10^4$  s. A particular class of PSRs, the Rotating Radio Transients (RRATs) show an extreme nulling behavior: no pulsed emission is observed between single radio flashes. PSRs showing strong nulling and RRATs are usually found close to the death-line in the  $P - \dot{P}$  diagram, suggesting that pair creation and acceleration in their magnetospheres might be close threshold conditions.

### 1.3.2 Magnetars

Magnetars are NSs characterized by a typical dipole magnetic field, inferred from spin-down, in the range  $10^{14} - 10^{15}$  G. Located in the up-right corner of the  $P - \dot{P}$  diagram with rotational periods in the range  $\sim 2 - 12$  s, they have typical spin-down ages of the order of  $10^4$  yr. They are isolated objects not belonging to any binary system. Magnetar as strongly magnetized NSs, were proposed in the early '90s to explain and unify two distinct classes of NSs: the Soft Gamma Repeaters (SGRs) and the Anomalous X-ray pulsars (AXPs). Both classes are characterized by a persistent X-ray emission with luminosities  $L_X \sim 10^{33} - 10^{36}$  erg s $^{-1}$ . AXPs show a phase modulation of their X-ray emission, with a large pulsed fraction. They were initially identified as canonical X-ray pulsars with unexpected high luminosity and pulsed fraction in soft X-rays. SGRs instead were first discovered thanks to their flaring activity with X-ray bursts whose duration is  $\sim 0.1 - 1$  s and whose peak luminosities are  $\sim 10^{40} - 10^{41}$  erg s $^{-1}$ . Originally thought to be a sub-classes of Gamma Ray Bursts (GRBs), only in 1987 they were recognized as different objects. Indeed, unlike GRBs which are single events, SGRs show recurrence. SGRs are also sources of violent events, known as *giant flares*, during which an amount of energy  $\sim 10^{44} - 10^{46}$  erg is released in a very short time  $< 1$  s.

**1.3.2.1 The Magnetar Idea** The properties of the quiescent emission in SGRs and AXPs put severe constraints on the possible source of the observed energy. A rough estimate of the rotational energy of a NS is given by:

$$E_{\text{rot}} = \frac{1}{2} I \Omega^2 \approx 10^{44} \left( \frac{P}{10\text{s}} \right)^{-2} \text{ erg} \quad (1.4)$$

where  $I \approx 10^{45}$  g cm $^2$  is the moment of inertia (for a NS with  $M \simeq 1.4M_{\odot}$  and  $R \simeq 10$  km),  $\Omega$  the rotation rate and  $P$  the period (of the order of 10 s for typical magnetars). This energy should be compared with the emitted energy that can be roughly estimated by the product of their X-ray luminosity with the typical spin-down age  $\tau L_X \sim 10^{44} - 10^{47}$  erg s $^{-1}$ . It is immediately evident that the rotation cannot support their persistent emission, much less their giant flares, which alone carry an amount of energy comparable to the rotational one.

On the other hand one can try to compute the amount of magnetic energy stored inside the neutron star, assuming the dipole estimate  $B \sim 10^{15}$  G to be correct. One finds:  $E_{\text{mag}} \approx R^3 B^2 \sim 10^{48}$  erg. This is enough to sustain the persistent emission and the flaring activity.

**1.3.2.2 Independent Estimates of the Magnetic Field** In the case of Magnetars/SGRs the giant flares can be used to obtain independent estimates of the strength of the magnetic field. The giant flares are characterized by an initial short  $< 1$  s spike of strong hard X-ray soft  $\gamma$ -ray emission with a luminosity that can be as high as  $10^{46}$  erg. The event then shows a long lasting (a few hundreds seconds) tails with a modulation at the rotational period of the NSs. This tail is due to an electron-positron fireball. Its modulation suggests that it must be confined in the inner magnetosphere of the NS. This implies that the magnetic pressure at the edge of the fireball at a radius  $\Delta R$  above the crust, must be strong enough to oppose the one from the pair-plasma  $E_{\text{FB}}/3$ .  $E_{\text{FB}}$  is the energy contained in the fireball that can be obtained multiplying the luminosity of the tail with its duration and is  $\sim 10^{44}$  erg.

$$\frac{B^2(R + \Delta R)}{8\pi} \gtrsim \frac{E_{\text{FB}}}{4\pi\Delta R^3} \quad (1.5)$$

Assuming a dipolar magnetic field  $B \propto R^{-3}$  the above relation implies:

$$B(R) \gtrsim 2 \times 10^{14} \left( \frac{\Delta R}{10\text{km}} \right)^{-3/2} \left( \frac{1 + \Delta R/R}{2} \right)^3 \text{ G} \quad (1.6)$$

where we can assume  $\Delta R \approx R$ , otherwise there will be no modulation.

Giant flares (in particular their initial spike) offer another way to estimate the magnetic field. For an astrophysical source of size  $R$  with luminosity  $L$  lasting for a time  $\Delta t$  the total energy must be  $L\Delta t$ , and it will be related to the mass contained in the source by:

$$L\Delta t = \eta \frac{4\pi}{3} R^3 n m_p c^2 \quad (1.7)$$

where  $n$  is the baryonic density,  $m_p$  the proton mass, and  $\eta < 1$  is the efficiency matter to energy conversion. For an instantaneous injection (the duration of the spike  $\sim 1$  s is much longer than the typical timescales at the base of the NS magnetosphere  $\sim R/c \sim 10^{-3}$  s) the duration of the source is related to the time it takes for a photon to escape.

$$\Delta t > \frac{R}{c} (1 + \tau_{\text{T}}) \quad (1.8)$$

where  $R/c$  is the light crossing time and  $\tau_{\text{T}}$  the optical depth. The correction comes from the fact that for  $\tau_{\text{T}} > 1$  photon diffuse with a random walk and the escape time increases accordingly. The opacity in the fireball is just the Thompson opacity due to electron  $\tau_{\text{T}} = \sigma_{\text{T}} n R$ , where we have assumed one electron per baryon (the case of H). Combining Eq. 1.7 and 1.8 to simplify the radius, one has:

$$\Delta t > \frac{3}{4\pi} \frac{\sigma_{\text{T}}}{m_p c^4} \frac{L}{\eta} \frac{(1 + \tau_{\text{T}})^2}{\tau_{\text{T}}} > \frac{3}{\pi} \frac{\sigma_{\text{T}}}{m_p c^4} \frac{L}{\eta} \quad (1.9)$$

given that the minimum is for  $\tau_{\text{T}} = 1$ . One then has:

$$\frac{L}{\Delta t} < 2\eta \times 10^{42} \text{ erg s}^{-2} \quad (1.10)$$

This is known as **Cavallo-Rees limit**, and it does not depend on any property of the source. Strangely in the initial spike of giant flares  $L/\Delta t \sim 10^{46} \text{ erg s}^{-2}$ . The solution to this paradox comes from the fact that for strong magnetic fields above the quantum threshold  $B_{\text{Q}} = 4.4 \times 10^{13} \text{ G}$ , the scattering cross section for photons with energy below 100keV differs from the Thompson value:

$$\sigma_{\text{B}} = \sigma_{\text{T}} \left( \frac{h\nu B_{\text{Q}}}{m_e c^2 B} \right)^2 \quad (1.11)$$

using this cross section, and adopting a typical photon energy of  $\sim 15 \text{ keV}$  one has:

$$B \approx 100 B_{\text{Q}} \left( \frac{0.1}{\eta} \right)^{1/2} \sim 10^{15} \text{ G} \quad (1.12)$$

consistent with the values obtained in other ways.

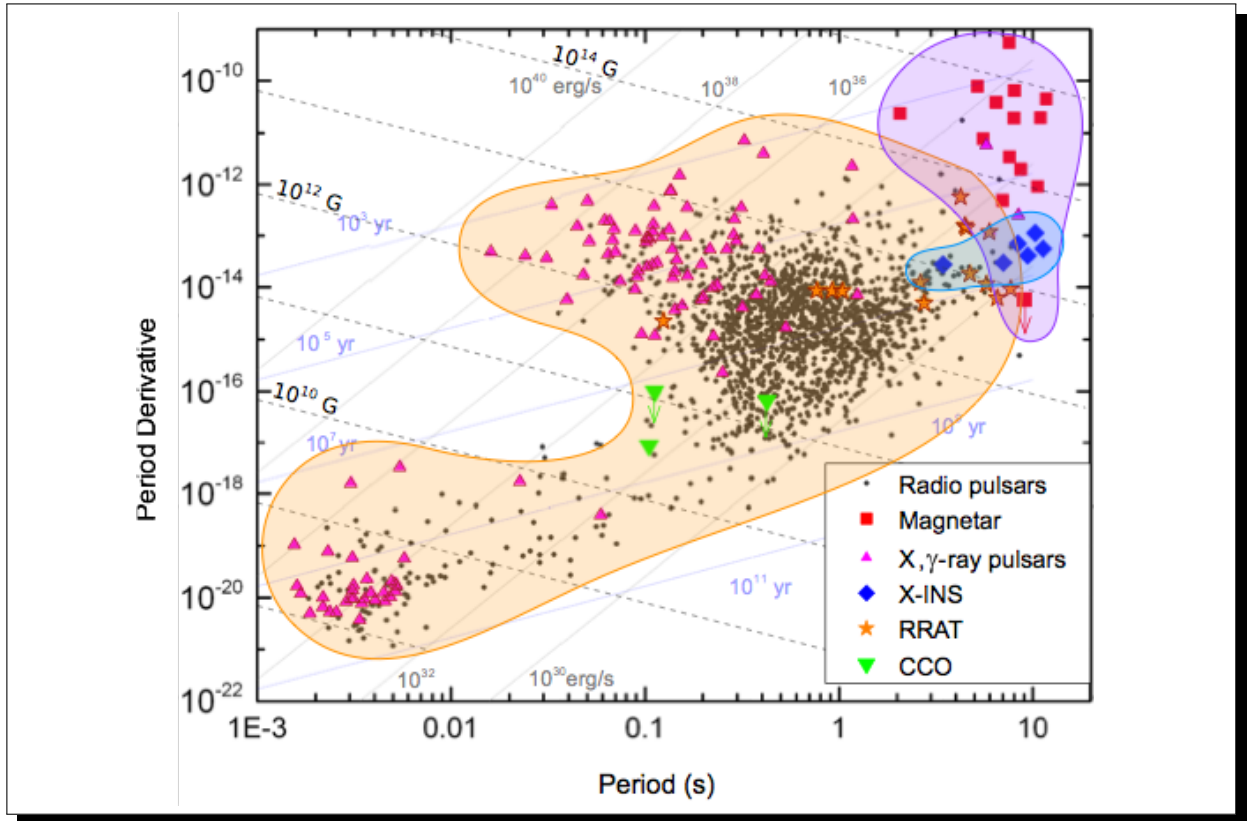


**Figure 1.3:** Diagram of the Period derivative vs Period for known NSs. The various classes are indicated with different symbols. The shaded are represent the portions of this diagram representative of those classes: orange PSRs; purple Magnetars; blue INS. Also shown are isochrones, isomagnetizations and iso-energetic curves.

### 1.3.3 INS and CCO

*Isolated Neutron Stars*, INSs (also known as XINSs due to the fact that they emit mostly in X-rays) are slowly rotating neutron stars with spin periods between 3 and 11 s, an inferred magnetic field slightly higher than that of rotational PSRs, and characteristic ages  $\tau \sim 2$  Myr. They show no pulsed emission similar to PSRs either in radio or other wavelengths, and are detected as isolated X-ray thermal sources, emitting soft X-rays due to cooling. The cooling is confirmed by the black body shapes of their spectra. For this reason we know only a few of them (7 to be precise) within a distance of 500 pc. They lack any observed associated supernova remnant or surrounding nebula. They do not show any magnetospheric activity.

Their emission peaks in the X-ray band with a faint optical/UV counterpart. The light curve shapes are quasi-sinusoidal and single-peaked, which is thought to be due to the presence of a hot spot on their surface. Their X-ray luminosity is  $\sim 10^{30} - 10^{32} \text{ erg s}^{-1}$ . In the case of RX J0720, it is even larger than the spin down luminosity. XMM-Newton's observations made it possible to detect wide absorption features in their spectra, either due to proton cyclotron resonances or atomic transitions in light elements. The values of  $B$  obtained from spin-down assuming magnetodipolar braking are in reasonable agreement with those inferred from the line energy.

INSs emission is believed to be powered by the residual thermal energy of the NS. The inferred temperatures and thermal luminosities are, however, one order of magnitude higher than those of PSRs of the same age. This may suggest that they were born with an initially higher magnetic field, which now has decayed supplying an additional source of heating. Because of the poor statistics, at the moment it is not clear if INS can be connected with other families of the NSs zoo: they may be extreme RRATs, high- $B$  PSRs viewed off-beam from their radio emission or, finally, old magnetars.

**Central Compact Objects**, CCOs are young NSs detected as X-ray sources at the center of supernova remnants of typical age  $\lesssim 10^4$  yr. The emission properties of CCOs are similar to those of XINSs. The observed spectra are purely thermal and can be fitted using multiple blackbody components. The luminosity spans the range  $L_X = 10^{33} - 10^{34}$  erg s $^{-1}$ . About ten CCOs are known to date but pulsations have been observed in only three of them. In the  $P - \dot{P}$  plane CCOs are between PSRs and millisecond PSRs, with spin period  $P \sim 0.1$  s and period derivative  $\dot{P} \sim 10^{17}$ . Contrary to INSs the inferred magnetic field is rather low  $B \sim 10^{10}$  G. Note that the characteristic age  $\tau \sim 100$  Myr is much longer than the age of the supernova remnant. This may suggest that CCOs are born with a low magnetic field and for this reason they are referred also as *anti-magnetars*. Despite the weakness of the dipolar magnetic field, the presence of modulated emission in some CCOs indicates a strongly non-uniform surface temperature distribution. This, in turn, seems to suggest that CCOs hide a stronger magnetic field in the interior. This magnetic field could have been buried by mass fallback accretion during core collapse.

### 1.3.4 LMXB and HMXB

NSs belonging to binary systems can undergo accretion of matter from the companion. In this case is the accretion that powers the observed X-ray emission. The details of the accretion process can be quite complex, depending on the mass accretion rate, the properties of the companion, the cooling properties of the accreting matter, the strength of the magnetic field. These kinds of systems are mainly divided into two separate classes: **Low Mass X-ray Binaries** (LMXBs) and **High Mass X-ray Binaries** (HMXBs).

A typical LMXB is a binary star system where one of the components is either a black hole or neutron star, while the other component, the donor, is less massive than the compact object, and can be a low mass main sequence star (usually a Red Dwarf), a WD, or an evolved star (Red Giant). Usually it fills its Roche lobe and therefore transfers mass to the compact star via **Roche lobe overflow**, forming an accretion disk. The orbital periods of LMXBs range from ten minutes to hundreds of days. Almost all the radiation is emitted as X-rays from the disk, or from the surface shear layer, and typically less than one percent in visible light (from the donor or from reprocessed X-rays), so they are among the brightest objects in the X-ray sky, but relatively faint in optical. In general the rotation rates of the NSs in these systems are very high (close to millisecond period), while their magnetic fields are  $\sim 10^9$  G. They show variability in the form of X-ray bursts, caused by thermonuclear explosions created by the accretion of Hydrogen and Helium. Approximately two hundred LMXBs have been detected in the Milky Way, and of these, about ten LMXBs have been discovered in globular clusters. They can be seen also in distant galaxies.

In the case of HMXBs the companion star is usually an O or B star, or a blue supergiant with mass  $\geq 5M_\odot$ . These stars have typically **strong winds**. A fraction of the stellar wind of the massive normal star can be captured by the compact object, if it flies close enough to be gravitationally bound, and produce X-rays as it falls onto the compact object itself. In a HMXB, the massive star dominates the emission of optical light, while the compact object is the dominant source of X-rays. The massive stars are very luminous and therefore easily detected. HMXBs are observed to vary with a smooth periodicity and do not show bursts. These because the accretion of matter is magnetically funneled into the poles of the accretor. As the poles rotate in and out of view, we observe pulses of X-rays. In HMXBs NSs have periods in the the range  $\sim 1 - 100$  s with magnetic field  $\sim 10^{12}$  G, sometimes estimated from cyclotron absorption lines in the X-ray spectra. Once a HMXB has reached its end, if the separation is large enough, and if the system remains bound after the supernova explosion of the massive donor ( $> 10M_\odot$ ), it can become a double neutron star binary.



# CHAPTER 2

---

## THE STATE OF MATTER IN NEUTRON STARS

---

### 2.1 Fermi-Dirac Distribution

We begin by reviewing some basics of classical statistical mechanics. In describing a system made up of a great many particles, it is usually possible to specify some macroscopically measurable independent parameters. These parameters are termed the *external parameters* of the system. Examples of such parameters are the volume, the total energy, the particle total number etc. A *macrostate* of the system is defined by specifying the external parameters, and any other constraint to which the system is subject. For example, if we are dealing with an isolated system (i.e., one that can neither exchange heat with, nor do work on its surroundings) then the macrostate might be specified by giving the values of the total particle number and the constant total energy. A *microstate* of the system, on the other hand, is defined as a state for which the conditions of all the individual particles are completely specified. For a many-particle system, there are generally a very great number of microstates which are consistent with a given macrostate.

At the typical densities one encounters in White Dwarves and Neutron Stars, quantum effects, and in particular the Pauli Exclusion principle for fermions, cannot be neglected. Indeed, as we will show, it is the fact that no two fermions can have the same quantum numbers, that allow these objects to exist in the first place. It is the so called *degeneracy pressure* that keeps them in equilibrium against the gravitational force. We are however going to begin our derivation of the equation of state for fermions at high densities, with the classical Boltzmann distribution.

#### 2.1.1 Classical Boltzmann Distribution

Let us consider a system of  $N$  particles, distributed over  $m$  energy levels, such that in this macrostate each level  $j$  has  $n_j$  particles. The number of way to assign  $n_1$  particles to the first energy level, is just the number of possible combinations of  $n_1$  elements out of a total of  $N$ :

$$W_1 = \frac{N!}{n_1!(N - n_1)!}. \quad (2.1)$$

The number of ways to assign  $n_2$  particles out of the remaining  $N - n_1$  particles to the second energy level is:

$$W_2 = \frac{(N - n_1)!}{n_2!(N - n_1 - n_2)!}, \quad (2.2)$$

and so on. The number of ways  $W$  to assign  $n_1$  particles to the first level,  $n_2$  to the second ....  $n_j$  to the  $j$ -th one etc., up to the  $m$ -th level, is:

$$W = \prod_{j=1}^m W_j = \frac{N!}{n_1!(N - n_1)!} \times \frac{(N - n_1)!}{n_2!(N - n_1 - n_2)!} \times \dots = \frac{N!}{n_1!n_2!\dots n_m!} = \frac{N!}{\prod_{j=1}^m n_j!}. \quad (2.3)$$

$W$  is related to the probability of the given distribution sequence, and corresponds to the total number of microstates for the given macrostate. The sequence  $n_1 \dots n_j \dots n_m$  that maximizes  $W$  is the **equilibrium configuration** and the relative macrostate is the **equilibrium macrostate**. The specific equilibrium distribution depends also on the constraints imposed on the system. For example, in a close system that does not exchange matter or energy (heat or work) with the surroundings, the total number of particles and their total energy  $E$  are conserved. Then the two constraints are:

$$\sum_{j=1}^m n_j = N \quad \sum_{j=1}^m n_j e_j = E \quad (2.4)$$

where  $e_j$  is the energy of level  $j$ . One can then look for the configuration that maximizes  $W$  [or equivalently  $\ln(W)$ ], enforcing the constraints by making use of Lagrangian multipliers.

$$\begin{aligned} d \ln(W) + \alpha \sum_{j=1}^m dn_j + \beta \sum_{j=1}^m e_j dn_j &= d \left[ \ln(N!) - \sum_{j=1}^m \ln(n_j!) \right] + \alpha \sum_{j=1}^m dn_j + \beta \sum_{j=1}^m e_j dn_j = 0 \\ d \left[ N \ln(N) - N - \sum_{j=1}^m [n_j \ln(n_j) - n_j] \right] + \alpha \sum_{j=1}^m dn_j + \beta \sum_{j=1}^m e_j dn_j &= 0 \\ d \left[ - \sum_{j=1}^m n_j \ln(n_j) \right] + \alpha \sum_{j=1}^m dn_j + \beta \sum_{j=1}^m e_j dn_j &= 0 \end{aligned} \quad (2.5)$$

where, in the first we have used Stirling's approximation for large  $N$ :  $\ln(N!) = N \ln(N) - N$ , and in the third we have used Eq. 2.4 and we have reabsorbed extra terms of the sum of  $dn_j$  into the coefficient  $\alpha$ . So we have:

$$\begin{aligned} \sum_{j=1}^m [dn_j - n_j \ln(n_j)] + \alpha \sum_{j=1}^m dn_j + \beta \sum_{j=1}^m e_j dn_j &= 0 \\ \sum_{j=1}^m dn_j [\ln(n_j) + (1 - \alpha) - \beta e_j] = 0 \Rightarrow \ln(n_j) = \beta e_j + (\alpha - 1) \Rightarrow n_j = e^{\alpha-1} e^{\beta e_j} \end{aligned} \quad (2.6)$$

**2.1.1.1 Equilibrium Temperature** The parameter  $\alpha$  enters just as a normalization, while the way different energy levels are populated is encoded by the parameter  $\beta$ . To understand the meaning of the latter, consider a system containing particles of two species ( $a$ ) and ( $b$ ), capable of interacting and exchanging energy among them, but not with the surrounding, and each populating different energy levels  $e_j^{(a)}$  and  $e_j^{(b)}$ . Now the total number of particles of each specie is separately conserved, while only the sum of total energy of the two will be:

$$\sum_{j=1}^m n_j^{(a)} = N^{(a)}, \quad \sum_{j=1}^m n_j^{(b)} = N^{(b)}, \quad \sum_{j=1}^m [n_j^{(a)} e_j^{(a)} + n_j^{(b)} e_j^{(b)}] = E \quad (2.7)$$

The number of ways  $W$  to assign  $n_j^{(a)}$  particles of specia ( $a$ ) to the  $j$ -th level of energy  $e_j^{(a)}$ , and  $n_j^{(b)}$  particles of specia ( $b$ ) to the  $j$ -th level of energy  $e_j^{(b)}$ , is just the product of  $W^{(a)}$  by  $W^{(b)}$ , each computed separately as in Eq. 2.3:

$$W = \frac{N^{(a)!}}{\prod_{j=1}^m n_j^{(a)}!} \times \frac{N^{(b)!}}{\prod_{j=1}^m n_j^{(b)}!} \quad (2.8)$$

If one repeats the maximization procedure done before, using now three Lagrangian multipliers, both in terms of  $dn_j^{(a)}$  and  $dn_j^{(b)}$ , one finds that the configurations that maximize  $W$  are:

$$n_j^{(a)} = e^{[\alpha^{(a)}-1]} e^{\beta e_j^{(a)}} \quad \text{and} \quad n_j^{(b)} = e^{[\alpha^{(b)}-1]} e^{\beta e_j^{(b)}} \quad (2.9)$$

We see that the same parameter  $\beta$  characterizes how the various energy levels are populated for both species. It is a common constant that characterizes two systems at equilibrium. We know from thermodynamics that this cannot be but the temperature (or any function of it).

**2.1.1.2 Equilibrium from Detailed Balance** It is well known that in order to establish thermodynamical equilibrium, particles need to interact among themselves, and exchange energy. In the previous discussion, however, no mention of interaction was made. The role of interactions was hidden under the concept of the macrostate with the maximum number of corresponding microstates. The idea is that a thermodynamics system, due to interactions, changes rapidly its microstate, each one being equally probable. Then the most probable macrostate in which a system can be found at any time is the one with the maximum number of corresponding microstates.

Here we will show how the same results can be derived if one takes interactions explicitly into account. We will refer to interaction events as **scattering**, even if usually the term is used with the idea that the system losses memory of its initial state, while for classical systems the interaction of two particles is always fully deterministic. Let us call  $C_{12 \rightarrow 1'2'}$  the probability per unit time for a couple of particles with energy  $e_1$  and  $e_2$  to interact through an interaction potential  $V$  (operating over distances much smaller than the distance travelled by a particle between successive interactions) and to end with energies  $e'_1$  and  $e'_2$  respectively. This is nothing else than the differential cross-section for the interaction  $d\sigma_V/de_1 de_2 de'_1 de'_2$ . Then the rate of scatterings from  $e_1$  and  $e_2$  to  $e'_1$  and  $e'_2$  is just:

$$R_{\rightarrow} = C_{12 \rightarrow 1'2'} f(e_1) f(e_2) \quad (2.10)$$

where  $f(e)$  is the distribution function, i.e. the probability to find a particle with an energy  $e$ . Note that the rate depends only on the probability of having particles in the initial states, and not on the final ones. The reverse interaction where particles with energy  $e'_1$  end into  $e_1$  to  $e_2$ , will have a rate:

$$R_{\leftarrow} = C_{1'2' \rightarrow 12} f(e'_1) f(e'_2) \quad (2.11)$$

Now as long as the potential  $V$  is conservative (i.e. the particles have no internal degree of freedom that can be excited in the interaction), then the dynamics of the interaction will be Hamiltonian, the differential cross-section will be unchanged, and  $C_{12 \rightarrow 1'2'} = C_{1'2' \rightarrow 12}$ .

**Detailed balance** requires the two rate to be the same at equilibrium  $R_{\rightarrow} = R_{\leftarrow}$ , and this implies  $f(e_1) f(e_2) = f(e'_1) f(e'_2)$ . Now if the total energy is conserved  $e_1 + e_2 = e'_1 + e'_2$ , one can set  $e'_1 = e_1 + x$ ,  $e'_2 = e_2 - x$ , leading to:

$$f(e_1) f(e_2) = f(e_1 + x) f(e_2 - x) \quad (2.12)$$

Given that this must hold for any value of  $x$ , it will also hold in the limit of small  $x$ , where we can perform a Taylor expansion

$$\begin{aligned} f(e_1) f(e_2) &= \left[ f(e_1) + \left. \frac{df}{de} \right|_{e_1} x \right] \left[ f(e_2) - \left. \frac{df}{de} \right|_{e_2} x \right] + \mathcal{O}(x^2) \\ &= f(e_1) f(e_2) \left[ 1 + \left( \left. \frac{d \ln(f)}{de} \right|_{e_1} - \left. \frac{d \ln(f)}{de} \right|_{e_2} \right) x \right] + \mathcal{O}(x^2) \\ &\Rightarrow \frac{d \ln(f)}{de} = \beta = \text{const} \end{aligned} \quad (2.13)$$

given that the equality must hold for any  $x$ . So we recover the previous result:

$$f(e_i) \propto e^{\beta e_i}. \quad (2.14)$$

**2.1.1.3 Maxwell-Boltzmann Equation of State** If one identifies  $\beta = -1/kT$  (for dimensional reasons), then one recovers the **Classical Maxwell-Boltzmann distribution**  $n_j \propto e^{-e_j/kT}$ . More generally if the level  $j$  has a degeneracy  $g_j$  (there are  $g_j$  somehow distinguishable levels all having the same energy) then:

$$n_j = g_j A e^{-e_j/kT} \quad (2.15)$$

The constraints can be used to fix the normalization. Assuming that the energy levels are finely spaced ( $e_{j+1} - e_j \ll kT$ ), one can assume that the energy varies continuously, and replace the summation with the integral:

$$N = \int_0^\infty Ag(e)e^{-e/kT} de, \quad E = \int_0^\infty Aeg(e)e^{-e/kT} de \quad \Rightarrow \quad E \propto NkT, \quad (2.16)$$

where the proportionality coefficient depends on the dimensionality [the degeneracy  $g(e)$ ] of the system. If one assumes that  $g(e) \propto e^d$  with  $d > -1$ , recalling that the definition of the Euler's Gamma function is:

$$\Gamma[d+1] = \int_0^\infty x^d e^{-x} dx, \quad (2.17)$$

then one finds:

$$E = NkT \frac{\Gamma[d+2]}{\Gamma[d+1]} \quad \Rightarrow \quad E = 3NkT/2 \quad \text{for} \quad d = 0.5 \quad (2.18)$$

telling us that degeneracy for the classical Maxwell-Boltzmann distribution in 3D is  $g(e) \propto \sqrt{e}$ .

## 2.1.2 Quantum mechanics and the Fermi-Dirac Distribution

The classical derivation presented above relies on two principles: particles are distinguishable (exchanging two particles among different energy levels leads to different configurations that are counted separately); each phase space volume (energy level) can contain as many particles as one wishes.

These assumptions contrast with quantum mechanical principles: similar particles (i.e. electrons, protons, neutrons) cannot be distinguished (any exchange of two particles leads to the same state, and must be counted only once); fermions obey **Pauli's Exclusion Principle**. Two fermions cannot have the same quantum numbers. Moreover, while in classical mechanics the phase space can be partitioned into an arbitrary number of volume elements, in quantum mechanics the **Uncertainty Principle** sets the minimal size of a phase space volume element to be  $dp_x dp_y dp_z dx dy dz \simeq h^3$ . Within each of these elementary volumes one can put at most one fermion, or  $g$  fermions if there are other  $g$  quantum numbers to be specified (i.e.  $g = 2$  for electrons given the different spins).

Suppose we have a number of energy levels, labeled by index  $j$ , each level having energy  $e_j$ , and containing each  $n_j$  particles. Suppose each energy level can be partitioned into  $g_j \geq n_j$  distinct sublevels, all of which have the same energy, but which are distinguishable by other quantum numbers ( $g_j$  is the degeneracy of the level). For example, two particles may have different momenta (i.e. their momenta may be along different directions), in which case they are distinguishable from each other, yet they can still have the same energy.  $g_j$  is just the number of phase space volume elements having all the same energy  $e_j$ .

The number of ways of distributing  $n_j$  indistinguishable particles among the  $g_j$  sublevels of an energy level, with a maximum of one particle per sublevel, is just the number of possible combinations of  $n_j$  elements out of  $g_j$ :

$$W_j = \frac{g_j!}{n_j!(g_j - n_j)!} \quad (2.19)$$

The number of ways that a macrostate characterized by a set of occupation numbers  $n_j$  ( $j = 1, \dots, m$ ) can be realized is the product of the ways in which each individual energy level can be populated:

$$W = \prod_{j=1}^m W_j = \prod_{j=1}^m \frac{g_j!}{n_j!(g_j - n_j)!} \quad (2.20)$$

Following the same procedure used in deriving the Maxwell-Boltzmann statistics, we wish to find the set of  $n_j$  for which  $\ln(W)$  is maximized, subject to the constraint that there are a fixed number of particles, and a fixed total energy. As before, we can apply a method based on Lagrangian multipliers:

$$\begin{aligned}
 d \ln(W) + \alpha \sum_{j=1}^m dn_j + \beta \sum_{j=1}^m e_j dn_j &= 0 \\
 d \left[ \sum_{j=1}^m [\ln(g_j!) - \ln(n_j!) - \ln(g_j - n_j)!] \right] + \alpha \sum_{j=1}^m dn_j + \beta \sum_{j=1}^m e_j dn_j &= 0 \\
 d \left[ \sum_{j=1}^m [-\ln(n_j!) - \ln(g_j - n_j)!] \right] + \alpha \sum_{j=1}^m dn_j + \beta \sum_{j=1}^m e_j dn_j &= 0
 \end{aligned} \tag{2.21}$$

given that the degeneracies  $g_j$  are constants of the energy levels. Then, applying Stirling formula, and reabsorbing terms in  $dn_j$  into  $\alpha$ , one gets:

$$\begin{aligned}
 d \left[ \sum_{j=1}^m [-n_j \ln(n_j) + n_j - (g_j - n_j) \ln(g_j - n_j) + g_j - n_j] \right] + \alpha \sum_{j=1}^m dn_j + \beta \sum_{j=1}^m e_j dn_j &= 0 \\
 d \left[ \sum_{j=1}^m [(n_j - g_j) \ln(g_j - n_j) - n_j \ln(n_j)] \right] + \alpha \sum_{j=1}^m dn_j + \beta \sum_{j=1}^m e_j dn_j &= 0 \\
 \sum_{j=1}^m \left[ d[(n_j - g_j) \ln(g_j - n_j) - n_j \ln(n_j)] + \alpha dn_j + \beta e_j dn_j \right] &= 0 \\
 \sum_{j=1}^m dn_j [\ln(g_j - n_j) - \ln(n_j) + \alpha + \beta e_j] &= 0
 \end{aligned} \tag{2.22}$$

which implies:

$$\ln \left( \frac{g_j - n_j}{n_j} \right) + \alpha + \beta e_j = 0 \quad \Rightarrow \quad n_j = \frac{g_j}{e^{-\alpha - \beta e_j} + 1} \tag{2.23}$$

Note that in the limit  $-\alpha - \beta e_j \gg 1$ , this reduces to the Maxwell-Boltzmann result Eq. 2.6. It is then natural to identify  $\beta = -1/kT$ . However, even in this case, it is possible to show explicitly that  $\beta$  represents a constant equal for all species at thermodynamic equilibrium. Let us repeat the same argument as in Sect. 2.1.1.1, and consider two species of particles, subject to the constraint that the number of each specie and the sum of their total energy is conserved, Eq. 2.8. The number of ways  $W$  to assign  $n_j^{(a)}$  particles of specie (a) to the  $g_j^{(a)}$  sublevels of the  $j$ -th level of energy  $e_j^{(a)}$ , and  $n_j^{(b)}$  particles of specie (b) to the  $g_j^{(b)}$  sublevels of the  $j$ -th level of energy  $e_j^{(b)}$ , is just the product of  $W^{(a)}$  by  $W^{(b)}$ , each computed separately as in Eq. 2.20. Maximization over  $dn_j^{(a)}$  and  $dn_j^{(b)}$ , leads to the following conditions:

$$n_j^{(a)} = \frac{g_j^{(a)}}{e^{-\alpha^{(a)} - \beta e_j^{(a)}} + 1} \quad \text{and} \quad n_j^{(b)} = \frac{g_j^{(b)}}{e^{-\alpha^{(b)} - \beta e_j^{(b)}} + 1} \tag{2.24}$$

which show that the Lagrangian multiplier  $\beta$  is the same for both, whence it follows its identification with a function of the temperature.

**2.1.2.1 Equilibrium from Detailed Balance** In Sect. 2.1.1.2 we showed that the Maxwell-Boltzmann distribution could be derived from detailed balance, considering explicitly the interaction of particles. The same can be done for the distribution of fermions, but now the argument must be recast in quantum mechanical terms, and we

need to account for Pauli's Exclusion Principle. This will illustrate a key feature of scattering processes in degenerate system. For simplicity we will neglect the degeneracy of energy levels, and assume  $g_j = 1$  for all  $j$ .

Let us consider a system formed by two particles with energies  $e_1$  and  $e_2$  whose quantum mechanical state is  $|1, 2\rangle$ . If they interact through a potential  $V$  leading to a final state  $|1', 2'\rangle$ , with energies  $e'_1$  and  $e'_2$  respectively, then the transition probability per unit time will be  $C_{12 \rightarrow 1'2'} = \langle 1', 2' | V | 1, 2 \rangle$ . The rate of transitions from  $|1, 2\rangle$  to  $|1', 2'\rangle$  is:

$$R_{\rightarrow} = C_{12 \rightarrow 1'2'} f(e_1) f(e_2) [1 - f(e'_1)] [1 - f(e'_2)] \quad (2.25)$$

where  $f(e)$  is the distribution function, i.e. the probability to find a particle with an energy  $e$ . Note that the rate depends now not only on the probability of having particles in the initial states, as it was before, but also on the probability that the final states are available (i.e. they are not already occupied). This is the manifestation of Pauli's Exclusion Principle. In a fermions system, a transition will be forbidden if the final state is already occupied. More generally the **Pauli's Exclusion Principle will lead to a suppression of the transition**, reducing the effectiveness of scattering. This will have important consequences in terms of transport of energy, or of charges (i.e. in terms of thermal/electric resistivity).

The rate of the reversed reaction will be:

$$R_{\leftarrow} = C_{1'2' \rightarrow 12} f(e'_1) f(e'_2) [1 - f(e_1)] [1 - f(e_2)] \quad (2.26)$$

where  $C_{1'2' \rightarrow 12} = \langle 1, 2 | V | 1', 2' \rangle$ . As long as  $V$  is Hermitian (i.e. the quantistic equivalent of an Hamiltonian potential), then  $C_{1'2' \rightarrow 12} = C_{12 \rightarrow 1'2'}$ . **Detailed balance** thus requires:

$$f(e_1) f(e_2) [1 - f(e'_1)] [1 - f(e'_2)] = f(e'_1) f(e'_2) [1 - f(e_1)] [1 - f(e_2)] \quad (2.27)$$

As before, if the total energy is conserved  $e_1 + e_2 = e'_1 + e'_2$ , one can set  $e'_1 = e_1 + x$ ,  $e'_2 = e_2 - x$ , leading to:

$$f(e_1) f(e_2) [1 - f(e_1 + x)] [1 - f(e_2 - x)] = f(e_1 + x) f(e_2 - x) [1 - f(e_1)] [1 - f(e_2)] \quad (2.28)$$

which can be written as:

$$\left[ \frac{1}{f(e_1)} - 1 \right] \left[ \frac{1}{f(e_2)} - 1 \right] = \left[ \frac{1}{f(e_1 + x)} - 1 \right] \left[ \frac{1}{f(e_2 - x)} - 1 \right] \\ \omega(e_1) \omega(e_2) = \omega(e_1 + x) \omega(e_2 - x) \quad (2.29)$$

where we have defined  $\omega(e) = -1 + 1/f(e)$ . Eq. 2.29 is formally equivalent to Eq. 2.12, and can be solved in the same way, giving:

$$\omega(e_i) \propto e^{-\beta e_i} \quad \Rightarrow \quad f(e_i) = \frac{1}{e^{-\alpha - \beta e_i} + 1} \quad (2.30)$$

where we have chosen the (arbitrary) sign of the integration constant for consistency. The result is the same as in Eq. 2.24.

**2.1.2.2 Fermi-Dirac Equation of State** Again, if one identifies  $\beta = -1/kT$ , then one recovers the **Fermi-Dirac statistics**:

$$n_j = \frac{g_j}{e^{(e_j - \mu)/kT} + 1} \quad (2.31)$$

where we have introduced the **chemical potential**  $\mu$ . The chemical potential has a clear interpretation as a function of density in the limit of zero temperature:

$$n(e) = \lim_{T \rightarrow 0} \frac{g(e)}{e^{(e - \mu)/kT} + 1} = \begin{cases} g(e) & \text{for } e \leq \mu \\ 0 & \text{for } e \geq \mu \end{cases} \quad (2.32)$$

The chemical potential is usually referred as **Fermi Energy**  $E_F$ , which is the highest energy a fermion can have at zero temperature. Moreover at zero temperature all state with  $e \leq E_F = \mu$  are fully occupied, as shown in Fig. 2.1.

In the limit  $e \gg \mu$  and  $e/kT \gg 1$  one recovers the classical Maxwell-Boltzmann solution.

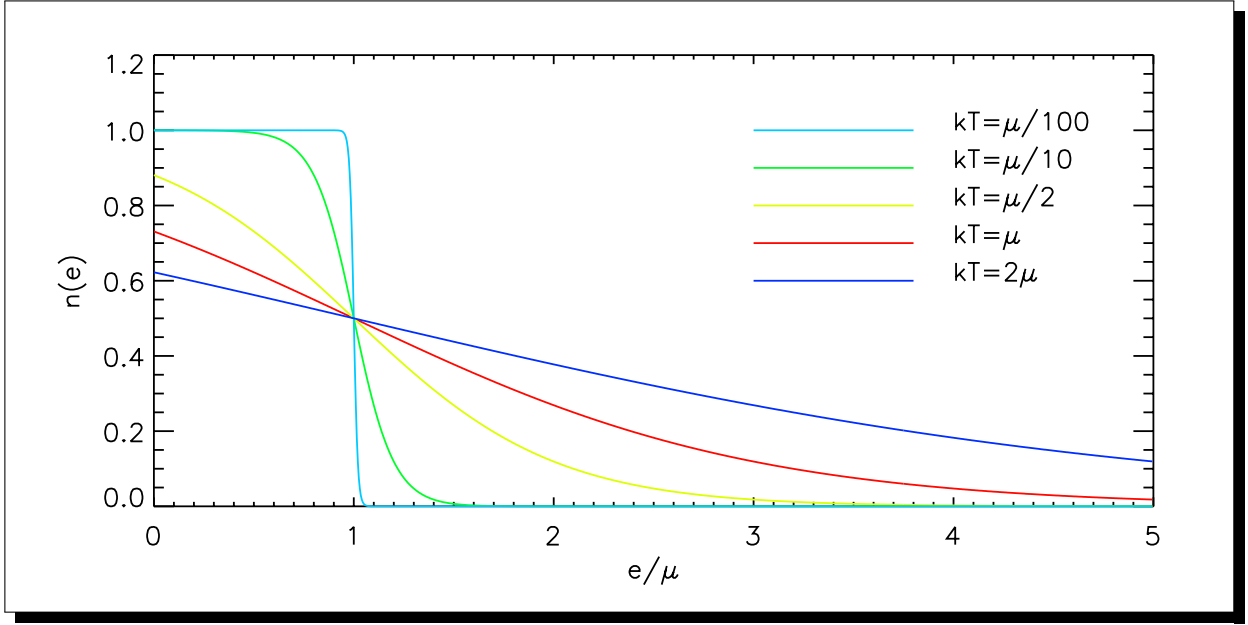


**Figure 2.1:** One-dimensional [ $g(e) = 1$ ] Fermi-Dirac distribution function for different values of the ratio of the thermal energy  $kT$  over the chemical potential  $\mu$ .

### 2.1.3 Heuristic interpretation of the Fermi Momentum

Consider a dense gas, with average distance in the  $x$ -direction between the particles of  $\Delta x$ . According to Heisenberg's uncertainty principle, the accuracy with which position and momentum of a single particle can be determined simultaneously is limited by  $\Delta x \Delta p_x > h$ . Pauli's exclusion principle now says that within this accuracy no two particles may be in the same state, i.e. that the minimal allowed difference in momentum for identical particles is given by  $\Delta p_x > h/\Delta x$ . An analogous reasoning can be made for the  $y$  and  $z$  directions. But the average distance between particles is related to their numerical density  $n$ . For an isotropic 3-dimensional system  $\Delta x = \Delta y = \Delta z \approx n^{-1/3}$ , and this implies that the uncertainty over momentum (let say in the  $x$ -direction) will be  $\Delta p_x \approx hn^{-1/3}$ . Momentum cannot be determined with a higher accuracy: larger momenta are possible but smaller ones are not (in the sense that it is not possible to establish them). So the system behaves as if the smaller possible momentum is  $\approx hn^{-1/3}$ .

This is the origin of the **Fermi Momentum**, as the smallest momentum allowed by a system of particles with average numerical density  $n$ . The Fermi energy, is nothing else than the energy associated with this momentum.

### 2.1.4 Equation of State in the Fully Degenerate Case

Consider a single free particle within a box of size  $L$ , with wave vector  $\mathbf{k} = (\pi/L)\mathbf{n}$  and corresponding momenta  $\mathbf{p} = (\pi\hbar/L)\mathbf{n}$  where  $\mathbf{n}$  is a triplet of positive integers. The number of possible states with momenta between  $\mathbf{p}$  and  $\mathbf{p} + d^3\mathbf{p} = \mathbf{p} + dp_x dp_y dp_z$  will be  $(\Delta n)^3 = \Delta n_x \Delta n_y \Delta n_z$  such that:

$$d^3\mathbf{p} = \left(\frac{\pi\hbar}{L}\right)^3 \Delta n_x \Delta n_y \Delta n_z = \frac{(\pi\hbar)^3}{V} (\Delta n)^3 \Rightarrow \frac{4\pi p^2 dp}{8} = \frac{(\pi\hbar)^3}{V} (\Delta n)^3 \quad (2.33)$$

where the factor  $1/8$  comes from the fact that, in the on-shell formalism, we counted only positive integers contributing to momenta only in one octant, and  $V = L^3$  is the volume. The on-shell approach is useful for free particles because their energy depends only on the norm of the momentum  $p$ , and not on its direction. So the

degeneracy of each energy level is equal to the degeneracy of the on-shell momentum space. One immediately sees that, the degeneracy of the on-shell phase space volume between  $p$  and  $p + dp$  is:

$$g = (\Delta n)^3 = \frac{4\pi p^2 dp}{(2\pi\hbar)^3} V = \frac{4\pi p^2 dp}{h^3} V \quad (2.34)$$

which immediately shows the existence of a minimal phase space volume:  $(2\pi\hbar)^3$ .

Using Eq. 2.31 one finds for the density

$$\frac{N}{V} = \int_0^\infty \frac{8\pi p^2 dp}{(2\pi\hbar)^3} \frac{1}{e^{(e(p)-E_F)/kT} + 1} \quad (2.35)$$

where  $e(p)$  is the energy corresponding to the momentum  $p$ , and the factor 2 comes from the spin. In the same way it is possible to compute the pressure given by the transverse momentum flux across a surface:

$$P = \int_0^\infty \frac{8\pi p^2 dp}{(2\pi\hbar)^3} \frac{(\mathbf{v} \cdot \mathbf{n})(\mathbf{p} \cdot \mathbf{n})}{e^{(p^2/2m-E_F)/kT} + 1} \quad (2.36)$$

where  $\mathbf{v}$  and  $\mathbf{n}$  are the velocity and surface normal respectively. For an isotropic distribution the integral in  $\sin(\theta)d\theta$  over all possible directions of  $(\mathbf{v} \cdot \mathbf{n})(\mathbf{p} \cdot \mathbf{n}) = vp \cos^2(\theta)$  is equal to  $pv/3$ .

For non relativistic particles of mass  $m$  the energy is  $e = p^2/2m$ . This implies that:

$$\frac{N}{V} = \int_0^\infty \frac{8\pi p^2 dp}{(2\pi\hbar)^3} \frac{1}{e^{(p^2/2m-E_F)/kT} + 1} \quad (2.37)$$

and in the fully degenerate limit  $T \rightarrow 0$  one finds:

$$n = \int_0^{p_F} \frac{8\pi p^2 dp}{(2\pi\hbar)^3} = \frac{8\pi p_F^3}{3(2\pi\hbar)^3} \Rightarrow E_F = \frac{p_F^2}{2m} = \frac{(2\pi\hbar)^2}{8\pi^{2/3}m} (3n)^{2/3} = \frac{\hbar^2}{2m} (3\pi^2 n)^{2/3} \quad (2.38)$$

In the non relativistic case  $v = p/m$  and:

$$P = \int_0^\infty \frac{8\pi p^2 dp}{3m(2\pi\hbar)^3} \frac{p^2}{e^{(p^2/2m-E_F)/kT} + 1} \quad (2.39)$$

which in the fully degenerate limit gives:

$$P = \int_0^{p_F} \frac{8\pi p^4 dp}{3m(2\pi\hbar)^3} = \frac{8\pi p_F^5}{15m(2\pi\hbar)^3} \Rightarrow P = \left(\frac{1}{5m}\right) (3\pi^2 \hbar^3)^{2/3} n^{5/3} \quad (2.40)$$

As the density increases so does the Fermi momentum and energy. At a certain point they will be higher than the rest mass energy of the particles  $E_F > mc^2$ . Beyond this density one must use relativistic energy-momentum relations to properly compute density and pressure. For relativistic particles the relation between energy and momentum is  $e = cp$ . While the relation between momentum and velocity is  $vp = cp$

This implies that:

$$\frac{N}{V} = \int_0^\infty \frac{8\pi p^2 dp}{(2\pi\hbar)^3} \frac{1}{e^{(cp-E_F)/kT} + 1} \quad (2.41)$$

and in the fully degenerate limit  $T \rightarrow 0$  one finds:

$$n = \int_0^{p_F} \frac{8\pi p^2 dp}{(2\pi\hbar)^3} = \frac{8\pi p_F^3}{3(2\pi\hbar)^3} \Rightarrow E_F = cp_F = \frac{c(2\pi\hbar)}{2\pi^{1/3}} (3n)^{1/3} = (\hbar c)(3\pi^2 n)^{1/3} \quad (2.42)$$

while for the pressure:

$$P = \int_0^\infty \frac{8\pi p^2 dp}{3(2\pi\hbar)^3} \frac{cp}{e^{(cp-E_F)/kT} + 1} \quad (2.43)$$

which in the fully degenerate limit gives:

$$P = \int_0^{p_F} \frac{8\pi p^3 cp}{3(2\pi\hbar)^3} = \frac{8\pi c p_F^4}{12(2\pi\hbar)^3} \Rightarrow P = \left(\frac{c}{4}\right) (3\pi^2 \hbar^3)^{1/3} n^{4/3} \quad (2.44)$$

independent from the mass of the particle.

It is possible to derive a generalized equation of state for the fully degenerate case, that smoothly connects the non relativistic to the relativistic regime. The general relation among energy, momentum and velocity is:

$$e = mc^2 \left(1 + \frac{p^2}{m^2 c^2}\right)^{1/2} \quad v = \frac{p}{m} \left(1 + \frac{p^2}{m^2 c^2}\right)^{-1/2} \quad (2.45)$$

leading to:

$$P = \frac{8\pi}{3m(2\pi\hbar)^3} \int_0^{p_F} \frac{p^4 dp}{(1 + p^2/m^2 c^2)^{1/2}} = \frac{8\pi c p_F^4}{12(2\pi\hbar)^3} \quad (2.46)$$

Using the following substitutions:

$$p/mc = \sinh(t/4) \quad p_F = mc \sinh(t_F/4) \quad E_F = mc^2 \cosh(t_F/4) \quad (2.47)$$

one finds:

$$n = \frac{1}{3\pi^2} \left(\frac{mc}{\hbar}\right)^3 \sinh^3(t_F/4) \quad P = \left(\frac{2m^4 c^5}{3\pi^2 \hbar^3}\right) (\sinh(t_F) - 8 \sinh(t_F/2) + 3t_F) \quad (2.48)$$

## 2.2 Atmosphere

We begin by describing the physical properties of the atmosphere and of the outer layers of the crust of a typical Neutron Star (NS). We will show that the values of density and temperature in the outer crust of a NS are not too dissimilar from those holding inside a WD.

If Fig. 2.2, the spectrum of three isolated NSs is shown. These are systems where there is no evidence of any magnetospheric activity, so that one can safely assume that the observed radiation comes from the NS photosphere (i.e. surface). It is evident that such spectra are not very informative: there is no evidence of emission or absorption features that might be used to constrain the composition of the NS atmosphere. In general a simple Black Body radiation provides a quite good fit to the data. The maximum of the emission is reached at frequencies  $\sim 10^{17}$  Hz, corresponding to a typical temperature  $\sim$  a few  $10^6$  K, and a typical thermal energy  $E_{Th} \sim 0.1$  keV. Only systems with very high magnetic field  $> 10^{13}$  G show higher temperatures  $\sim 10^7$  K, most likely because of continuous heating due to magnetic field dissipation (see Fig. 2.3). It is found that throughout the entire crust the temperature ranges from  $10^6$  to  $10^8$  Kelvin, reaching the highest value at the base of the inner crust, where it merges into the core.

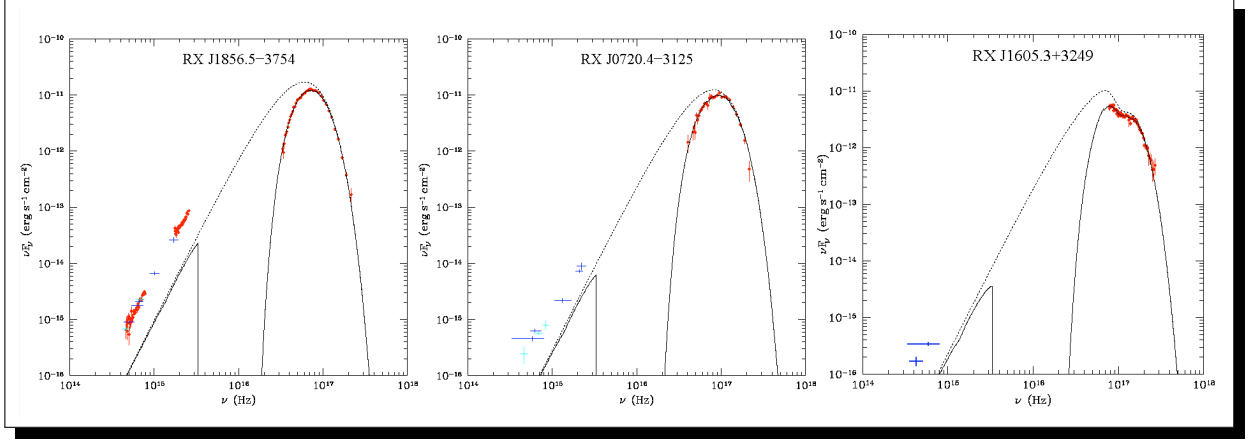


**Figure 2.2:** Spectrum of three isolated NSs. Color points are the data. The dashed line is an unabsorbed Black Body. The solid line is a Black Body plus ISM absorption.

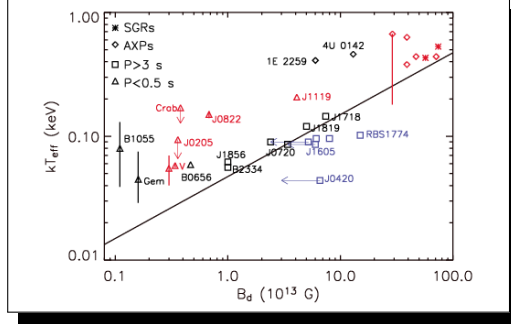


**Figure 2.3:** Surface temperature of NSs vs magnetic field

The complete ionization energy for an atom of charge  $Z$ , is  $E_{\text{ion}} = 13.6 Z^2 \text{eV}$ , corresponding to typical ionization temperature of  $10^5 \text{K}$  for H,  $4 \times 10^5 \text{K}$  for He,  $4 \times 10^6 \text{K}$  for C, up to  $\sim 10^8 \text{K}$  for Fe. Obviously at the typical surface temperatures of NSs, light elements up to C-N-O are fully ionized. Heavier elements might still be partly ionized.

For an isothermal neutrally charged atmosphere, in hydrostatic equilibrium, the density  $\rho$  has an exponential profile with the high  $h$ :

$$\rho(h) = \frac{A}{Z} m_p n_e = \frac{A}{Z} m_p n_e(h_0) e^{(h-h_0)/H}, \quad (2.49)$$

where  $A$  is the atomic number of the element forming the atmosphere (1 for H, 4 for He, 12 for C),  $m_p$  is the proton mass,  $n_e$  is the electron number density,  $h_0$  is a reference high, and  $H$  is the scale-height of the atmosphere (see Fig. 2.4).

It is found that  $H = kT/Am_p g$  where  $k$  is the Boltzmann constant,  $T$  the temperature, and  $g$  the surface gravity. At the NS surface  $g \approx GM_{\text{NS}}/R_{\text{NS}}^2 \approx \frac{6.6 \times 10^{-8} \times 3 \times 10^{33}}{10^{12}} \text{cm s}^{-2} \approx 2 \times 10^{14} \text{cm s}^{-2}$ , and the typical scale-high is  $H \approx 0.5 A^{-1} \text{cm}$ .

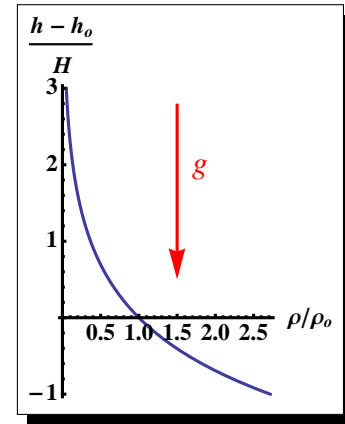


**Figure 2.4:** Density profile in an exponential atmosphere

The typical density at the photosphere can be estimated recalling that the photosphere is defined requiring its optical depth to be unity:  $n_e \sigma_T H = 1$ , where we have assumed the opacity to be due to Thompson scattering. This gives  $n_e = 3A \times 10^{24} \text{cm}^{-3}$  corresponding to  $\rho = 2.5 \frac{A}{Z} A g \text{cm}^{-3} \approx 5A g \text{cm}^{-3}$ . For a He-C atmosphere the density reaches values  $\sim 10^4 - 10^5 \text{g cm}^{-3}$  in less than one cm.

## 2.3 Degeneracy and Ionization

Matter at high density is properly described by the Fermi-Dirac statistics. The characteristic energy scale is the so called Fermi energy  $E_F$ , related to the Fermi momentum  $P_F$ . For electrons it is:

$$E_F = \begin{cases} \frac{P_F^2}{2m_e} = \left(\frac{\hbar^2}{2m_e}\right) (3\pi^2 n_e)^{2/3} & \text{if } E_F \ll m_e c^2 \\ cP_F = (\hbar c)(3\pi^2 n_e)^{1/3} & \text{if } E_F \gg m_e c^2 \end{cases} \quad (2.50)$$

The transition from the Non-Relativistic to the Relativistic regime takes place where:

$$(3\pi^2 n_e)^{1/3} \approx \left(\frac{2m_e c}{\hbar}\right) \Rightarrow n_e \approx \frac{1}{3\pi^2} \left(\frac{2m_e c}{\hbar}\right)^3 \approx 4.7 \times 10^{30} \text{ cm}^{-3} \quad (2.51)$$

$$\Rightarrow \rho \approx \frac{A}{Z} m_p n_e \approx 1.6 \times 10^7 \text{ g cm}^{-3} \quad (2.52)$$

One defines the Fermi temperature  $T_F$  as the temperature where thermal energy equals the Fermi energy:

$$kT_F = \begin{cases} \left(\frac{\hbar^2}{2m_e}\right) \left(\frac{3\pi^2 Z\rho}{Am_p}\right)^{2/3} = 2.6 \times 10^{-11} \rho^{2/3} & \text{if } \rho \ll 1.6 \times 10^7 \text{ g cm}^{-3} \\ (\hbar c) \left(\frac{3\pi^2 Z\rho}{Am_p}\right)^{1/3} = 6.5 \times 10^{-9} \rho^{1/3} & \text{if } \rho \gg 1.6 \times 10^7 \text{ g cm}^{-3} \end{cases} \quad (2.53)$$

or:

$$\left(\frac{kT_F}{1\text{keV}}\right) = \begin{cases} 1.6 \times 10^{-2} \left(\frac{\rho}{1\text{g cm}^{-3}}\right)^{2/3} \approx 1.6 \left(\frac{\rho}{10^3\text{g cm}^{-3}}\right)^{2/3} & \text{if } \rho \ll 1.6 \times 10^7 \text{ g cm}^{-3} \\ 4.1 \left(\frac{\rho}{1\text{g cm}^{-3}}\right)^{1/3} \approx 41 \left(\frac{\rho}{10^3\text{g cm}^{-3}}\right)^{1/3} & \text{if } \rho \gg 1.6 \times 10^7 \text{ g cm}^{-3} \end{cases} \quad (2.54)$$

It is immediately evident that electrons will always be degenerate, already in the NS outer layers at the base of the atmosphere. They will also rapidly become relativistic.

We can repeat the same arguments for the nuclei, just substituting  $n_e \rightarrow n_i$  and  $m_e \rightarrow Am_p$ . The transition from the relativistic to the non relativistic regime takes place at:

$$n_i \approx \frac{1}{3\pi^2} \left(\frac{2Am_p c}{\hbar}\right)^3 \Rightarrow \rho \approx \frac{Am_p}{3\pi^2} \left(\frac{2Am_p c}{\hbar}\right)^3 = 5 \times 10^{16} A^4 \text{ g cm}^{-3} \quad (2.55)$$

much larger than the typical average density of a NS. Nuclei, protons and neutrons will always be non relativistic inside NSs.

On the other hand the Fermi temperature of the nuclei is:

$$\left(\frac{kT_F}{1\text{keV}}\right) = 9 \times 10^{-4} A^{-5/3} \left(\frac{\rho}{10^3\text{g cm}^{-3}}\right)^{2/3} \Rightarrow 1.1 \times 10^{-6} \left(\frac{\rho}{10^3\text{g cm}^{-3}}\right)^{2/3} \text{ for Fe} \quad (2.56)$$

at the typical temperatures of the outer layers of NSs, degeneracy for the nuclei requires densities  $\approx 10^{12} \text{ g cm}^{-3}$ , far larger than the values in the outer crust. Nuclei can be dealt with as non degenerate thermal particles, obeying classical dynamics.

Interestingly at densities  $\approx 10^8 \text{ g cm}^{-3}$  the Fermi energy of electrons reaches a value of  $\approx 1.5 \text{ Mev}$  which corresponds to the mass difference between neutron and proton  $m_n - m_p = 1.3 \text{ Mev}$ . At such densities electrons have

enough energy for inverse  $\beta$  decay. The electron number is no longer a conserved quantity, and nuclei become progressively more neutron rich.

Because of degeneracy, at high densities electrons can behave as free particles even at small temperatures. One can compare the Coulomb interaction energy between electrons and nuclei, to the Fermi energy of electrons. Assuming that the typical electron-nucleus distance is  $\approx n_i^{-1/3}$ , the ratio of the Coulomb energy to the Fermi energy is:

$$\frac{E_C}{E_F} = \frac{Ze^2 n_i^{1/3}}{(3\pi^2 n_e)^{2/3}} \frac{2m_e}{\hbar^2} \approx 0.07Z \left( \frac{A\rho}{10^3 \text{g cm}^{-3}} \right)^{-1/3} \quad (2.57)$$

In the case of Fe, such ratio is equal to unity at  $\rho \approx 1 \times 10^2 \text{g cm}^{-3}$ . At  $\rho \approx 10^5 \text{g cm}^{-3}$  the ratio is already  $\sim 0.1$ , and saturates in the relativistic regime to  $\sim 0.01$ . This suggests that the Coulomb interaction with nuclei can be neglected to a first approximation.

At high density matter will behave as if it is fully ionized even if the thermal temperature is below the ionization threshold. The full ionization energy for a nucleus of charge  $Z$  is  $Z^2 e^2 / 2a_o$ . The Fermi energy of electrons will be equal to the full ionization energy when:

$$\left( \frac{\hbar^2}{2m_e} \right) (3\pi^2 n_e)^{2/3} = \frac{Z^2 e^2}{2a_o} \Rightarrow n_e^{-1/3} \simeq 3a_o Z^{-1} \quad (2.58)$$

This implies that the average distance between electrons becomes smaller than the typical size of the orbital of the last bound electron, which is just  $Z^{-1} a_o$ .

$$n_e^{-1/3} = \left( \frac{\rho}{Am_p} \right)^{-1/3} \simeq a_o Z^{-1} \Rightarrow \rho \simeq AZ^2 \frac{m_p}{a_o^3} \approx AZ^2 \text{g cm}^{-3} \quad (2.59)$$

corresponding to a density  $\rho \simeq 2 \times 10^4 \text{g cm}^{-3}$  for Fe.

## 2.4 Gas - Liquid - Solid

The above discussion makes clear that at the densities of interest between  $10^5$  and  $10^8 \text{g cm}^{-3}$ , the electrons form a fully degenerate Fermi gas, behaving as free particles. The nuclei on the other hand are fully ionized, and behaves as classical thermal particles.

The condition for nuclei to behave as a gas is that their thermal energy should exceed the energy of the mutual Coulomb interaction. Such energy is dominated by the closest neighbors, given that the background of free electrons shields the contribution from distant charges. Such a system is known as One Component Plasma (OCP).

For a nucleus of charge  $Z$ , the transition from the gas phase to condensed (liquid or solid) phase takes place when the internuclear distance  $d_o \approx 4\pi n_i^{-1/3} / 3$  is such that :

$$\frac{Z^2 e^2}{d_o} = kT \Rightarrow \left( \frac{Z^2 e^2}{kT} \right) \left( \frac{4\pi}{3} n_i \right)^{1/3} = \left( \frac{Z^2 e^2}{kT} \right) \left( \frac{4\pi}{3Am_p \rho} \right)^{1/3} = \Gamma_i = 1 \quad (2.60)$$

For  $\Gamma_i \ll 1$  one has a gas while for  $\Gamma_i \gg 1$  one has a solid. For Fe the transition takes place when:

$$\left(\frac{1\text{keV}}{kT}\right) \left(\frac{\rho}{10^3\text{g cm}^{-3}}\right)^{1/3} = 35 \quad (2.61)$$

which shows that the nuclei are always in a condensed phase.

Determining the transition from liquid to solid, the so called crystallization/melting threshold, is not as simple, because solids and liquids are both phases where the mutual Coulomb interaction energy of nuclei is bigger than the thermal energy, and in general of similar magnitudes. Such transition cannot be determined from simple analytical arguments based on orders of magnitude. There are however empirical criteria, based on experiments with alkali metals that can be used to a first approximation.

Theoretically, statistical models are used. From Montecarlo simulations of OCP it is found that the solid to liquid transition takes place for  $\Gamma_i \simeq 150$ . The Coulomb energy is about two orders of magnitude larger than the thermal energy. This implies that the amplitude of the thermal oscillations is about 1/10 of the average internuclear distance.

## 2.4.1 Modeling melting OCP

We describe here briefly the technique that is used to estimate the value  $\Gamma_i \simeq 150$ . The OCP is modelled as a set of nuclei of charge  $Z$  embedded into a neutralizing uniform electron background. Each nucleus has a potential energy that is given by the Coulomb interaction energy with the other nuclei and with the background. The electrostatic potential  $\Phi$  is computed according to:

$$\nabla^2\Phi(\mathbf{r}) = 4\pi\rho_c(\mathbf{r}) \quad \text{with} \quad \rho_c(\mathbf{r}) = Ze \left[ \sum_{j=1}^N \delta(\mathbf{r} - \mathbf{r}_j) - \frac{N}{V} \right] \quad (2.62)$$

where the sum is done over the  $N$  other nuclei at locations  $\mathbf{r}_j$ . It is found that only the nearest neighbors contribute to the energy, given the neutralizing background. It is possible to use a limited number of ions ( $N \simeq 200$  and imposing periodicity) to obtain converged results.

The Montecarlo technique consists in the following steps:

- One choses an initial distribution for the nuclei (for example a BCC lattice that minimizes the interaction energy, but one can even chose or a random one), and compute the initial potential energy of the entire set of nuclei.
- A random nucleus is displaced by a random amount and the energy of the new configuration is computed, (Fig. 2.5).
- If the energy is lower than the previous one, the configuration is accepted. If it is greater by an amount  $\Delta$  then it is accepted with probability  $e^{-\Delta/kT}$ . Otherwise it is rejected.
- The procedure is repeated and new configurations are obtained.

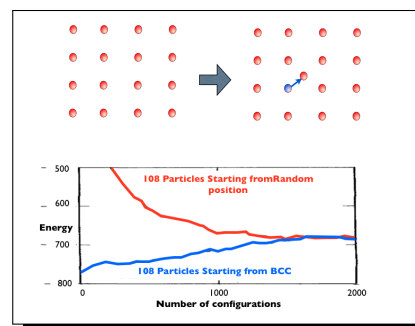


**Figure 2.5:** Displacement of a nucleus. Evolution toward equilibrium of the energy of the configurations for  $\Gamma_i = 10$

One can compute statistical quantities for each configuration, like the total potential energy, and in general one finds that, after an initial relaxation, the configurations settle into a regime where global quantities remain constant, independent of the initial configuration, as shown in Fig. 2.5. It means that the system has reached its thermodynamic equilibrium.

A quantity of interest is the mean displacement from the original position. If the conditions (the value of  $\Gamma_i$ ) imply a solid, one expects that the nuclei should settle to their final position and at most oscillate around them. The displacement should saturate to a finite value. For a liquid instead one expects the nuclei to keep moving around, and the displacement should increase indefinitely. The value of  $\Gamma_i$  at which this happens traces the transition from solid-crystal to liquid. It is found that this value is  $\Gamma_i \simeq 150$ .

Another quantity of interest is the distribution function of the nuclei, as a function of their separation. For gas this should be uniform, apart from a repulsive core at very short range, where electron shielding is ineffective. For a crystal at zero temperature, without thermal oscillations, this should be discrete, and different from 0 only for the separations characteristic of the lattice structure. A liquid is expected, to have an intermediate behavior, as shown in Fig. 2.6.

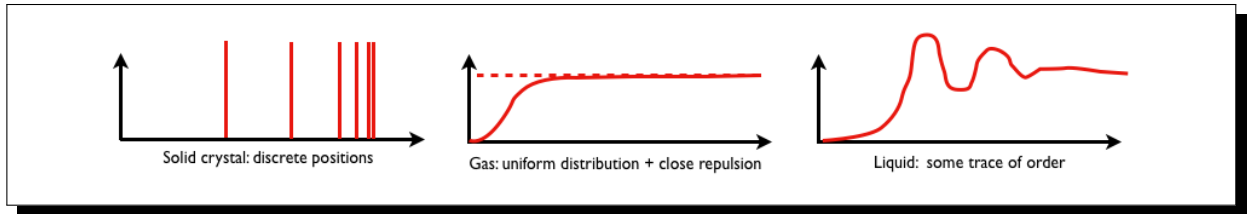


**Figure 2.6:** Nuclei distribution as a function of relative distance.

## 2.5 Phase Diagram of Outer Crust

The conditions in the outer crust of a NS can be summarized in the phase diagram shown in Fig. 2.7 where conditions of matter at high density and temperature is shown. The conditions in the outer crust correspond to densities in the range  $10^5$  to  $10^8$   $\text{g cm}^{-3}$ , and typical temperatures ranging from 0.1keV to about 1keV.

The pressure in the outer crust is provided almost completely by non relativistic degenerate electrons. Relativistic conditions are reached only at the highest density, when electron capture by inverse  $\beta$ -decay becomes important. At low density, below  $10^5$   $\text{g cm}^{-3}$ , Coulomb corrections become important. Coulomb attraction reduces the pressure with respect to the case of free electrons. At  $10^3$   $\text{g cm}^{-3}$  the pressure is about half the value for completely free degenerate electrons.

## 2.6 Neutronization and the Liquid Drop Model

At a density of  $\approx 10^8$   $\text{g cm}^{-3}$ , the Fermi energy of electrons exceeds the mass difference between neutron and proton, and electron capture is possible. In practice electron capture becomes a relevant process already at densities of  $\sim 10^7$   $\text{g cm}^{-3}$ , because the relevant energy threshold is that for inverse  $\beta$ -decay of  $^{56}\text{Fe}$ .

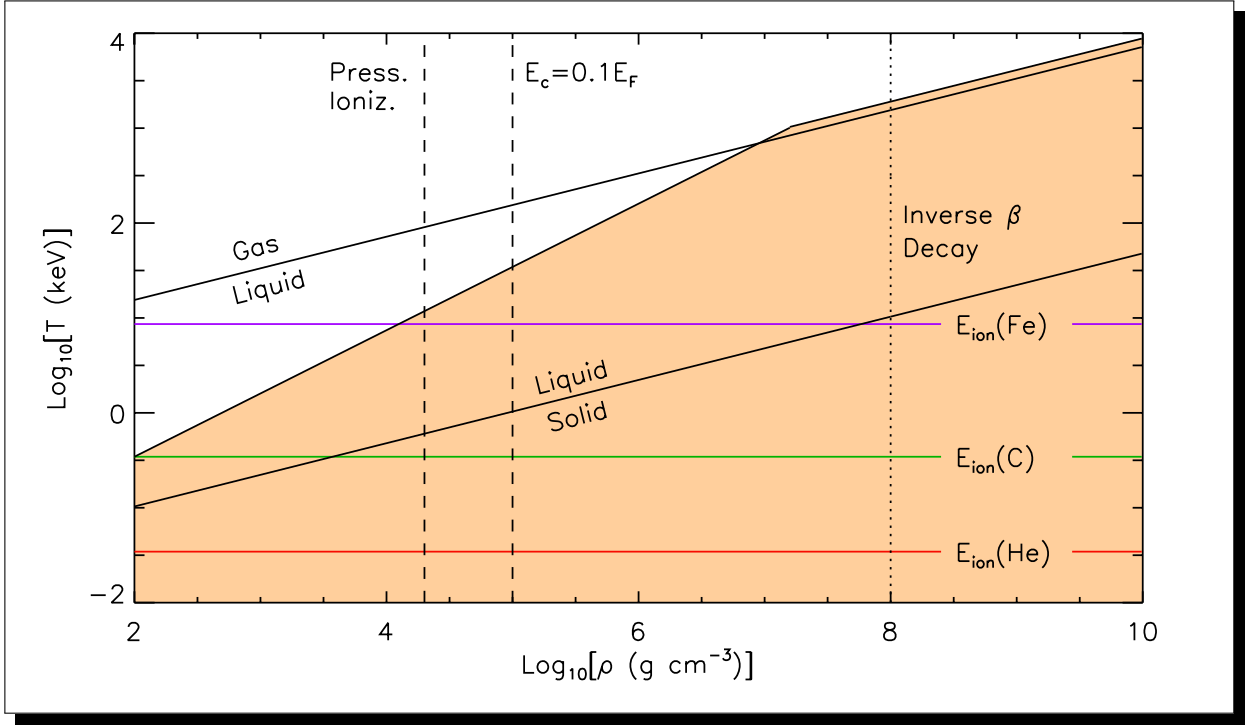


**Figure 2.7:** Phase diagram of matter at high densities and temperatures typical of the outer layers of the crust of a NS. In orange shaded area electrons are degenerate.  $E_{\text{ion}}$  are the thermal full ionization energies. Dashed vertical lines define the density threshold for pressure ionization of where the Coulomb energy is only 0.1 of the kinetic energy of electrons. The dotted vertical line is the density limit for inverse  $\beta$ -decay. The solid lines indicate the transition from gas to liquid to solid, for the ions in the crust.

To study how neutronization proceeds at densities above  $\sim 10^7 \text{ g cm}^{-3}$  one needs a model telling how the energy of the nuclei depends on the number of neutrons and protons. The simplest of such model is the so called *Liquid Drop Model*, where the nuclear energy is given by the *semi-empirical mass formula*. A nucleus of atomic number  $A$  and proton number  $Z$ , has a total energy given by:

$$E_{\text{nuc}} = m_n(A - Z)c^2 + m_p c^2 Z + E_b + E_c + E_s \quad (2.63)$$

where  $m_n$  is the neutron mass,  $m_p$  the proton mass,  $E_b$  the nuclear droplet energy,  $E_c$  the Coulomb electrostatic energy, and  $E_s$  the Symmetry energy. In the Liquid Drop Model, the nucleus is treated as a uniform sphere of size  $R_n = A^{1/3} r_o$ , where  $r_o$  is the typical nucleon size  $r_o \approx 10^{-16} \text{ cm} = 0.1 \text{ fm}$ . The Coulomb energy, can be simply estimated to be equal to the electrostatic energy of a uniformly charged sphere of charge  $Ze$ , and radius equal to  $R_n$ ;

$$E_c = 4\pi \int_0^{R_n} \frac{3Ze}{4\pi R_n^3} \frac{Zer^3}{R_n^3} r^2 dr = \frac{3}{5} \frac{Z^2 e^2}{r_o} A^{-1/3} = \mathcal{E}_c Z^2 A^{-1/3} \approx 0.7 Z^2 A^{-1/3} \text{ MeV} \quad (2.64)$$

The symmetry energy, is what tends to favor an equal number of protons and neutrons in normal nuclei and is given by:

$$E_s = \mathcal{E}_s A \left(1 - 2\frac{Z}{A}\right)^2 \approx 24A \left(1 - 2\frac{Z}{A}\right)^2 \text{ MeV} \quad (2.65)$$

The droplet energy itself can be decomposed into a volume and surface term:

$$E_b = \mathcal{E}_v A + \mathcal{E}_\sigma A^{2/3} \approx 34A + 12A^{2/3} \text{ MeV} \quad (2.66)$$

At a given density  $\rho$  the energy density associated to the nuclei will be:

$$u_n = \frac{\rho}{Am_u} E_{\text{nuc}} \quad (2.67)$$

where  $m_u \approx m_p \approx m_n$  is the mean nucleon mass. At that same density the energy density associated with the fully degenerate electrons will be:

$$u_e = \frac{Z\rho}{Am_u} E_F \quad (2.68)$$

such that the total energy will be

$$u_t = \frac{\rho}{m_u} \left( m_n c^2 + Y_p (m_p - m_n) c^2 + \mathcal{E}_v + \mathcal{E}_\sigma A^{-1/3} + \mathcal{E}_c Y_p^2 A^{2/3} + \mathcal{E}_s \left( 1 - 2\frac{Z}{A} \right)^2 + Y_p E_F \right) \quad (2.69)$$

where  $Y_p = Z/A$  is the proton fraction. The equilibrium nucleus  $(A, Z)$  is obtained minimizing this energy at a fixed density. Notice that the density enters only through the electron Fermi energy  $E_F$ .

The minimization proceeds in two steps. First one minimizes with respect to  $A$ , at constat  $Y_p$ . In this case one obtain the following condition;

$$\mathcal{E}_\sigma A^{-4/3} = 2\mathcal{E}_c Y_p^2 A^{-1/3} \quad \Rightarrow \quad A = \frac{\mathcal{E}_\sigma}{2\mathcal{E}_c Y_p^2} \approx \frac{12}{Y_p^2} \quad (2.70)$$

This step corresponds to a minimization with respect to the strong interaction, that fixes the total nucleon number in nuclei. It means that, having to chose between many light nuclei or a few massive ones (keeping the density fixed) the favored nuclei are those that have minimal energy. It is interesting to compare this result with the criterion for spontaneous fission. A nucleus will undergo spontaneous fission if its total energy is bigger that the total energy of two separate nuclei having each half of the nucleon of the original one. Obviously the volume term  $\propto A$  is the same for both configurations (and similarly the Symmetry term), while the surface and Coulomb term change. The condition for fission is then:

$$\mathcal{E}_\sigma A^{2/3} + \mathcal{E}_c Y_p^2 A^{5/3} \geq 2(\mathcal{E}_\sigma (A/2)^{2/3} + \mathcal{E}_c Y_p^2 (A/2)^{5/3}) \quad \Rightarrow \quad A \geq 0.7 \frac{\mathcal{E}_\sigma}{\mathcal{E}_c Y_p^2} \approx \frac{17}{Y_p^2} \quad (2.71)$$

and one sees that nuclei satisfying Eq. 2.70, are always stable for spontaneous fission.

The second step corresponds to a minimization with respect to  $Y_p$  at fixed  $A$ . This represents a minimization with respect to the weak interaction that is responsible for the exchange of protons into neutrons. Changing  $Y_p$  at fixed density means that a proton is exchanged into a neutron and viceversa; which obviously keeps  $A$  constant. If one substitutes the result of Eq. 2.70 then:

$$(m_p - m_n) c^2 + E_F - 4\mathcal{E}_s(1 - 2Y_p) + (2\mathcal{E}_\sigma^2 \mathcal{E}_c)^{1/3} Y_p^{-1/3} = 0 \quad (2.72)$$

Note that the above condition can be written in term of the so called chemical potentials:

$$\mu_p + \mu_e = \mu_n \quad (2.73)$$

where, using Eq. 2.69:

$$\begin{aligned} \mu_p &= \frac{\partial u_t}{\partial n_p} = m_p c^2 + \mathcal{E}_v - \mathcal{E}_s(1 - 2Y_p)(3 - 2Y_p) + (2\mathcal{E}_\sigma^2 \mathcal{E}_c)^{1/3} Y_p^{2/3} \left( \frac{1}{2} + \frac{1}{Y_p} \right) \\ \mu_n &= \frac{\partial u_t}{\partial n_n} = m_n c^2 + \mathcal{E}_v + \mathcal{E}_s(1 - 4Y_p^2) + \frac{1}{2} (2\mathcal{E}_\sigma^2 \mathcal{E}_c)^{1/3} Y_p^{2/3} \\ \mu_e &= \frac{\partial u_t}{\partial n_e} = E_F \end{aligned} \quad (2.74)$$

The minimum condition, implies that the chemical potentials must be in equilibrium. The chemical potentials represent the amount of energy necessary to increase by one the number respectively of free electrons, protons and neutrons in the nuclei. It must cost the same energy to add a neutron or a couple electron-proton to the system.

Eq. 2.72 establishes a relation between the density, that enters the electron Fermi energy according to Eq.2.50, and the nuclear proton fraction. The results of Eqs.2.70-2.72 are shown in Fig. 2.8.

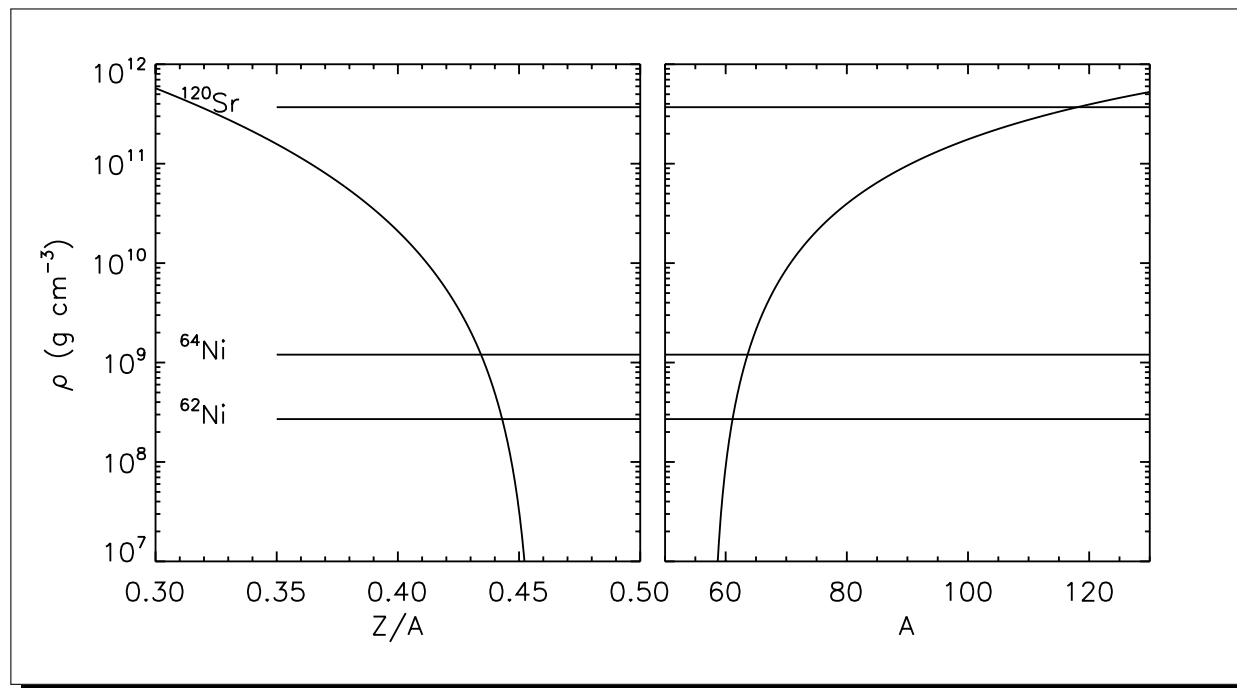


**Figure 2.8:** Evolution of the proton fraction  $Z/A$  and the atomic number  $A$  as a function of density. Typical nuclei are shown for densities  $\sim 10^8 - 10^9 \text{ g cm}^{-3}$ , and then for density  $\sim 4 \times 10^{11} \text{ g cm}^{-3}$ . At intermediate value the existence of magic number alters the behavior of the curves.

Note that for simplicity one can assume that the electron Fermi energy is always given by the formula derived using  $Z/A \approx 0.5$ . This is not strictly true, however the Fermi energy scales as  $(Z/A)^{1/3}$ , and in the range of interest this effect is marginal.

More important is the fact that the semi-empirical mass formula, does not correctly reproduce the binding energy of nuclei. It is well known that there are nuclear configurations characterized by so called *magic numbers* of neutrons/protons, that are particularly stable. This is due to *shell effects* of the nucleon interaction inside nuclei. Of particular importance for NS are the magic number 50 and 80. Indeed while the model we presented correctly describes the neutronization (change in  $Y_p$ ), it fails to properly recover the correct nuclei (correct  $A$ ) in the density range  $10^9 - 10^{11} \text{ g cm}^{-3}$ , exactly because at those densities nuclei are found with the neutron magic number 50 and 80.

## 2.7 Neutron Drip

At density  $\rho \sim 4 \times 10^{11} \text{ g cm}^{-3}$ , the chemical potential of the neutrons satisfy:

$$\mu_n = \frac{\partial u_t}{\partial n_n} = m_n c^2 + \mathcal{E}_v + \mathcal{E}_s(1 - 4Y_p^2) + \frac{1}{2}(2\mathcal{E}_\sigma^2 \mathcal{E}_c)^{1/3} Y_p^{2/3} = 940 \text{ Mev} \approx m_n c^2 \quad (2.75)$$

Above this density it becomes energetically favorable to add an extra neutron as a free one, outside the nuclei, instead of adding it to a nucleus. This conditions, and the related density, are known as *neutron drip*. Physically speaking this corresponds to a phase transition: the matter ceases to be formed by nuclei surrounded by free degenerate electrons, and free degenerate neutrons appear. However the pressure support at this point is still due to the free relativistic degenerate electrons. Further increasing the density, however, leads to an increase in the number of free neutrons, that do not contribute much to the pressure. The electron pressure as a consequence does not rise as much.

The neutron drip is considered the point where the crust begin to *dissolve* into the core which as we will see is mostly formed by unbound nucleons. The density at neutron drip is about  $10^{-3}$ , of the nuclear density. This means that the average separation of nuclei is about ten times their size.

At the neutron drip  $Z/A \sim 0.3$  and this implies that the electron pressure is about  $(0.3/0.5)^{4/3} \sim 0.5$  of what one would have naively obtained, extrapolating the behavior of degenerate electrons for Iron nuclei, that we derived in the previous chapter.

## 2.8 Above Neutron Drip

The model developed previously to describe neutronization, can be easily extended to take into account the presence of free neutrons beyond neutron drip. The total energy now will have to include the energy of the free neutrons, which we can to first order describe as a fully degenerate, non relativistic fermion gas (relativity will set in at densities above  $10^{16}$  g cm $^{-3}$ ). Recalling that now the density includes the contribution from free neutrons:

$$\begin{aligned} u_N &= \frac{\rho(1 - Y_n)}{Am_u} E_{\text{nuc}} \\ u_e &= \frac{Z(1 - Y_n)\rho}{Am_u} E_F \\ u_n &= \frac{Y_n\rho}{m_u} E_n \end{aligned} \tag{2.76}$$

$$u_t = \frac{\rho(1 - Y_n)}{m_u} \left( m_n c^2 + Y_p(m_p - m_n)c^2 + \mathcal{E}_v + \mathcal{E}_\sigma A^{-1/3} + \mathcal{E}_c Y_p^2 A^{2/3} + \mathcal{E}_s \left( 1 - 2\frac{Z}{A} \right)^2 + Y_p E_F + \frac{Y_n}{1 - Y_n} E_n \right) \tag{2.77}$$

where with  $Y_n$  we have indicated the fraction of free neutrons with respect to bound nucleons and  $E_n$  is their energy. At this point one proceeds as before, except that now one need to minimize also with respect to  $Y_n$ . The first step is a minimization with respect to  $A$  at fixed  $Y_p$  and  $Y_n$ . This has the same meaning as discussed previously, of selecting the most stable nucleus. The result is the same as before:

$$\mathcal{E}_\sigma A^{-4/3} = 2\mathcal{E}_c Y_p^2 A^{-1/3} \quad \Rightarrow \quad A = \frac{\mathcal{E}_\sigma}{2\mathcal{E}_c Y_p^2} \approx \frac{12}{Y_p^2} \tag{2.78}$$

implying that even above neutron drip nuclei are still stable against spontaneous fission. Note that the presence of free neutrons does not affect, in this simple model, the stability of the nuclei.

Then one minimizes with respect to  $Y_p$  at fixed  $A$  and  $Y_n$ . One recovers the equilibrium conditions for the chemical potentials, which again is the same as before:

$$\mu_e + \mu_p = \mu_n^{(N)} \quad (2.79)$$

where the superscript ( $N$ ) implies that those neutrons are inside nuclei. This again relates to a process where a proton is exchanged for a neutron inside a nucleus. The result is again independent from the presence of free neutrons.

And finally one minimizes with respect to  $Y_n$  at fixed  $Y_p$ . Note that if one keeps the density constant, one cannot change  $Y_n$  without affecting also  $A$ . Infact one has  $dA \propto -dY_n$ . This process in fact relates to the exchange of a neutron between the nuclei and the outer gas, and obviously, a change in one correspond to an opposite change in the other. What remains fixed in the process is actually the number of protons and of electrons. This is equivalent to the statement that it costs the same energy to add a neutron to the nucleus or to add it as a free one. The energy necessary to add a neutron to a nucleus at fixed  $Z$  is:

$$\left. \frac{dE_{\text{nuc}}}{dA} \right|_Z = m_n c^2 + \mathcal{E}_v + \frac{2\mathcal{E}_\sigma}{3A^{1/3}} - \frac{\mathcal{E}_c Z^2}{A^{4/3}} + \mathcal{E}_s \left(1 - 4\frac{Z^2}{A^2}\right) = E_N \quad (2.80)$$

The quantity  $E_N - m_n c^2$  is nothing else than the Fermi energy for degenerate neutrons.

Now:

$$E_F = \hbar c (3\pi^2)^{1/3} \frac{\rho(1 - Y_n)Y_p}{m_u} \quad (2.81)$$

$$E_n = m_n c^2 + \frac{\hbar^2}{2m_n} (3\pi^2)^{2/3} \frac{\rho Y_n}{m_u} \quad (2.82)$$

such that the equilibrium conditions become:

$$(m_p - m_n)c^2 - 4\mathcal{E}_s(1 - 2Y_p) + (2\mathcal{E}_\sigma^2 \mathcal{E}_c)^{1/3} Y_p^{-1/3} = -\hbar c (3\pi^2)^{1/3} \left( \frac{\rho(1 - Y_n)Y_p}{m_u} \right)^{1/3} \quad (2.83)$$

$$\mathcal{E}_v + \frac{1}{3} \left( \frac{\mathcal{E}_\sigma^2 \mathcal{E}_c}{4} \right)^{1/3} Y_p^{2/3} + \mathcal{E}_s (1 - 4Y_p^2) = \frac{\hbar^2}{2m_n} (3\pi^2)^{2/3} \left( \frac{\rho Y_n}{m_u} \right)^{2/3} \quad (2.84)$$

The results are show in Fig. 2.9.

The free neutrons contribute to the density, and they also contribute to the pressure, so that the total pressure will be:

$$P = P_e + P_n = \left(\frac{c}{4}\right) (3\pi^2 \hbar^3)^{1/3} \left[ \frac{\rho}{m_u} Y_p (1 - Y_n) \right]^{4/3} + \left(\frac{1}{5m}\right) (3\pi^2 \hbar^3)^{2/3} \left[ \frac{\rho}{m_u} Y_n \right]^{5/3} \quad (2.85)$$

In Fig. 2.10 the pressure is shown as a function of the density. At a density of  $\sim 4 \times 10^{12} \text{ g cm}^{-3}$ , the free neutrons contribute about one half of the density and one half of the pressure. From this point on the nuclei and free electrons will be less and less important and to a good approximation matter will behave as a system of degenerate nucleons and electrons, with neutrons providing most of the density and pressure support. Note moreover that just beyond neutron drip, the total pressure rises much less with density than the  $n^{4/3}$  behaviour of the degenerate electron just before it. The reason being that the increase in density is mostly associated with the appearance of free degenerate neutrons, that do not contribute to the total pressure. The pressure will begin to rise as  $n^{5/3}$ , after  $\rho \sim 5 \times 10^{12} \text{ g cm}^{-3}$ , once the free degenerate neutrons become the dominant contributor.

In Fig. 2.10 we show how pressure changes as a function of density above neutron drip, and the contribution from electrons and neutrons separately. Immediately after the neutron drip the adiabatic coefficient drops from  $4/3$  typical of electron dominated pressure, to  $\sim 0.5$ , to rise again to  $5/3$  once neutrons become dominant.

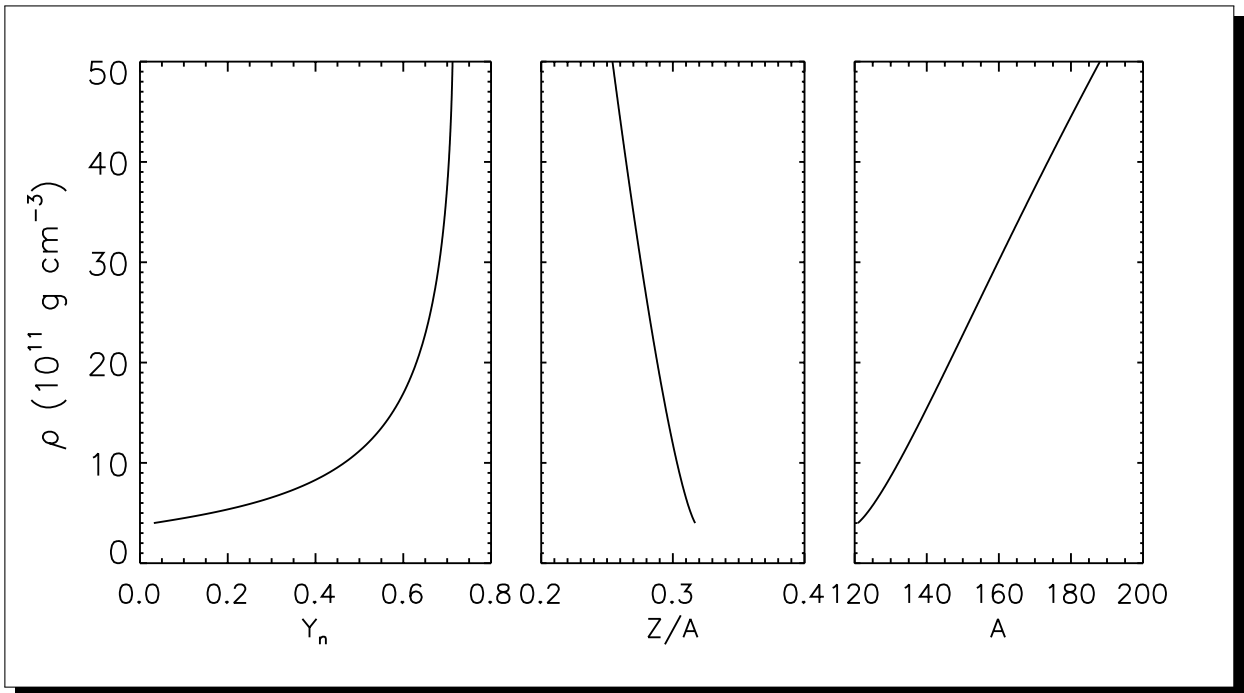


**Figure 2.9:** Evolution of the free neutron fraction  $Y_n$ , the proton fraction  $Z/A$  in atoms, and the atomic number  $A$  as a function of density, above neutron drip.

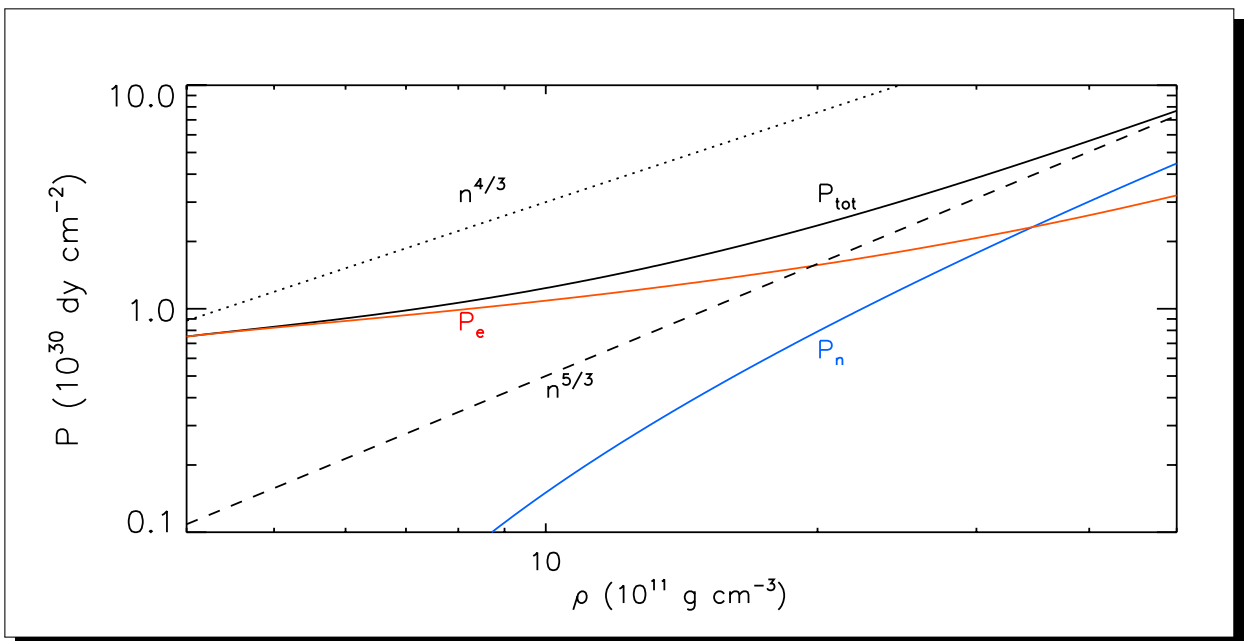


**Figure 2.10:** Pressure as a function of density above neutron drip. Solid dark line is the total pressure, the red line if the electron contribution, and the blue line the one from the free neutrons.

### 2.8.1 Corrections

The model we presented above is extremely simplified. While, apart from nuclear shell effects, it is quite accurate below neutron drip, above that density, there are several effects that our model does not take into account, and that become progressively stronger as the nuclear density  $\rho_{nuc} \sim 2 \times 10^{14} \text{ g cm}^{-3}$  is approached.

- given that  $Y_p$  keeps dropping (till it gets to value  $\sim 0.1$ ) one needs to take this into account in the definition of the electron Fermi energy.
- one needs to correct the energy associated to the free neutrons. First the available volume for free neutrons must be reduced by the volume occupied by the nuclei. This is only about  $10^{-3}$  at neutron drip but reaches value of order unity close to nuclear density. Second the neutrons cannot be treated as free particles all the way to nuclear density. The strong interaction has an attractive character that will begin to affect neutrons once their typical distance is  $\sim 0.1 \text{ fm}$ . This means that their energy rises slightly less than for the completely free case.
- the energy of the nuclei cannot be described by the same semi-empirical mass formula, that is used for normal nuclei surrounded by a *vacuum*. First the Coulomb energy, which was originally derived taking into account only the mutual interaction of protons belonging to the same nucleus, must be corrected to include now the electrostatic interaction with nearby nuclei (a lattice correction), as well as the fact that for large nuclei, electron penetration tends to reduce the electrostatic energy.

$$E_c = \frac{3}{5} \frac{Z^2 e^2}{r_o} A^{-1/3} - \frac{9}{10} \frac{Z^2 e^2}{r_o} \left[ \frac{\rho}{\rho_n} \right]^{1/3} \left( 1 - \frac{5}{9} \left[ \frac{\rho}{\rho_n} \right]^{2/3} \right) \quad (2.86)$$

Second the surface energy must also be corrected for the presence of free neutrons outside. Free neutrons reduce the surface energy. One expects that as the density of nucleons outside reaches the same value of the density of nucleons inside the nuclei, the concept of a surface ceases to have a meaning. So the surface energy should vanish when the neutron density outside reaches the same value as the one inside the nuclei. Third the nuclei themselves cannot be considered as hard spheres, whose size grows proportional to  $A^{1/3}$ . The presence of free neutrons outside will exert a pressure on the nuclei, and their volume will be compressed with respect to a case in vacuum. Such compression will alter the nuclear binding energy. Fourth, as the nuclei become progressively more neutron rich, the values of the various coefficients in the semiempirical mass formula will not be accurate any longer, and one will have to resort to better models for the energy of nuclear matter, that take into account also how it depends on  $Y_p$ .

## 2.9 The Core

We saw that starting from a density  $\rho \sim 5 \times 10^{12} \text{ g cm}^{-3}$  the mass and pressure are dominated by the free neutron gas. The average distance of nuclei is just four times their size. Once nuclear densities are reached one expects that the nuclei will dissolve into a uniform background of neutrons protons and electrons. To a first approximation one could think of treating such system as composed by a fermi gas of fully degenerate protons neutrons and electrons, recalling that at the typical nuclear density neutrons and protons are still sub-relativistic. Such simplified models can be used to get an idea of the possible behavior of nuclear matter, but it is well known that it gives wrong quantitative results.

One can get a much better understanding of the physical conditions, starting from the liquid drop model for nuclei. Once nuclei are fully dissolved into a uniform fluid of nucleons and electrons the energy density will be:

$$u_t = \frac{\rho}{m_u} \left( m_n c^2 + X_p (m_p - m_n) c^2 + \mathcal{E}_v + \mathcal{E}_s (1 - 2X_p)^2 + X_p E_F \right) \quad (2.87)$$

where the main difference with respect to Eq. 2.69 is that now there is no surface term, given that we are dealing with a uniform fluid, and no Coulomb term because the uniform distribution of protons and electrons implies charge neutrality. Now  $X_p$  is the total proton fraction. At density  $\rho \sim 5 \times 10^{12} \text{ g cm}^{-3}$ , the total proton fraction is  $X_p = (1 - Y_n)Y_p \approx 0.06$ . Differentiating with respect to  $X_p$  at fixed density one find the chemical equilibrium condition:

$$(m_n - m_p)c^2 + 4\mathcal{E}_s(1 - 2X_p) = E_F = \hbar c(3\pi^2)^{1/3} \frac{\rho X_p}{m_u} \quad (2.88)$$

which can be solved for  $X_p$ . At density close to the nuclear density  $\rho \approx 2 \times 10^{14} \text{ g cm}^{-3}$ , one finds  $X_p \approx 0.03$ . In general the coefficient in Eq. 2.69 are themselves a function of the density. For example  $\mathcal{E}_s$  is known to increase above nuclear density. As a consequence above nuclear density the proton fraction increases again, and it can be as much as twice bigger around  $\rho \approx 5 \times 10^{14} \text{ g cm}^{-3}$ .

Modeling the nucleon fluid as a systems of free degenerate fermions (which as we remarked before is not correct), in the limit of very high density, when also baryons become relativistic, one has:

$$\mu_n = (\hbar c)(3\pi^2 n_n)^{1/3} = (\hbar c)(3\pi^2 n_e)^{1/3} + (\hbar c)(3\pi^2 n_p)^{1/3} = \mu_e + \mu_p \quad \Rightarrow \quad n_n^{1/3} = 2n_p^{1/3} \quad (2.89)$$

The solution provides the asymptotic value for the proton fraction:  $n_p/n_n = 1/8 \Rightarrow X_p = 0.1$  that is the reason why these objects are often assumed to be formed almost exclusively by neutrons. These small proton fractions are very important because they guarantee the presence inside the NS of charged particles that can carry currents, and support the presence of a magnetic field.

However as shown in Chapter 3.2 a NS cannot be described as a system of free fermions, because they fail to reproduce the correct masses. The reason is that at and above nuclear density, nucleons cannot be treated as free. The strong interaction has a hard repulsive core, whose effect becomes important once the typical nucleon density becomes  $\sim 4 \times 10^{14} \text{ g cm}^{-3}$ . This causes a stiffening of the pressure, that rises more rapidly with density than in the free case.

A very simple model of the effect of the hard core of nuclear interaction can be obtained using a model based on Yukawa potentials.

The hard core is modelled using a potential of the form:

$$V(r) = g \frac{e^{-kr}}{r} \quad (2.90)$$

the effect of this potential on the total energy of the nucleon gas can be estimated as follows. The total energy will be the sum of the kinetic term and the potential term. The potential term of the fluid is just the sum of the potential energy for each pair of nucleons. If the baryons are treated as a uniform fluid with density  $n$ , for a single nucleon the interaction energy will be given by the integral of the potential energy over the rest of the baryon fluid:

$$4\pi \int_{\mathcal{V}} n g \frac{E e^{-kr}}{r} r^2 dr = \frac{4\pi g}{k^2} n = \propto n \quad (2.91)$$

so that the total potential energy density will be  $4\pi gn^2/k^2$ . The total energy will then be:

$$E = \frac{\hbar^2}{2m_u} (3\pi^2)^{2/3} n^{5/3} + \frac{4\pi g}{k^2} n^2 \quad (2.92)$$

Where we have assumed non relativistic degenerate nucleons. The value of  $g$  and  $k$  depend on the properties of the repulsive core. The pressure of the baryon fluid can be obtained recalling that at zero temperature  $dE = PdV \Rightarrow P = n(\partial E/\partial n)$ , leading to:

$$P \approx \frac{(3\pi^2 \hbar^3)^{2/3}}{m_u} n^{5/3} + \frac{4\pi g}{k^2} n^2 \quad (2.93)$$

which shows that as the density increases the term due to the potential becomes progressively more important and the adiabatic index goes to 2. This stiffening of the Equation of State leads to masses in excess of  $1.4M_\odot$ .

### 2.9.1 Higher densities

As we saw in the previous discussion, as the density increase it becomes energetically favorable for the system to include states/particles, that in normal conditions would be unstable. This happens first for neutron rich nuclei, that can exist for densities above  $\sim 10^8 \text{ g cm}^{-3}$ , and that would be normally unstable for beta decay. Then above  $4 \times 10^{11} \text{ g cm}^{-3}$ , also free neutrons can exist. One immediately sees that as the chemical potentials of the various component increase, it becomes possible to have particles that in normal conditions would decay in those constituents. The spontaneous decay relation  $X + Y \rightarrow Z$  implies that the system will contain particle  $Z$  if the chemical potentials satisfy  $\mu_X + \mu_Y = \mu_Z \approx m_Z$ . For example at densities of the order of  $3 \times 10^{14} \text{ g cm}^{-3}$ , the electron chemical potential (its Fermi energy) reaches  $\approx 105 \text{ MeV}$ , which is comparable to the mass of the muon, so that muons will start to appear. This is the reason why the physics of such very high super-nuclear density is so complex, because many different new particles can appear depending on the how the chemical potentials behave.



# CHAPTER 3

---

## POLYTROPIC MODELS FOR NEUTRON STARS

---

Here we present simple polytropic models both for classical and general relativistic configurations. We will show the existence of a maximum mass, and discuss how observations of Neutron Stars, can constrain the mass-radius relationship.

### 3.1 Lane-Emden Equation and the Classical Polytropic Model

For a degenerate system, the pressure is just a function of the density. The equation of state in this case is said to be barotropic. Among all barotropic cases, a polytropic equation of state is such that the pressure  $p$  is related to the density as  $p = K\rho^\gamma$ , where  $\gamma$  is known as the adiabatic index. In this case the equation describing the self-gravitating hydrostatic equilibrium for a non-rotating system can be cast into a simplified form, that allows self-similar solutions.

Assuming an equation of state in the form  $p = K\rho^{1+1/n}$  [corresponding to  $n = 1/(\gamma - 1)$ ], the hydrostatic equilibrium condition reads:

$$\frac{\partial p(r)}{\partial r} = -\frac{GM(r)\rho(r)}{r^2} \Rightarrow K\rho(r)^{1/n} \frac{n+1}{n} \frac{\partial \rho(r)}{\partial r} = -\frac{GM(r)\rho(r)}{r^2}. \quad (3.1)$$

The mass equation is:

$$M(r) = 4\pi \int_0^r \rho(r')r'^2 dr' \Rightarrow \frac{\partial M(r)}{\partial r} = 4\pi\rho(r)r^2. \quad (3.2)$$

Further differentiating Eq.3.1 one gets:

$$4\pi G\rho(r) = \frac{K}{r^2} \frac{\partial}{\partial r} \left( r^2 \rho(r)^{(1-n)/n} \frac{n+1}{n} \frac{\partial \rho(r)}{\partial r} \right) \quad (3.3)$$

We introduce the following variable  $\theta$  such that  $\rho = \rho_c \theta^n$ , then:

$$-4\pi G\rho_c \theta^n = \frac{K\rho_c^{1/n}}{r^2} \frac{\partial}{\partial r} \left( r^2 \theta^{(1-n)} (n+1) \theta^{(n-1)} \frac{\partial \theta}{\partial r} \right) = \frac{K\rho_c^{1/n}}{r^2} \frac{\partial}{\partial r} \left( r^2 (n+1) \frac{\partial \theta}{\partial r} \right) \quad (3.4)$$

with the substitution  $\xi = ar$  with  $a^2 = (n+1)K\rho_c^{1/n-1}/(4\pi G)$  the equation can be cast in adimensional form:

$$-\frac{4\pi Ga^2}{(n+1)K\rho_c^{1/n-1}}\theta^n = \frac{1}{r^2} \frac{\partial}{\partial r} \left( r^2 \frac{\partial \theta}{\partial r} \right) \Rightarrow -\theta^n = \frac{1}{\xi^2} \frac{\partial}{\partial \xi} \left( \xi^2 \frac{\partial \theta}{\partial \xi} \right) \quad (3.5)$$

This is known as *Lane-Emden Equation*. It is a second order differential equation, and must be solved subject to the following boundary conditions at the center  $\theta(\xi = 0) = 1$  and  $\partial_\xi \theta(\xi = 0) = 0$ . The first condition uses the freedom of scale, and the second condition follows from symmetry with respect to  $r = 0$ , so that  $\partial_r p = 0$  at  $r = 0$ . The solutions for non relativistic degenerate fermions  $n = 1.5$  ( $\gamma = 5/3$ ) and for relativistic degenerate fermions  $n = 3$  ( $\gamma = 4/3$ ) are shown in Fig. 3.1. The point where  $\theta = 0$  is the stellar radius  $R$ . One finds:

$$R = \begin{cases} 3.6 \left( \frac{2.5K\rho_c^{-1/3}}{4\pi G} \right)^{1/2} & \text{for } \gamma = 5/3 \\ 6.8 \left( \frac{4K\rho_c^{-2/3}}{4\pi G} \right)^{1/2} & \text{for } \gamma = 4/3 \end{cases} \quad (3.6)$$

Note that the higher the central density the smaller the stellar radius.

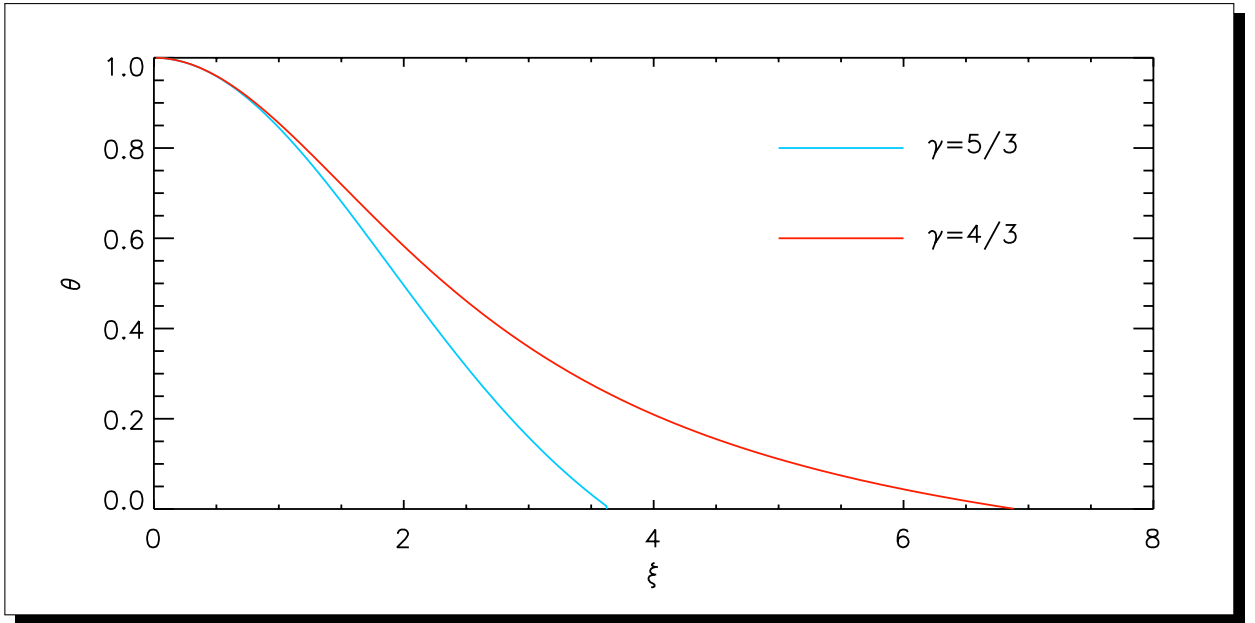


**Figure 3.1:** Solutions of the Lane-Emden Equation for a system of fully degenerate fermions, both in the relativistic and non-relativistic regime.

### 3.1.1 Chandrasekhar Mass

In the same way it is possible to derive the stellar mass. One has:

$$M(r) = 4\pi \int_0^r \rho(r') r'^2 dr' \Rightarrow M(\xi) = 4\pi \int_0^\xi \rho_c a^3 \theta(\xi')^n \xi'^2 d\xi' \quad (3.7)$$

recalling Eq.3.5 one has:

$$M(\xi) = -4\pi \int_0^\xi \rho_c a^{3/2} \frac{\partial}{\partial \xi} \left( \xi^2 \frac{\partial \theta}{\partial \xi} \right) d\xi' \Rightarrow M(\xi) = -4\pi \left[ \frac{(n+1)K}{4\pi G} \right]^{3/2} \rho_c^{(3-n)/(2n)} \xi^2 \frac{\partial \theta}{\partial \xi} \quad (3.8)$$

The stellar mass is given by taking the value of  $\xi$  and the derivative of  $\theta$  at the surface.

$$M = \begin{cases} 10.8\pi \left[ \frac{5K}{8\pi G} \right]^{3/2} \rho_c^{1/2} & \text{for } \gamma = 5/3 \\ 7.6\pi \left[ \frac{K}{\pi G} \right]^{3/2} & \text{for } \gamma = 4/3 \end{cases} \quad (3.9)$$

Note two important properties:

- for  $\gamma = 5/3$  the stellar mass and radius are related as  $R \propto M^{-1/3}$ . More massive stars have smaller radii. This implies that as the total mass increases so does the central density.

$$R = 5 \left[ \frac{K}{G} \right] \pi^{-2/3} M^{-1/3} \quad (3.10)$$

- when the density reaches the value where the degenerate particles become relativistic the mass saturates to a finite value, independent of its radius. Such value is known as the *Chandrasekhar Mass*  $M_{ch}$ . There are no solutions with higher mass, so this must be considered as an upper limit for degenerate stars.

For WDs with typical densities of the order of  $\rho_c \sim 10^5 \text{ g cm}^{-3}$ , electrons are in the non relativistic limit (which is reached at densities  $\sim 10^{6-7} \text{ g cm}^{-3}$ ), and the mass radius relation reads:

$$\frac{R}{R_\odot} = 0.0012 \left( \frac{M}{M_\odot} \right)^{-1/3} \Rightarrow R \approx 1000 \text{ km} \quad (3.11)$$

where we have assumed 2 baryons per electron. While the Chandrasekhar Mass derived in the relativistic limit is:

$$M_{ch} = 1.38 M_\odot \quad (3.12)$$

If one considers a NS, with central density of the order of, or slightly above, nuclear density  $\rho_c \sim 10^{15} \text{ g cm}^{-3}$ , then one finds that the pressure support is due to non relativistic degenerate neutrons (the relativistic limit sets in at density  $\sim 10^{16} \text{ g cm}^{-3}$ ) the mass radius relation is:

$$\frac{R}{R_\odot} = 2 \times 10^{-5} \left( \frac{M}{M_\odot} \right)^{-1/3} \Rightarrow R \approx 15 \text{ km} \quad (3.13)$$

where we have assumed 1 baryon per neutron. While the Chandrasekhar Mass is:

$$M_{ch} = 5.5 M_\odot \quad (3.14)$$

Note however that for NSs such estimates are only correct within an order of magnitude (the difference with respect to a WD supported by electrons is due solely to the fact that there is one electron per two baryons). The radii that are found are comparable in magnitude with the Schwarzschild radius and this implies that general relativistic corrections cannot be neglected.

## 3.2 TOV equations

We begin by recalling the two main equations defining the TOV equilibrium. The equation for the included mass is:

$$\frac{d}{dr} [r(1 - e^{-2\lambda})] = 8\pi r^2 \epsilon \Rightarrow e^{-2\lambda} = 1 - \frac{2M(r)}{r} \quad \text{with } M(r) = 4\pi \int_0^r \epsilon r^2 dr \quad (3.15)$$

Outside the star the quantity  $M$  is a constant, that in the weak field limit coincides with the Newtonian gravitational mass of the star.

The TOV equilibrium is given by:

$$\frac{dp}{dr} = - \frac{[p(r) + \epsilon(r)][M(r) + 4\pi r^3 p(r)]}{r(r - 2M(r))} \quad (3.16)$$

### 3.2.1 Constant Density Model

The TOV equation introduces several non-linearities due to GR effects and the fact that now the internal energy contributes to the mass and inertia. This prevents a simple renormalization (adimensionalization) as it was done for the Lane-Emden equation.

Instead the TOV must be solved as an initial value ODE, given a central density (energy density or barion density). Realistic EoS can only be handled numerically. However it is possible to derive a simple solution in the simple case of constant energy density  $\epsilon = \epsilon_o$  (corresponding to a *stiff* equation of state, large variations of pressure are associated with weak variations of density). The energy density usually contains the rest mass density (associated with the baryon number density) and the internal energy density.

Eq. 3.15 integrates trivially:

$$M(r) = \frac{4\pi}{3} \epsilon_o r^3 \quad M = \frac{4\pi}{3} \epsilon_o R^3. \quad (3.17)$$

These stars follow a  $M \propto R^3$  mass-radius relation, with the proportionality coefficient dependent on the energy density.

The TOV equation is:

$$\frac{dp}{dr} = - \frac{4\pi r^3}{3} \frac{[p(r) + \epsilon_o][\epsilon_o + 3p(r)]}{r(r - 8\pi \epsilon_o r^3/3)} = - \frac{4\pi r}{3} \frac{[p(r) + \epsilon_o][\epsilon_o + 3p(r)]}{(1 - 8\pi \epsilon_o r^2/3)} \quad (3.18)$$

that can be rearranged and integrated to:

$$- \int_r^R \frac{dp}{(p + \epsilon_o)(3p + \epsilon_o)} = \frac{4\pi}{3} \int_r^R \frac{r dr}{1 - 8\pi \epsilon_o r^2/3} \quad (3.19)$$

Recalling that at the surface  $p(R) = 0$ , one has:

$$- \frac{1}{2\epsilon_o} [\ln(3p + \epsilon_o) - \ln(p + \epsilon_o)] \Big|_r^R = - \frac{1}{4\epsilon_o} \ln(1 - 8\pi \epsilon_o r^2) \Big|_r^R \quad (3.20)$$

$$\frac{1}{2\epsilon_o} [\ln(3p(r) + \epsilon_o) - \ln(p(r) + \epsilon_o)] = - \frac{1}{2\epsilon_o} \ln \left[ \frac{p(r) + \epsilon_o}{3p(r) + \epsilon_o} \right] = - \frac{1}{2\epsilon_o} \ln \left[ \frac{1 - 8\pi \epsilon_o R^2}{1 - 8\pi \epsilon_o r^2} \right]^{1/2} \quad (3.21)$$

$$\frac{p(r) + \epsilon_o}{3p(r) + \epsilon_o} = \sqrt{\frac{1 - 8\pi \epsilon_o R^2}{1 - 8\pi \epsilon_o r^2}} = \sqrt{\frac{1 - 2M/R}{1 - 2Mr^2/R^3}} \quad (3.22)$$

which solves to:

$$\frac{p(r)}{\epsilon_o} = \left[ \frac{\sqrt{1 - 2M/R} - \sqrt{1 - 2Mr^2/R^3}}{\sqrt{1 - 2Mr^2/R^3} - 3\sqrt{1 - 2M/R}} \right] \quad (3.23)$$

From Eq. 3.22 one also finds, in terms of the central pressure  $p_c$ :

$$\frac{2M}{R} = 1 - \left[ \frac{p_c + \epsilon_o}{3p_c + \epsilon_o} \right]^2 \quad (3.24)$$

This can be used to express the ratio  $M/R$  as a function of the central pressure. Assuming  $p_c = \eta\epsilon_o$ , and  $\xi = r/R$  Eq. 3.23 becomes:

$$\frac{p(r)}{\epsilon_o} = \frac{1 + \eta - \sqrt{(1 + 3\eta)^2 - 4\eta(1 + 2\eta)\xi^2}}{-3 - 3\eta + \sqrt{(1 + 3\eta)^2 - 4\eta(1 + 2\eta)\xi^2}} \rightarrow \eta(1 - \xi^2) \quad \text{for } \eta \ll 1 \quad (3.25)$$

### 3.2.2 Polytropic Model

Assuming the NS to be composed only of fully degenerate, non-relativistic neutrons (relativity sets in above  $10^{16}$  g cm<sup>-3</sup>, while typical central density in NSs do not exceed a few  $10^{15}$  g cm<sup>-3</sup>), one can use for the pressure the result of Eq.2.40. The solution is only numerical, but in Fig. 3.2 we show the results, the total mass is plotted as a function of the central density, and the mass-radius relation is shown.

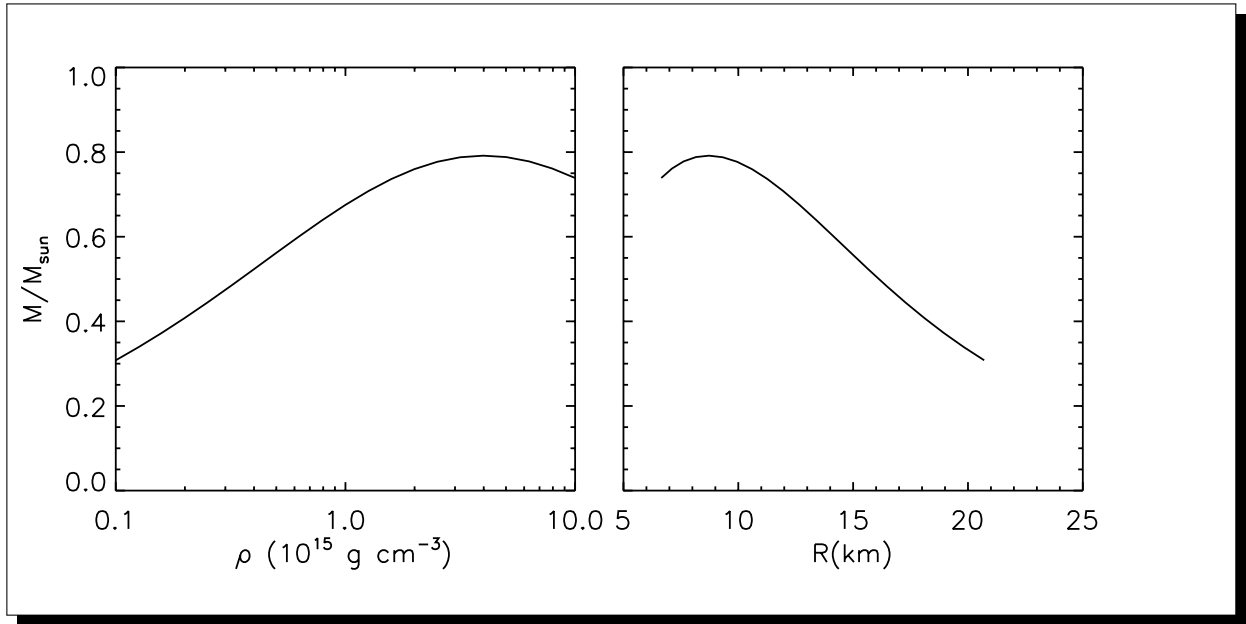
Those results show that there is a maximum mass  $\approx 0.8M_\odot$  (the correct value using Eq. 2.48 is  $0.7M_\odot$ ), that is reached for central density  $4 \times 10^{15}$  g cm<sup>-3</sup>, corresponding to a radius of 8 km. Above this density solutions are unstable, so there are no stable configurations in the relativistic regime. For stable configurations  $M \approx [1 - (R/30\text{km})]M_\odot$ .

It is immediately evident that the maximum mass derived in this regime is smaller than the Chandrasekhar Mass for WDs. This implies a formation bottleneck. The degenerate iron core of Red Supergiant Star, will collapse to form a NS only once its mass becomes bigger than the Chandrasekhar limit. But total mass is conserved during collapse, so it is impossible, for the collapsing iron core, to reach a stable NS configuration.

The solution of this problem was obtained only in the '50s, once it was realized that at the typical densities of NS, the average distance of neutrons is so small that the relative strong attraction cannot be neglected, and neutrons cannot be treated as free fermions. More realistic EoS lead to maximum mass  $\sim 1.7 - 2.0 M_\odot$  solving the bottleneck problem.

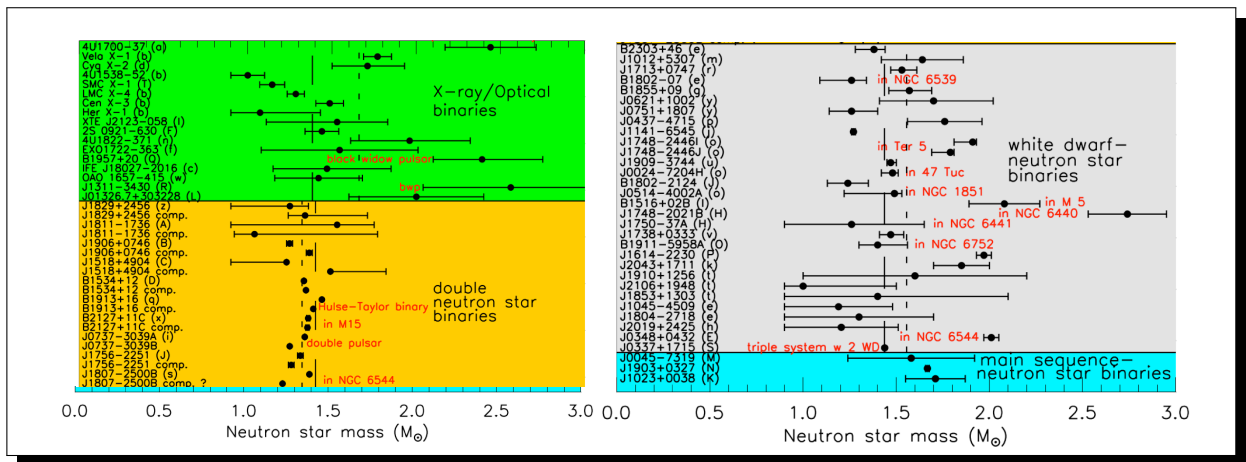
## 3.3 Mass and Radius

Fig. 3.3 shows the measured masses of NSs. As in the case of other astrophysical objects, measurements of mass are possible only in binary systems, once the orbital properties of the NS and its companion are known. NSs do not have spectral features (lines) whose Doppler modulation due to the orbital motion can be measured. However there



**Figure 3.2:** Solutions of the TOV Equation for a system of fully degenerate neutrons in the non-relativistic regime. Left panel: mass as a function of central density. Right panel: mass as a function of radius

is a class of NS known as Pulsars (see Chapter 1) that produce a highly periodic radio pulsed emission, that can be timed with high accuracy. The orbital modulation of this pulsed emission can be used to reconstruct the orbit and hence the mass. If the companion is a Main Sequence star or a WD, its mass can be derived from his spectrum. Sometimes the companion is another NS (in the case of PSR J0737-3039 detectable also as a pulsar). The timing accuracy is nowadays so high that one can also measure GR deviations from the Newtonian orbit: precession of periastron, orbital decay due to gravitational wave emission, etc.... These post-Newtonian corrections offer independent estimates of the masses (in addition to the classical Newtonian orbital parameters), that can fix the masses in a binary system even if the companion is unseen. The highest measured mass is  $\approx 2M_{\odot}$  for PSR J0348+0432 and PSR J1614–2230.



**Figure 3.3:** Measured masses of NSs.

Measuring the radius of NSs is more complex. There is a very small group of NS (less than 10) known as Isolated Neutron Star (INSS), that show an X-ray thermal emission, with a typical Black Body spectrum (see Fig. 2.2). These are old isolated objects, with no evidence of magnetospheric activity, or accretion from a binary companion. It is reasonable to expect that the emission we observe, come from the very surface. In this case, knowledge of

the Black Body temperature  $T_{bb}$ , that can be derived from spectral fitting, and of their luminosity  $L$  can be used to infer a radius  $R_{bb}$  from the Black Body relation  $L = 4\pi\sigma_{SB}R_{bb}^2T_{bb}^4$ , where  $\sigma_{SB}$  is the *Stefan-Boltzmann constant*. However, the radii derived in this way are far too small ( $\sim 3 - 5$  km) to be compatible with NSs.

There are two possible reasons for this discrepancy: either emission is dominated by a hot spot on the NS surface, such that  $R_{bb}$  is actually a measure of the spot size, or absorption in the NS atmosphere suppresses the emission, with respect to a pure Black Body. Unfortunately the absence of spectral features does not allow us to derive the atmospheric composition, and hence its absorption.

There are two further issues with INs: the black body spectrum inferred in X-ray is not compatible with their optical emission, and the fact that they are isolated prevents the measure of their mass.

Mass and radii can be measured, in a sub-class of NSs, belonging to binary systems with a Main Sequence companion, from which they accrete matter. The densities and temperatures reached by the accreting matter as it deposits on the NS surface, are so high that hydrogen nuclear burning takes place. Depending on the mass accretion rate, in a few systems such burning can give rise to rapid outbursts. Some of these bursts can be so intense that the luminosity reaches the *Eddington limit*:

$$L_{Edd} = \frac{4\pi GMm_p c}{\sigma_T} \approx 1.3 \times 10^{38} \left( \frac{M}{M_\odot} \right) \text{ erg s}^{-1} \quad (3.26)$$

where  $\sigma_T$  is the Thompson cross section. Once this limit is reached the accreting matter is lifted out by radiation pressure.

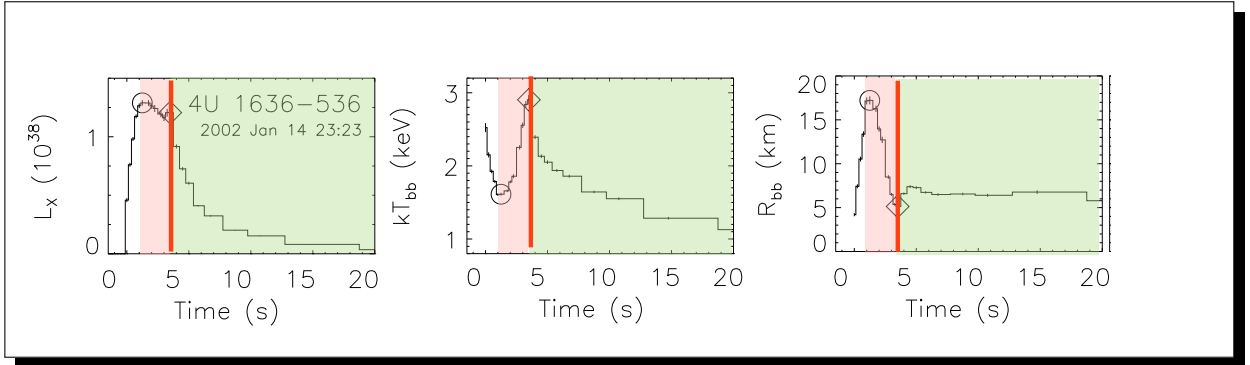


**Figure 3.4:** Luminosity, Black Body temperature and Black Body radius in an Eddington limited burst. The pink area shows the first phase of shrinking photosphere, while the green area shown the second phase after touchdown (the red line).

In these bursts one distinguishes two phases (Fig. 3.4): after a rapid rise, in the first phase the luminosity remains almost constant for a few seconds and the Black Body temperature  $T_{bb}$  rises, then in the second phase the luminosity steadily declines, and so does the Black Body temperature. The duration of the first phase is much longer than the typical free falling time on a NS ( $\sim \sqrt{R^3/GM}$ ) which is  $\sim$  a few ms. This implies that the photosphere must be supported against gravity, which means that the luminosity must be close to the Eddington limit. As the NS cools, following the initial nuclear burning burst, the photosphere will shrink until it relaxes back to the NS surface (the touchdown). In the first phase the photospheric radius can be estimated from the Black Body relation  $L_{edd} = 4\pi\sigma_{SB}R_{ph}^2T_{bb}^4$ . The radius at touchdown is the NS radius. This is confirmed by the evolution of the second phase when the luminosity is seen to decline as  $L \propto T_{bb}^4$ , which implies a fixed size. The burst itself allows one to derive a relation between mass and radius:

$$\frac{4\pi GMm_p}{\sigma_T} = 4\pi\sigma_{SB}R^2T_{bb}^4 \Rightarrow \frac{M}{R^2} = \frac{\sigma_T\sigma_{SB}}{Gm_p}T_{bb}^4 \quad (3.27)$$

with quantities measured at touchdown. Together with orbital information from the binary system this can constrain both mass and radius.

### 3.3.1 Constraints on the Mass-Radius relation

In the mass radius diagram there are regions than can be excluded based on theoretical constraints. This together with measured masses and radii can be used to constrain the possible EoS, describing degenerate matter at super-nuclear densities.

The first constraint comes from GR, and it is simply the statement that a NS must be bigger than its own Schwarzschild radius:

$$R > \frac{2GM}{c^2} \quad (3.28)$$

Another constraint can be derived in the limit of infinite central pressure. From Eq. 3.24, setting  $p_c \gg \epsilon_o$ , one finds:

$$\frac{Rc^2}{GM} = \frac{9}{4} \Rightarrow R > \frac{9GM}{4c^2} \quad (3.29)$$

Finally the last constraint comes from causality. For a causal equation of state the sound speed  $c_s^2 = dp/d\epsilon < 1$ . Now at low density  $p < \epsilon$ . So causality will be violated if at some higher density  $p = \epsilon$ . Setting  $p_c = \epsilon_o$  thus necessarily implies a causality violation. Again using Eq. 3.24, this requirement reads:

$$\frac{Rc^2}{GM} = \frac{8}{3} \Rightarrow R > \frac{8GM}{3c^2} \quad (3.30)$$

These forbidden regions are shown in Fig. 3.5.

### 3.3.2 Mass Limits and Rotation

Observations also pose important constraints on the possible Equation of State. The existence of a NS with mass  $\approx 2.0M_\odot$  implies that only EoS giving mass radius relations that extend above that limit are allowed. On the other hand there are a handful of Pulsars seen to spin with millisecond period. The fastest spinning PSR known is PSR J1748-2446 with a frequency of 716 Hz, corresponding to a period of 1.4 ms.

The maximum rotation of a NS can be obtained setting the rotation frequency at the equator equal to the Keplerian frequency. Unfortunately correct estimates require the knowledge of the structure of the rotating NS as well as the metric of the spacetime. In a system with angular momentum, the metric outside the star cannot be described by the Schwarzschild solution. The deviation of the metric from the spherically symmetric case, is given by the so called *Kerr parameter*  $a = GI\Omega^2/(M^{1/2}c^2R^{-3/2})$ , where  $I$  is the moment of inertia and  $\Omega$  is the rotation rate. At the

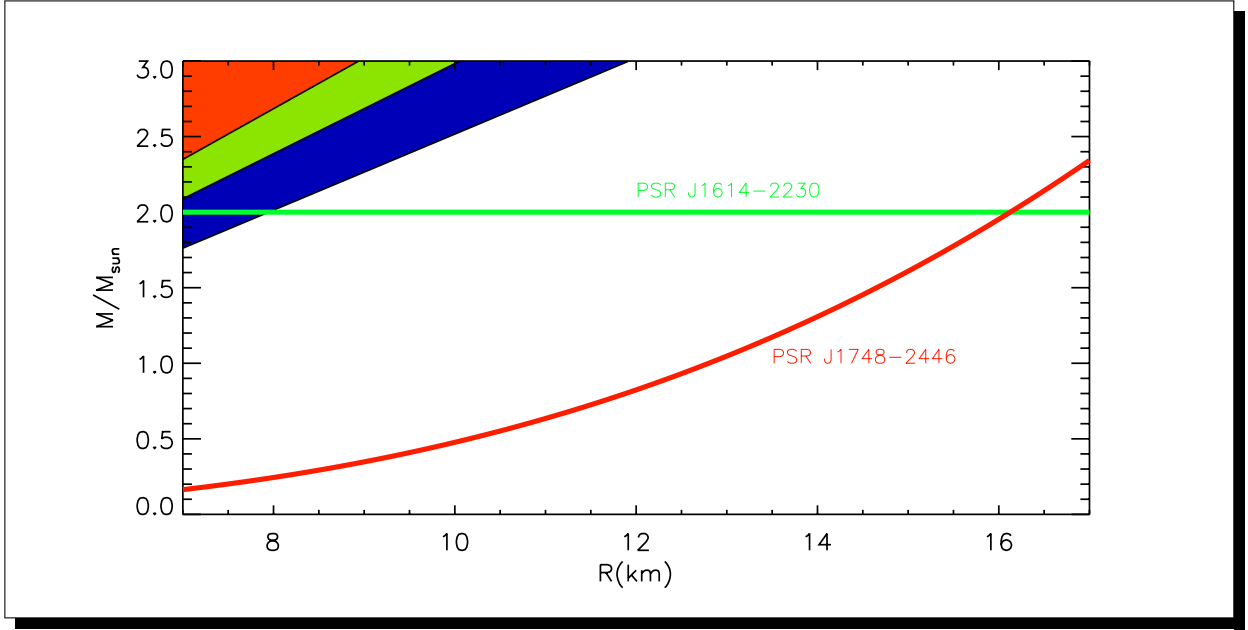


**Figure 3.5:** Mass radius diagram for NSs. Colored areas represent regions that are forbidden: GR limit (red); infinite pressure limit (green), causality limit (blue). Green line is the maximum measured mass of a NS. Red line is the Keplerian limit for the fastest spinning NS known.

surface of a typical NS ( $M \sim 1.4M_{\odot}$ ,  $R \sim 10$  km,  $I = 10^{45}$  g cm<sup>2</sup>) the Kerr parameter is  $\sim 0.1$  for a millisecond rotator. This implies that the metric outside the NS can be reasonably approximated by the Schwarzschild solution. Recalling the formula of the Keplerian frequency in Kerr metric, one has:

$$\Omega_K^2 = \frac{GM}{(R^2 + a^2)^{3/2}} \approx \frac{GM}{R^3} \quad \text{for } a \ll 1 \quad (3.31)$$

Identical to the Newtonian case. On the other hand a star rotating at the keplerian speed, will be deformed into an oblate ellipsoid. It is well known that for a system in hydrostatic equilibrium, the isobaric surfaces are also isopotential ones. The stellar surface, will be an isopotential surface, where the effective gravity will now include the centrifugal force. Assuming for simplicity the Newtonian regime, with the same gravitational potential as the non rotating case, one has for the polar and equatorial radii  $R_p$  and  $R_e$  respectively:

$$\frac{GM}{R_p} = \frac{GM}{R_e} + 0.5\Omega_K(R_e)^2 R_e^2 = \frac{3GM}{2R_e} \quad \Rightarrow \quad R_e = 3R_p/2 \quad (3.32)$$

More accurate computations show that at mass shedding  $R_e \approx 2R_p$ . It is possible at this point to define an effective radius (the radius of a sphere having the same volume of the ellipsoid)  $\tilde{R}^3 = R_e^2 R_p \approx 0.5R_e^3$ , hence  $\tilde{R} \approx 0.8R_e$ . Using this value as a proxy for a non rotating star of the same volume (mass) in the mass radius diagram (where EoS are usually plotted for non rotating systems) one gets a corrected Keplerian formula:

$$\Omega_K^2 \approx 0.5 \frac{GM}{\tilde{R}^3} \quad \Omega_K \simeq 9000\text{Hz} \left( \frac{M}{M_{\odot}} \right)^{1/2} \left( \frac{10\text{km}}{R} \right)^{3/2} \quad (3.33)$$

More accurate numerical models, in full GR, give a coefficient  $\sim 0.4$ . Setting this equal to the observed frequency allows one to define another curve in the mass radius plane that any realistic EoS must cross.



# CHAPTER 4

---

## PULSAR ELECTRODYNAMICS

---

In this chapter we will investigate the Electrodynamics of Pulsars (PSRs). We will show that, for typical PSR conditions, a magnetosphere forms above the Neutron Star (NS) surface, and the conditions in the magnetosphere are such that an outflow develops, which exerts a torque on the star.

### 4.1 Spinning Dipole and the Lighthouse model

It was immediately suggested, soon after their discovery, that PSR could be understood as rotating NSs endowed with a magnetic field, and that the properties of their emission and slowing down could be due to the magnetic field itself.

The simplest model is to assume that the rotating NS is endowed with a dipolar magnetic field. A rotating dipole is known to emit EM radiation. The energy emitted per unit time is simply given by the *Larmor formula*:

$$W = \frac{2}{3} \frac{\ddot{\mu}^2}{c^3} \quad (4.1)$$

where  $\mu$  is the *magnetic dipole moment*. For a NS with radius  $R_{\text{NS}} \sim 10^6$  cm and magnetic field  $B_{\text{NS}}$ , the dipole moment is  $R_{\text{NS}}^3 B_{\text{NS}}$ . If the magnetic axis is inclined an angle  $\chi$  with respect to the rotation axis, and the rotation rate is  $\Omega$ , the time derivatives of the dipole moment will be  $\dot{\mu} = \mu\Omega \sin \chi$ , and  $\ddot{\mu} = \mu\Omega^2 \sin \chi$ . The NS will then lose rotational energy by the emission of dipole radiation according to the spin-down formula:

$$\dot{E} = I\Omega\dot{\Omega} = -\frac{2}{3} \frac{B_{\text{NS}}^2 R_{\text{NS}}^6}{c^3} (\sin \chi)^2 \Omega^4. \quad (4.2)$$

where  $I \simeq M_{\odot} R_{\text{NS}}^2 \simeq 10^{45}$  g cm<sup>2</sup> is the typical moment of inertia of a NS. For typical PSR values, assuming  $\sin \chi \sim 1$  one gets:

$$\dot{\Omega} = -10^{-12} \left( \frac{\Omega}{30 \text{ s}^{-1}} \right)^3 \left( \frac{B_{\text{NS}}}{10^{12} \text{ G}} \right)^2 \text{ s}^{-2} = -\frac{2\pi\dot{P}}{P^2} \rightarrow \dot{P} \simeq 10^{-14} \left( \frac{P}{0.1 \text{ s}} \right)^{-1} \left( \frac{B_{\text{NS}}}{10^{12} \text{ G}} \right)^2 \text{ s s}^{-1}. \quad (4.3)$$

This implies that, for the canonical PSRs, the magnetic field should be of the order of  $10^{12}$  G, while for the millisecond ones it should be  $\sim 10^8$  G.

While the details of the formation of a PSR magnetic field are still largely debated, a simple estimate can be done considering what happens at the NS formation. A NS is just the remnant of the collapsing core of a massive

star. The typical Fe core of a massive star is supported against gravitational collapse by the degeneracy pressure of its electrons. Its typical mass, before collapse, will be  $\sim 1.4M_{\odot}$ , the Chandrasekhar limit. This implies that the size of the Fe core of a massive star will be of the order of the size of a WD,  $R_{\text{core}} \sim 10^9$  cm. If this core is endowed with a magnetic field  $B_{\text{core}}$ , the net magnetic flux through the core will be  $\sim B_{\text{core}}R_{\text{core}}^2$ . As the core collapses, its high conductivity will ensure flux freezing (the magnetic flux through a closed loop will be conserved). Once the core reaches the size of a NS,  $R_{\text{NS}}$ , its magnetic field will be enhanced by a factor  $(R_{\text{core}}/R_{\text{NS}})^2 \sim 10^6$ . This shows that any preexisting magnetic field can be amplified several orders of magnitude, but needs to be at least  $\sim 10^6$  G, to give the expected values. Little is known about the strength of the magnetic field in the pre-collapsing core. A simple argument states that, taken a star like the Sun, with a typical magnetic dipole field at the surface  $\sim 1$  G, if one extrapolates this dipole field from the surface at  $\sim 10^{11}$  cm to  $R_{\text{core}}$ , one finds  $\sim 10^6$  G.

The spin-down formula can be integrated to give the spin evolution in time for a NS. First note that the curves  $P\dot{P} = \text{const}$  represent PSRs with the same magnetic field. If one assumes that the magnetic field (the magnetic dipole moment) is constant in time, a PSR should evolve along the  $P\dot{P} = \text{const}$  curve corresponding to its initial magnetic field. The spin-down equation can be generalized to:

$$\frac{d\Omega}{dt} = -k\Omega^n \quad (4.4)$$

where  $n$  is called the braking index, and  $n = 3$  for a pure magnetic dipole. The solution of this equation allows one to relate the age of the pulsar  $t_{\text{PSR}}$  to the observed period, period derivative, and initial period  $P_o = 2\pi/\Omega_o$ .

$$dt = -\frac{d\Omega}{k}\Omega^{-n} \rightarrow t_{\text{PSR}} = \frac{k^{-1}}{1-n}[\Omega_o^{1-n} - \Omega^{1-n}] = \frac{\Omega}{(1-n)\dot{\Omega}} \left[ 1 - \left( \frac{\Omega}{\Omega_o} \right)^{n-1} \right] \quad (4.5)$$

$$t_{\text{PSR}} = \frac{P}{(n-1)\dot{P}} \left[ 1 - \left( \frac{P_o}{P} \right)^{n-1} \right]. \quad (4.6)$$

Assuming the initial rotation to be much faster than the present value, one can neglect the term  $P_o/P$  and derive the so called *characteristic dipole age*  $\tau_c = P/2\dot{P}$ . The curves  $P/\dot{P} = \text{const}$  are isochrones, representing PSRs of similar ages. The braking index,  $n = \dot{\Omega}\Omega/\Omega^2$ , is measured only for few PSRs, and is always less than 3 (with values ranging from 1.4 for the Vela PSR to 2.85 for the pulsar in the SNR Kes 75). The typical ages of the canonical pulsars are  $\sim 10^6$  yr, while for the millisecond ones, one finds spin-down ages comparable to the Hubble time. This is a clear evidence that the millisecond PSRs do not evolve with the mechanism of the canonical ones.

The spin-down formula can also be used to compute how energy losses from the PSR change in time:

$$\Omega = \Omega_o \left( 1 - \frac{k(n-1)\Omega_o^n t_{\text{PSR}}}{\Omega_o} \right)^{-\frac{1}{n-1}} \quad (4.7)$$

$$\rightarrow \dot{E} = I\Omega\dot{\Omega} = I\Omega_o\dot{\Omega}_o \left( 1 - \frac{(n-1)\dot{\Omega}_o t_{\text{PSR}}}{\Omega_o} \right)^{-\frac{n+1}{n-1}} = \dot{E}_o \left( 1 + \frac{t_{\text{PSR}}}{\tau_{\text{sd}}} \right)^{-\frac{n+1}{n-1}} \quad (4.8)$$

where we have defined the characteristic spin-down time  $\tau_{\text{sd}} = P_o/(n-1)\dot{P}_o$ .

Based on the idea that PSRs are NSs with a dipolar field, one can explain their pulsed radio emission assuming that the radiation originates in a spot close to the magnetic pole, the so called *polar cap*, and that it is beamed in the direction of the magnetic axis. If the magnetic axis is inclined with respect to the rotation axis, the rotation of the star causes this beam to rotate, like a *Lighthouse*. If the beam intersects the direction toward us, it gives a pulse, which repeats every rotation. The narrower is this beam, the sharper is the pulse. Given that a PSR has two magnetic poles, it might happen that we can receive radiation from both of them (a pulse every half period).

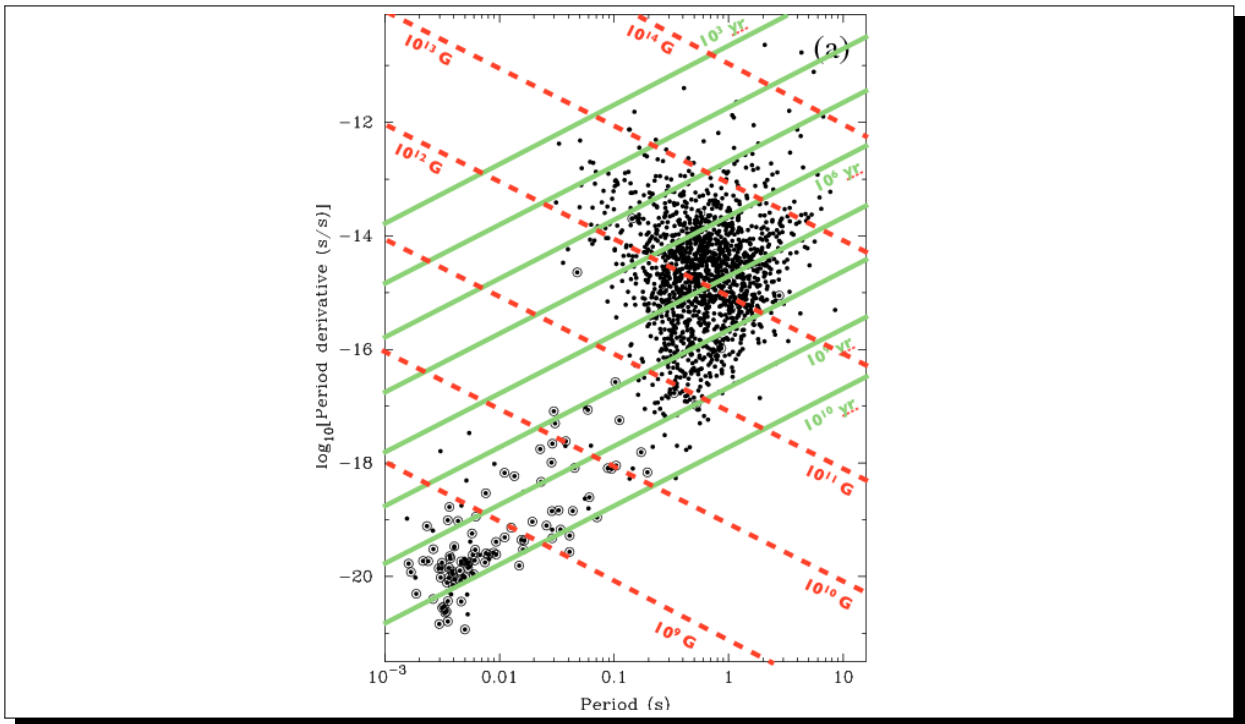


**Figure 4.1:** Distribution of periods and periods derivatives for the known pulsar population from the ATNF catalogue. Red lines are curves of constant dipole magnetic field (evolutionary curves for pure dipoles) with strength ranging from  $10^9$  to  $10^{14}$  G. Green lines are curves of constant characteristic dipole age (isochrones for pure dipoles), rangin from  $10^{10}$  to  $10^3$  yr.

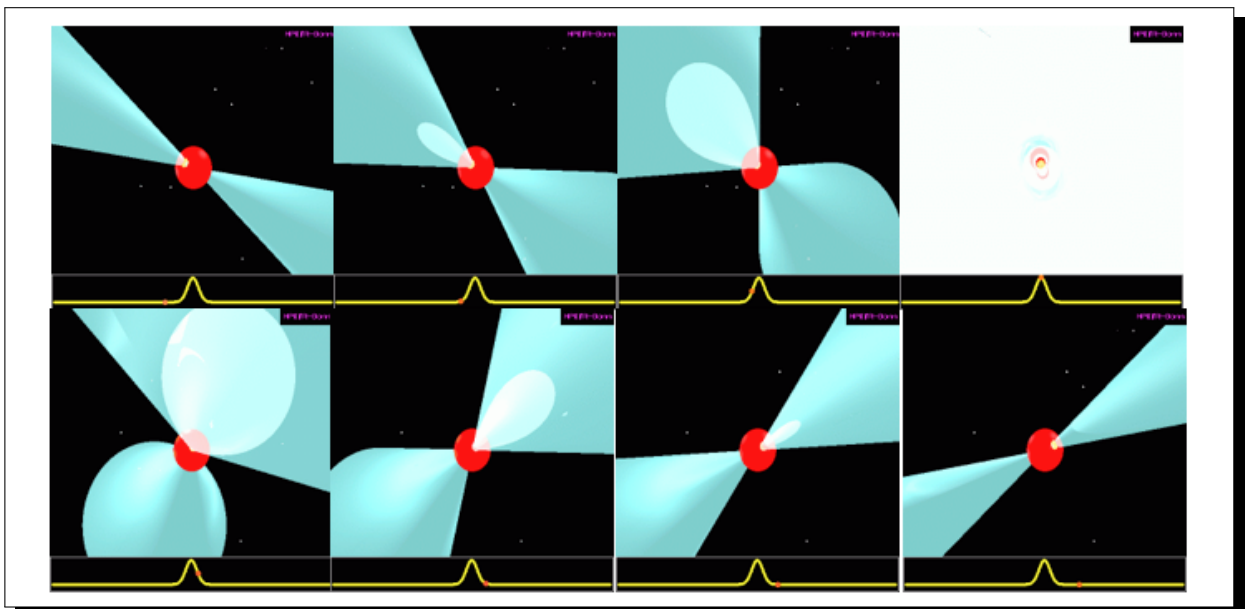


**Figure 4.2:** How a pulse is produced in the Lighthouse model for PSRs. The full animation of the rotating system is available at <http://pulsar.ca.astro.it/pulsar/Figs/smallmodpulsar.gif>

## 4.2 The Unipolar Inductor

Before presenting in detail realistic models for PSRs, it is instructive to discuss a simple system, formed by a rotating conductor embedded in a magnetic field. Such system is known as *unipolar inductor*. The simplest symmetry is for the rotation axis to be parallel to a uniform external magnetic field. The first and simplest unipolar inductor was proposed by Faraday and it is just a rotating disk, as in Fig. 4.3. For a conductor at rest, the laws of electrostatic state that the outer surface is an equipotential surface, and the internal electric field vanishes (any electric field will be rapidly cancelled out by charges moving inside). The situation is however different for the “unipolar inductor”. The magnetic field  $\mathbf{B}$  inside a rotating conductor provides an unbalanced Lorentz force that can act on the charge carriers:

$$\frac{q}{c} \mathbf{v} \wedge \mathbf{B} \quad (4.9)$$

where  $q$  is the charge of the particle and  $\mathbf{v}$  its velocity. The consequence of this force is to separate the charges axially moving all the electrons in one direction and all the ions in the other. This would immediately create an electric field  $\mathbf{E}$  that opposes the force due to the magnetic one. The system will then relax to a situation where the total Lorentz force vanishes:

$$q \left( \mathbf{E} + \frac{\mathbf{v} \wedge \mathbf{B}}{c} \right) = 0. \quad (4.10)$$

This equation is just stating that in a frame comoving with the conductor, the electric field must vanish. This is known as the *Ideal MHD condition*, and the electric field, that satisfies it, is known as the *induction electric field*.

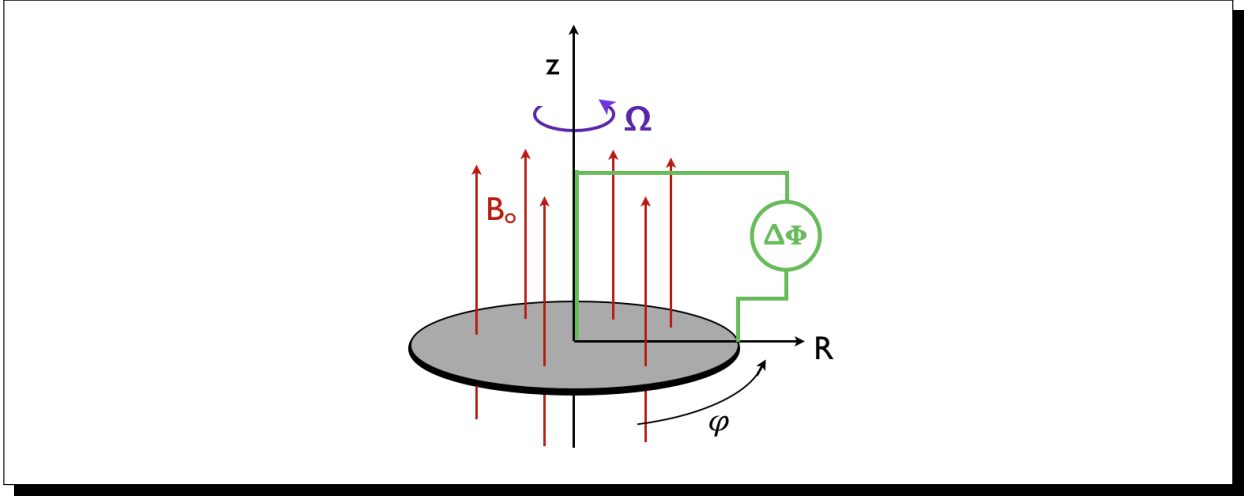


**Figure 4.3:** Scheme of a Faraday disk acting as a unipolar inductor.

Using a cylindrical reference frame, with the  $z$ -axis aligned with the rotation axis of the disk, and assuming a uniform field  $\mathbf{B} = B_o \mathbf{e}_z$  one can easily compute the induction electric field:

$$\mathbf{E} = -\frac{\Omega}{c} R B_o \mathbf{e}_R \quad (4.11)$$

where  $\Omega$  is the rotation rate of the disk, and  $R$  is the distance from the rotation axis. In our disk, one finds that the electric field is directed along the disk radius, and it induces a potential difference  $\Delta\Phi$  between the centre and the edge of the disk,  $R_{\text{disk}}$ , equal to:

$$\Delta\Phi = \Omega R_{\text{disk}}^2 B_o / 2c. \quad (4.12)$$

In principle this potential difference can drive a current. It is indeed this potential difference and the current that it drives that power the entire phenomenology of PSRs.

To this potential difference, and electric field, one can associate a charge density:

$$\rho = \frac{1}{4\pi} \frac{\partial}{R\partial R} (RE_r) = \frac{1}{2\pi} \frac{\Omega}{c} B_o \quad (4.13)$$

The disk is uniformly charged. The net charge on the disk is clearly different from zero (it is the charge density, and the net charge in the corotating frame that vanishes).

Despite its simplicity, the Faraday disk already contains the main physical ingredients of more complex configurations. We will see that, apart from changes in the numerical coefficients, due to the more complex geometry of a realistic PSR case, the general scalings derived above in terms of electric field, potential and charge density hold.

### 4.3 The Aligned Rotator

A PSR could be naively modelled, to a first approximation, as a rotating magnetized conducting sphere in vacuum. For simplicity we will here assume again that the magnetic field axis is aligned with the rotational axis (misaligned cases will be discussed in ....). Given the symmetry of the problem, the result will be time independent, and the fields will be stationary.

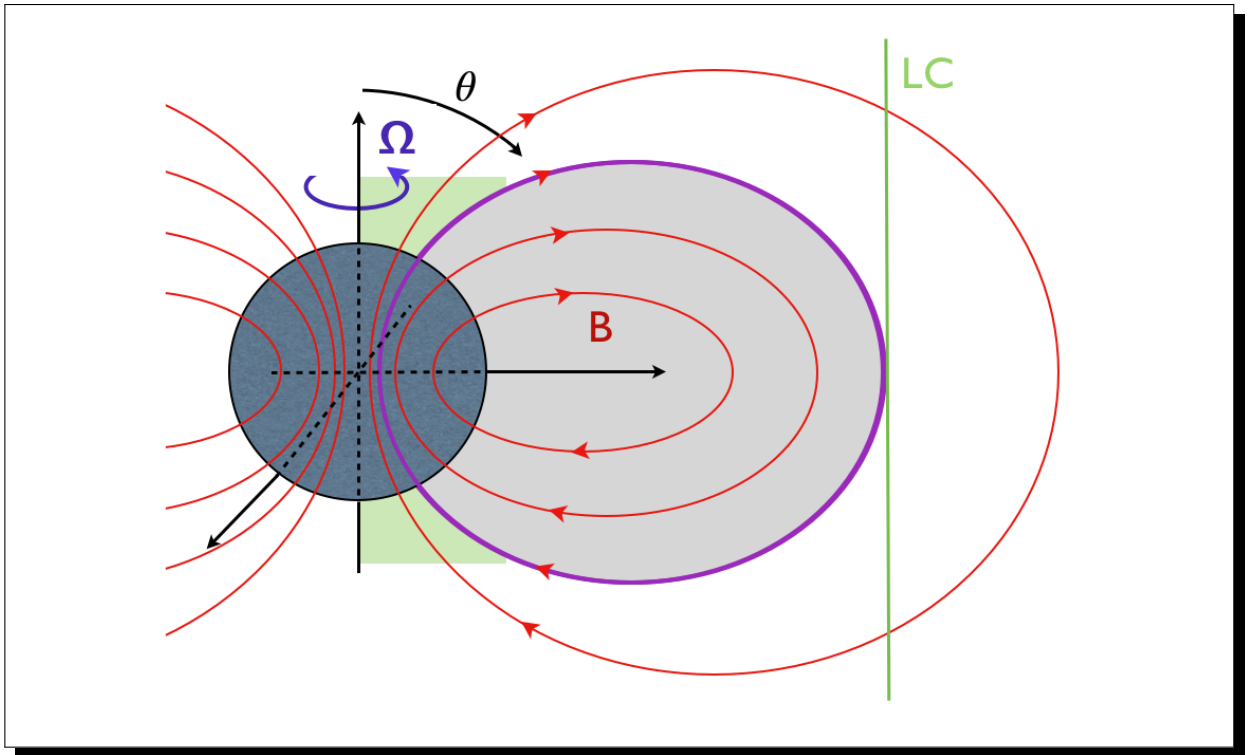


**Figure 4.4:** The aligned rotator. LC is the Light Cylinder, the gray shaded area is the closed field lines region, the green shaded one the open field lines region.

The magnetic field outside the rotating sphere, and just underneath its surface, is assumed to be dipolar. The structure of magnetic field in the deep interior is irrelevant for our discussion. So, using spherical coordinates  $(r, \theta, \phi)$ ,  $\mathbf{B}$  from the outer surface layers of the star all the way to infinity is:

$$B_r = 2B_o \left( \frac{R_{NS}}{r} \right)^3 \cos \theta, \quad B_\theta = B_o \left( \frac{R_{NS}}{r} \right)^3 \sin \theta \quad (4.14)$$

where  $B_o$  is the surface magnetic field strength at the equator. Given a rigid rotation,  $\mathbf{v} = \Omega r \sin \theta \mathbf{e}_\phi$ , the induction electric field just below the surface will be:

$$E_r = B_o \left( \frac{R_{\text{NS}}^3 \Omega}{cr^2} \right) \sin^2 \theta, \quad E_\theta = -2B_o \left( \frac{R_{\text{NS}}^3 \Omega}{cr^2} \right) \sin \theta \cos \theta. \quad (4.15)$$

Note that this induction electric field is perpendicular to the magnetic field:  $\mathbf{B} \cdot \mathbf{E} = 0$ . The electric field in the outside vacuum can be derived by solving the *Laplace equation* for the electric field potential  $\nabla^2 \Phi = 0$  (its solution can be expressed in terms of Spherical Harmonics). The potential must vanish at infinity, and must satisfy the proper boundary conditions at the surface of the sphere. Given that the magnetic and electric fields are time independent, the tangential component of the electric field just outside the conductor surface, must equal the one just inside:  $E_\theta(r = R_{\text{NS}}^+) = E_\theta(r = R_{\text{NS}}^-)$ . The only possible choice for the potential  $\Phi$  that satisfies the  $\theta$  dependence of the induction electric field at the surface is:

$$\Phi = Ar^{-3}[1 - 3 \cos^2 \theta] + Br^{-1} \quad (4.16)$$

the parameter  $A$  is determined by the surface value of  $E_\theta$ . The term  $B$  is in principle arbitrary, but can be fixed requiring the radial electric field,  $E_r$ , to vanish at the pole (in reality its value depends on the internal structure of the magnetic field, which is not known, the assumption we are doing minimizes the radial electric field at the pole):

$$A = -\frac{1}{3} \frac{B_o R_{\text{NS}}^5 \Omega}{c}, \quad B = 6AR_{\text{NS}}^{-2} = -\frac{2B_o R_{\text{NS}}^3 \Omega}{c} \quad (4.17)$$

which gives for the external electric field:

$$E_r = \frac{\partial \Phi}{\partial r} = \frac{B_o R_{\text{NS}}^5 \Omega}{cr^4} [1 - 3 \cos^2 \theta] + \frac{2B_o R_{\text{NS}}^3 \Omega}{cr^2}, \quad E_\theta = \frac{1}{r} \frac{\partial \Phi}{\partial \theta} = -\frac{2B_o R_{\text{NS}}^5 \Omega}{cr^4} \sin \theta \cos \theta \quad (4.18)$$

This electric field has a component parallel to the magnetic field. Just outside the conductor surface one has:

$$\begin{aligned} \mathbf{B} \cdot \mathbf{E} &= E_r B_r + E_\theta B_\theta = \frac{2B_o^2 R_{\text{NS}} \Omega}{c} [1 - 3 \cos^2 \theta] \cos \theta + \frac{4B_o^2 R_{\text{NS}} \Omega}{c} \cos \theta + \frac{2B_o^2 R_{\text{NS}} \Omega}{c} \sin^2 \theta \cos \theta \\ &= \frac{2B_o^2 R_{\text{NS}} \Omega}{c} \cos \theta [1 - 3 \cos^2 \theta + 2 + \sin^2 \theta] = \frac{8B_o^2 R_{\text{NS}} \Omega}{c} \cos \theta \sin^2 \theta \end{aligned} \quad (4.19)$$

The parallel electric field is:

$$E_{\parallel} = \frac{\mathbf{B} \cdot \mathbf{E}}{B} = \frac{8B_o R_{\text{NS}} \Omega}{c} \frac{\cos \theta \sin^2 \theta}{\sqrt{1 + 3 \cos^2 \theta}} \simeq \frac{4B_o R_{\text{NS}} \Omega}{c} \theta^2 \quad \text{at the pole} \quad (4.20)$$

Apart from a numerical coefficient and the geometric factor, the same result obtained for the Faraday disk. Note that the sign of the field (if it pushes out positive or negative charges) depends on the sign of  $\boldsymbol{\Omega} \cdot \mathbf{B}$ . For typical PSR parameters:

$$E_{\parallel} = 10^9 \left( \frac{B_o}{10^{12} \text{G}} \right) \left( \frac{R_{\text{NS}}}{10 \text{km}} \right) \left( \frac{\Omega}{10^2 \text{s}^{-1}} \right) \theta^2 \quad \text{stv.} \quad (4.21)$$

The force exerted by this electric field on an electron (or proton) is several orders of magnitude larger than the gravitational force. This electric field can lift particles from the NS surface, and, over a short distance  $l$ , can accelerate them, along the magnetic field lines, to very high Lorentz factors:

$$\gamma_e \simeq 5 \times 10^{10} \left( \frac{B_o}{10^{12} \text{G}} \right) \left( \frac{R_{\text{NS}}}{10 \text{km}} \right) \left( \frac{\Omega}{10^2 \text{s}^{-1}} \right) \left( \frac{l}{1 \text{km}} \right) \theta^2 \quad (4.22)$$

Such high relativistic particles will emit curvature radiation as they move along the curved magnetic field lines. This radiation will be beamed along the magnetic field. This is the mechanism that is thought to be at the base of the collimated emission in the Lighthouse model.

It is clear that a rapidly rotating NS, with a strong magnetic field, cannot be surrounded by a vacuum. Charges will be pull off the surface, and a charge density will be established in the magnetosphere, to shorten the parallel electric field.

### 4.3.1 The polar cap size

Particles that are lifted by the parallel electric field, can be enforced to corotate with the PSR only within a region where  $\Omega r \sin \theta < c$ . The boundary of this region is known as *Light Cylinder* (LC):

$$r_{\text{LC}} = \frac{c}{\Omega \sin \theta}. \quad (4.23)$$

The ratio  $c/\Omega$  sets a typical length scale for the magnetosphere. The magnetosphere itself can be divided into two parts. The region of field lines that close within the Light Cylinder, known as *closed field line region*, and the region of field lines that extend beyond the Light Cylinder, known as *open field lines region*. Within the closed field line region, particles extracted by the parallel electric field, can set into a corotating equilibrium, giving rise to a charge distribution that eventually will shorten the parallel electric field itself. Instead, particles extracted in the open field line region, might in principle stream away outside the LC. Once beyond the LC, particles cannot be stopped, and they will simply fly away, eventually opening the field lines. So it is possible that a charge density never form, strong enough to completely shorten the parallel electric field, and a continuous extraction of charges takes place at the foot points of the open field line region. It is thus meaningful to identify the emitting polar cap with the open field line region at the surface of the star.

The boundary between the open and closed field line regions corresponds to the field line that exactly closes at the LC, the *last closed field line*. For a dipolar magnetic field, the field lines have the parametric equation  $r = A \sin^2 \theta$ . The equation for the last closed field line is:

$$r = \frac{c}{\Omega} \sin^2 \theta. \quad (4.24)$$

The foot point of this line at the stellar surface is just the size of the polar cap:

$$\sin \theta_{\text{cap}} \simeq \theta_{\text{cap}} = \left( \frac{R_{\text{NS}} \Omega}{c} \right)^{1/2} = 0.1 \left( \frac{R_{\text{NS}}}{10 \text{km}} \right)^{1/2} \left( \frac{\Omega}{100 \text{s}^{-1}} \right)^{1/2} \quad (4.25)$$

The typical Lorentz factor of an electron accelerated at the polar cap, over a distance  $l$  will be:

$$\gamma_e \simeq \frac{e B_o R_{\text{NS}}^2 \Omega^2 l}{m_e c^4} \simeq 5 \times 10^8 \left( \frac{B_o}{10^{12} \text{G}} \right)^2 \left( \frac{R_{\text{NS}}}{10 \text{km}} \right) \left( \frac{\Omega}{10^2 \text{s}^{-1}} \right)^2 \left( \frac{l}{1 \text{km}} \right) \quad (4.26)$$

### 4.3.2 Outer Gaps

We have seen that close to the pole, in the region of field lines that do not close within the Light Cylinder, particles can be extracted and accelerated. There is also another location in the pulsar magnetosphere where a strong potential can develop. In order to shorten the parallel component of the electric field, a given charge must be present in the magnetosphere. If one assumes to first order a corotating magnetosphere one can derive a typical charge from:

$$\rho_e = \nabla \cdot \mathbf{E} = -\frac{1}{c} \nabla \cdot (\mathbf{v} \wedge \mathbf{B}) \quad (4.27)$$

Assuming that the magnetospheric magnetic field can be described as a dipole, at least as a first approximation within the Light Cylinder, then one finds:

$$\rho_e = \nabla \cdot \mathbf{E} = -\frac{1}{c} [\mathbf{B} \cdot \nabla \wedge \mathbf{v} - \mathbf{v} \cdot \nabla \wedge \mathbf{B}] = -\frac{\Omega \mathbf{e}_z \cdot \mathbf{B}}{c} \quad (4.28)$$

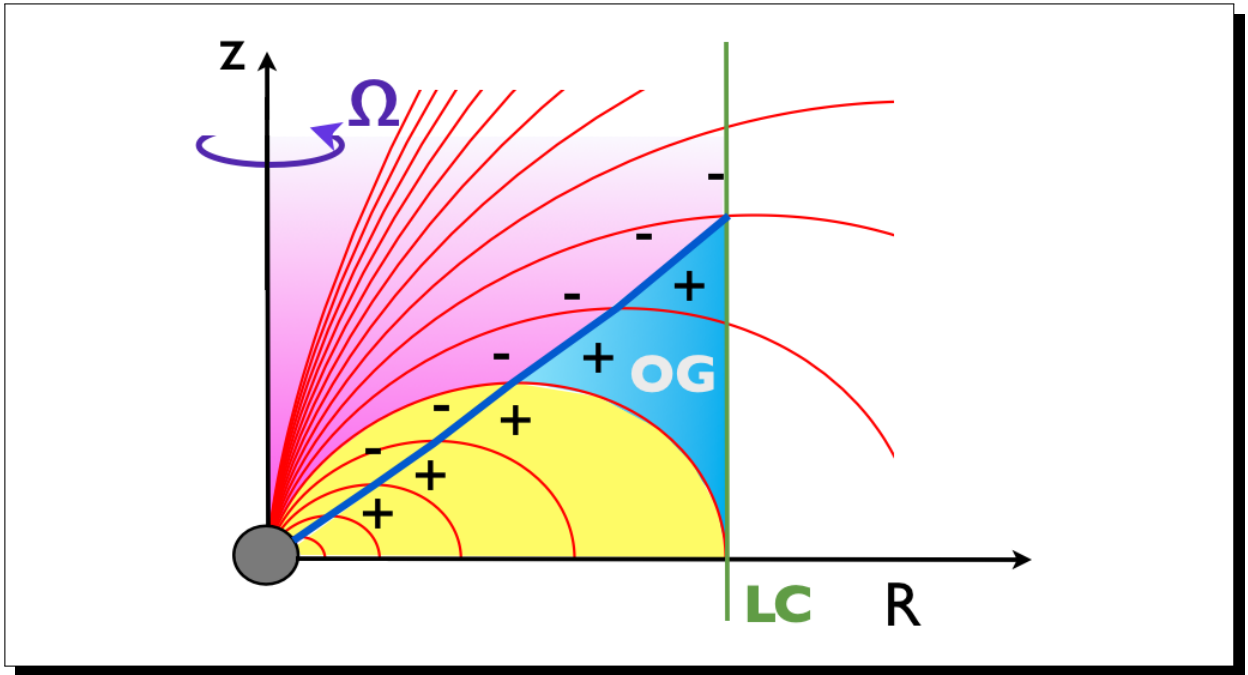


**Figure 4.5:** The concept of outer gaps. The blue line represents the null surface, separating magnetospheric regions that require a positive charge from those requiring a negative one. The outer gap region requires positive charge but its magnetic field lines connect to part of the NS surface where the charge is negative.

which is known as **Goldreich-Julian** charge density. It is evident that the sign of this charge changes depending on the sign of  $B_z$ . The surface where  $B_z = 0$  is known as the null surface. This surface separates the magnetosphere into two regions: one where the charge necessary to shorten the parallel electric field is negative, from one where it is positive.

In principle the only possible source of charges is the Neutron Star. However it is immediately evident that in the outer part of the magnetosphere there are regions that require, for example, a positive charge density, but that are connected to portion of the NS, where only a negative charge density can be extracted. How charge of a given sign can reach the outer part of the magnetosphere if only charge of the opposite sign can be extracted from the star along those field lines? This is at the origin of the concept of **outer gaps**: regions in the outer magnetosphere, close to the Light Cylinder, where the necessary neutralizing charge density cannot come from the stellar surface.

#### 4.4 The Orthogonal Rotator

We will investigate here the case of an orthogonal rotator. This can be considered as the opposite extreme to the aligned case. For an orthogonal spinning dipole, the electromagnetic field will have a radiation term, function of the retarded time, which will dominate at large distances, and that is ultimately responsible for the radiation energy loss. However, as we discussed for the aligned case, we are interested just to the conditions at the surface of the star, to show that a parallel electric field develops. Thus we will neglect in the following derivations the wave part of the field. The orthogonal case will allow us to consider a configuration that is time dependent, and to see what changes this introduces.

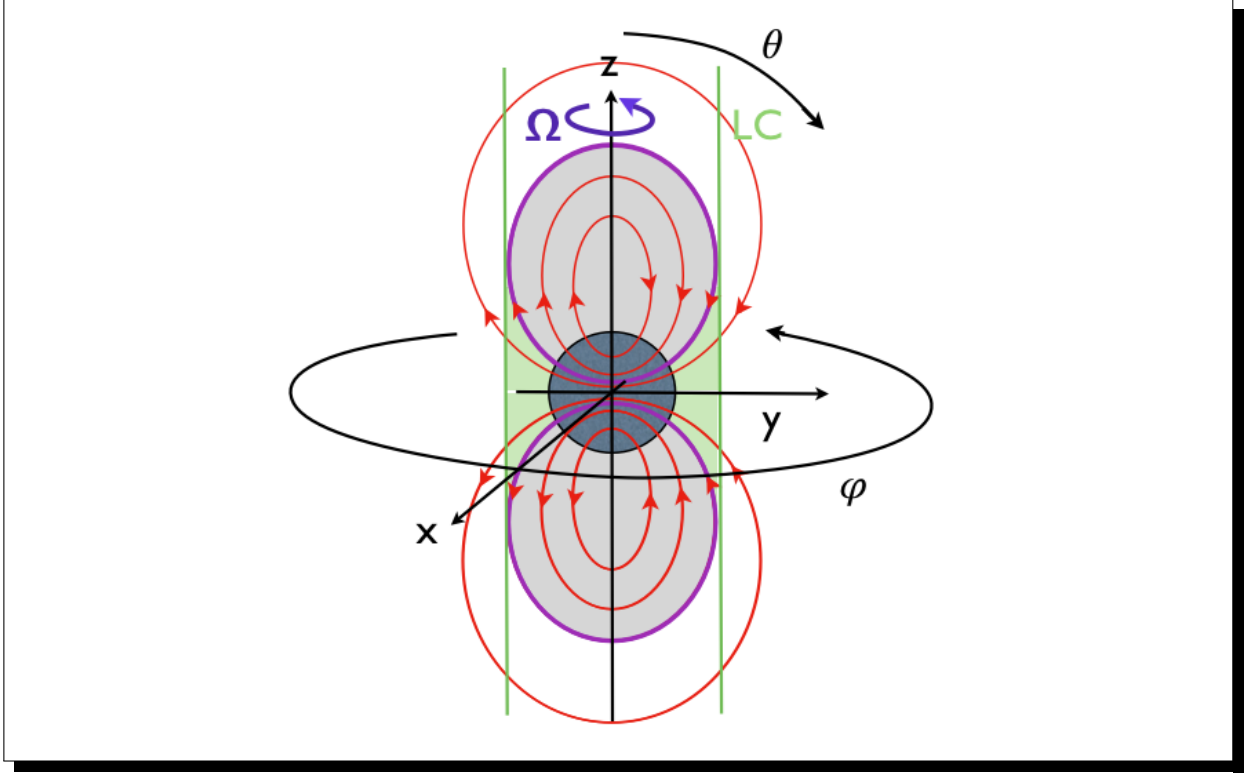


**Figure 4.6:** Geometry of the orthogonal rotator.

For simplicity we will make reference to a cartesian coordinate system  $[x, y, z]$  to derive the magnetic field. An orthogonal (to the  $z$ -axis) dipole, rotating at a frequency  $\Omega$ , is characterized by a magnetic dipole moment that in cartesian coordinates is:

$$\boldsymbol{\mu} = \mu_o \cos(\Omega t) \mathbf{e}_x + \mu_o \sin(\Omega t) \mathbf{e}_y. \quad (4.29)$$

with  $\mu_o = B_o R_{\text{NS}}^3$ . Close to the NS surface we can assume that the magnetic field has purely dipolar geometry:

$$\mathbf{B} = \frac{(\mathbf{e}_r \cdot \boldsymbol{\mu})\mathbf{e}_r - \boldsymbol{\mu}}{r^3} \quad (4.30)$$

$$\Rightarrow B_r = 2 \frac{(\mathbf{e}_r \cdot \boldsymbol{\mu})}{r^3} = 2B_o \left( \frac{R_{\text{NS}}}{r} \right)^3 \sin \theta \cos(\phi - \Omega t) \quad (4.31)$$

$$\Rightarrow B_\theta = -\frac{(\mathbf{e}_\theta \cdot \boldsymbol{\mu})}{r^3} = -B_o \left( \frac{R_{\text{NS}}}{r} \right)^3 \cos \theta \cos(\phi - \Omega t) \quad (4.32)$$

$$\Rightarrow B_\phi = -\frac{(\mathbf{e}_\phi \cdot \boldsymbol{\mu})}{r^3} = B_o \left( \frac{R_{\text{NS}}}{r} \right)^3 \sin(\phi - \Omega t) \quad (4.33)$$

$$(4.34)$$

where we recall here that  $\mathbf{e}_r = \sin \theta \cos \phi \mathbf{e}_x + \sin \theta \sin \phi \mathbf{e}_y + \cos \theta \mathbf{e}_z$ , while  $\mathbf{e}_\theta = \cos \theta \cos \phi \mathbf{e}_x + \cos \theta \sin \phi \mathbf{e}_y - \sin \theta \mathbf{e}_z$ , and  $\mathbf{e}_\phi = -\sin \phi \mathbf{e}_x + \cos \phi \mathbf{e}_y$ .

In the case of a time varying magnetic field, the electric field inside the star will be of the form  $\mathbf{E} = \mathbf{E}_{\text{ind}} + \mathbf{E}_{\text{rot}}$ , with  $\mathbf{E}_{\text{rot}} = \nabla \Phi_{\text{rot}}$ . The term  $\mathbf{E}_{\text{ind}}$  is due to the time varying magnetic field, through induction. The term  $\mathbf{E}_{\text{rot}}$  instead is an additive term, having zero curl, that ensures the vanishing of the net Lorentz force for corotating

charges. One has:

$$\nabla \wedge \mathbf{E}_{\text{ind}} = -\frac{1}{c} \frac{\partial \mathbf{B}}{\partial t} \quad \text{and} \quad (\mathbf{E}_{\text{ind}} + \mathbf{E}_{\text{rot}}) = -\frac{\Omega r \sin \theta}{c} \mathbf{e}_\phi \wedge \mathbf{B} \quad (4.35)$$

One finds that:

$$\mathbf{E}_{\text{ind}} = -\frac{\Omega B_o}{c} \left( \frac{R_{\text{NS}}^3}{r^2} \right) [\cos(\phi - \Omega t) \mathbf{e}_\theta - \cos \theta \sin(\phi - \Omega t) \mathbf{e}_\phi] \quad (4.36)$$

$$\begin{aligned} \mathbf{E}_{\text{rot}} = & -\frac{\Omega B_o}{c} \left( \frac{R_{\text{NS}}^3}{r^2} \right) [\sin \theta \cos \theta \cos(\phi - \Omega t) \mathbf{e}_r + (\sin^2 \theta - \cos^2 \theta) \cos(\phi - \Omega t) \mathbf{e}_\theta + \\ & + \cos \theta \sin(\phi - \Omega t) \mathbf{e}_\phi] \end{aligned} \quad (4.37)$$

The net electric field just underneath the surface is:

$$E_r = -\frac{\Omega B_o}{c} \left( \frac{R_{\text{NS}}^3}{r^2} \right) \sin \theta \cos \theta \cos(\phi - \Omega t) \quad (4.38)$$

$$E_\theta = -\frac{2\Omega B_o}{c} \left( \frac{R_{\text{NS}}^3}{r^2} \right) \sin^2 \theta \cos(\phi - \Omega t) \quad (4.39)$$

$$E_\phi = 0 \quad (4.40)$$

For the electric field outside the NS surface one proceeds following the same approach as in the aligned case. Assuming a vacuum, one looks for a solution of the form:  $\mathbf{E} = \mathbf{E}_{\text{ind}} + \mathbf{E}_{\text{vac}}$  such that:

$$\nabla \wedge \mathbf{E}_{\text{ind}} = -\frac{1}{c} \frac{\partial \mathbf{B}}{\partial t} \quad \text{and} \quad \mathbf{E}_{\text{vac}} = \nabla \Phi_{\text{vac}} \quad \text{such that} \quad \nabla^2 \Phi_{\text{vac}} = 0 \quad (4.41)$$

given that  $\nabla \cdot \mathbf{E}_{\text{ind}} = 0$ , and  $\nabla \wedge \mathbf{E}_{\text{vac}} = 0$ . The induction part  $\mathbf{E}_{\text{ind}}$  is the same as the one computed before. The vacuum part instead can again be expressed using spherical harmonics. In particular, the only harmonic that provides the correct angular dependence to match the tangential electric field at the surface, is the  $l = 2$ ,  $m = 1$ ,  $Y_2^1$ , real harmonic  $\propto r^{-3} \sin \theta \cos \theta \cos \phi$ . One finds:

$$\Phi_{\text{vac}} = \frac{\Omega B_o}{c} \left( \frac{R_{\text{NS}}^5}{r^3} \right) \sin \theta \cos \theta \cos(\phi - \Omega t) + \frac{B}{r} \quad (4.42)$$

where the coefficient is selected to match the electric field at the surface. As before we have added a monopolar component, which is arbitrary. For simplicity we will now neglect it. We recall however that this implies that there might be a net surface charge at the magnetic pole. We will show that now this charge is zero for  $B = 0$ .

The net electric field just outside the NS surface is:

$$E_r = -\frac{3\Omega B_o}{c} \left( \frac{R_{\text{NS}}^5}{r^4} \right) \sin \theta \cos \theta \cos(\phi - \Omega t) \quad (4.43)$$

$$E_\theta = -\frac{\Omega B_o}{c} \left[ \left( \frac{R_{\text{NS}}^5}{r^4} \right) \cos(2\theta) - \left( \frac{R_{\text{NS}}^3}{r^2} \right) \right] \cos(\phi - \Omega t) \quad (4.44)$$

$$E_\phi = \frac{\Omega B_o}{c} \left[ \left( \frac{R_{\text{NS}}^3}{r^2} \right) - \left( \frac{R_{\text{NS}}^5}{r^4} \right) \right] \cos \theta \sin(\phi - \Omega t) \quad (4.45)$$

which, as required, at the surface matches the internal tangential component.

So one has that just above the surface:

$$\mathbf{E} \cdot \mathbf{B} = \frac{4\Omega R_{\text{NS}} B_o^2}{c} \sin^2 \theta \cos \theta \cos^2(\phi - \Omega t) \quad (4.46)$$

Close to the the polar cap, whose location is defined by  $\phi = \Omega t$ ,  $\theta = \pi/2$ , one has:

$$E_{\parallel} = \frac{\mathbf{E} \cdot \mathbf{B}}{B_o} \approx \frac{2\Omega R_{\text{NS}} B_o}{c} \sin^2 \theta \cos \theta \cos^2 (\phi - \Omega t) \approx 0 + \mathcal{O}(\theta - \pi/2) + \mathcal{O}(\phi - \Omega t)^2 \quad (4.47)$$

Again apart from a different numerical coefficient, and a more complex angular dependence, the same result as in the aligned case. As we anticipated with  $B = 0$  one find that at the magnetic pole, the outer radial electric field vanishes, and the net surface charge is thus zero.

## 4.5 QED Pair Creation

In this section we present a heuristic derivation of the photon pair production in a strong magnetic field. The correct derivation of this process requires the full machinery of QED: quantization of the EM field and the use of Dirac equation for electrons and positrons. Here instead we will take a *poor-man approach* based on a physical picture of the behavior of virtual pairs in a magnetic field.

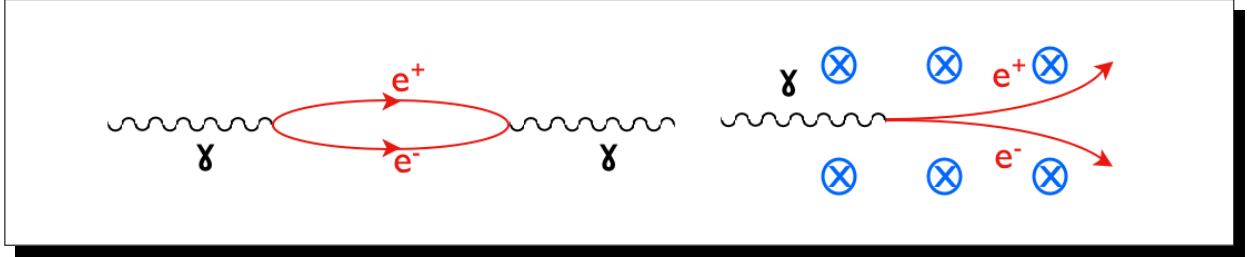


**Figure 4.7:** Left part: virtual pair creation by a photon during its propagation. Right part: virtual/real pair creation by a photon in a magnetic field.

It is a known result of QED that photons can turn into a virtual  $e^{\pm}$  pair as they propagate. Usually this pair annihilates back to the original photon. However there is a finite possibility for this pair to interact with the environment (for example an external EM field) before annihilation. This leads to *QED non-linear effects*.

Let us concentrate on high energy photons  $h\nu > 2m_e c^2$ . Lower energy photon can never produce pairs, because they do not have enough energy. However, even higher energy photons cannot spontaneously create a pair. This because the creation of a pair cannot simultaneously satisfy conservation of momentum and energy. The momentum and energy of a photon of frequency  $\nu$  go into the momentum and energy of the pair according to;

$$h\nu/c \rightarrow 2m_e c \gamma \beta, \quad h\nu \rightarrow 2m_e c^2 \gamma. \quad (4.48)$$

If we assume a high energy photon, such that  $\beta \rightarrow 1$ , and assume momentum conservation, we get that the energy law is violated. The pair has an excess energy  $\Delta E$  given by:

$$\Delta E = 2m_e c^2 \gamma - h\nu = h\nu/\beta - h\nu = h\nu \frac{1-\beta}{\beta} \approx \frac{h\nu}{2\gamma^2} \approx \frac{h\nu}{\gamma^2} \quad (4.49)$$

where we have used  $\beta = \sqrt{1-1/\gamma^2}$ . This excess energy sets the typical lifetime of the pair, according to Heisenberg uncertainty principle:

$$\Delta t \simeq \frac{\hbar}{\Delta E} \approx \frac{\gamma^2}{\nu} \quad (4.50)$$

Pay attention that the same result can be derived if one assumes energy conservation and momentum violation, and then defines the lifetime as the position uncertainty over the speed of light.

In a magnetic field, the two virtual charges would drift apart due to the action of the Lorentz force. If, during their lifetime, they drift apart enough that their wave-function do not overlap, then the probability of annihilation will be strongly reduced. Physically speaking, the magnetic field will provide the required energy/momentum to satisfy momentum conservation. The intensity of non-linear QED effects will be related to how much the pair can drift apart during its lifetime.

Before proceeding, we introduce two quantities, that will be useful in the discussion. One is the so called *critical magnetic field*:

$$B_Q = \frac{m_e^2 c^3}{e \hbar} = 4.413 \times 10^{13} \text{ G} \quad (4.51)$$

It is the magnetic field at which the classical cyclotron energy (the energy of the ground Landau level) equals the rest mass energy of the electron.

$$\hbar \omega_c = \hbar \frac{eB}{m_e c} = m_e c^2 \frac{B}{B_Q} \quad (4.52)$$

where  $\omega_c$  is the cyclotron frequency. The other is the *electron Compton wavelength*:

$$\lambda_c = \frac{\hbar}{m_e c} = 3.86 \times 10^{-11} \text{ cm} \quad (4.53)$$

The Compton wavelength can be thought of as a fundamental limitation on measuring the position of a particle. As such it sets the typical extent of the electron/positron wave function of the virtual pair (their size). It also sets the cross-section of interactions in QED.

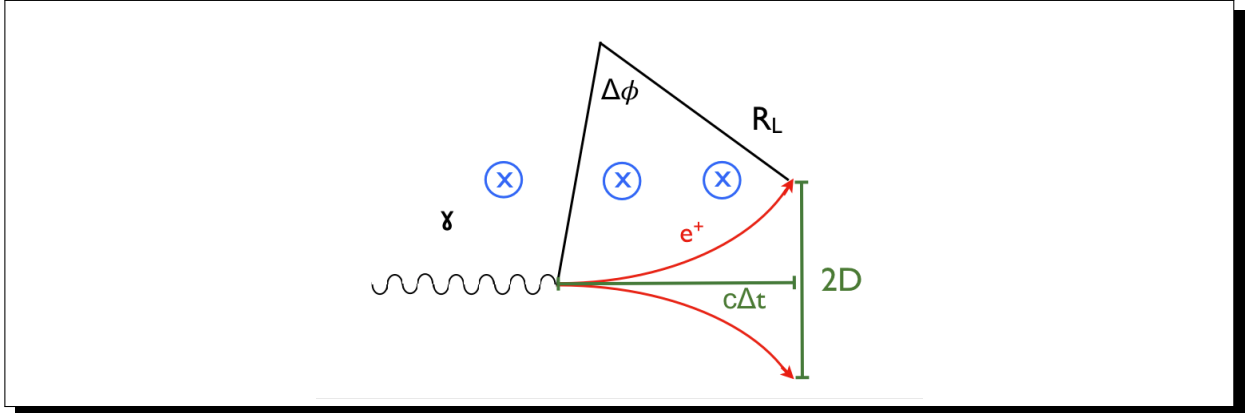


**Figure 4.8:** Geometry of the virtual/ral pair created by a photon as the drift in the external magnetic field..

Let us now compute how much the pair drift apart, assuming the magnetic field to be perpendicular to the photon propagation. The Larmor radius of the virtual pair in the external magnetic field is:

$$R_L = \frac{\gamma m_e c^2}{eB} = \frac{e \hbar}{m_e^2 c^3} \frac{B_Q}{B} \frac{\gamma m_e c^2}{e} = \gamma \frac{B_Q}{B} \lambda_c \quad (4.54)$$

Overt its typical lifetime  $\Delta t$  a pair will move along the photon direction an amount  $\approx c \Delta t$ . Due to the magnetic field the trajectory is curved, and the gyration angle will be  $\Delta \phi \approx c \Delta t / R_L$ . The drift distance will be  $D \approx c \Delta t \Delta \phi \approx (c \Delta t)^2 / R_L$ .

Note that we are allowed to use the classical trajectory in the limit  $B < B_Q$  (valid for PSRs), because  $\hbar \nu \gg \hbar \omega_c = \hbar e c / m_e B = m_e c^2 B / B_Q$  (we are implicitly assuming that the photon energy is high enough to produce a pair,  $\hbar \nu \gg m_e c^2$ ).

Working out the math:

$$D \approx \frac{B}{B_Q} \frac{1}{c\lambda_c} \left( \frac{\gamma^2 c}{\nu} \right)^2 = \left[ \frac{h\nu}{m_e c^2} \right]^4 \left( \frac{c}{\nu} \right)^2 \frac{m_e c^2}{h\nu} \frac{1}{\lambda_c} \frac{B}{B_Q} = \frac{h\nu}{m_e c^2} \frac{B}{B_Q} \left( \frac{h}{m_e c} \right)^2 \frac{1}{\lambda_c} \approx \lambda_c \left[ \frac{h\nu}{m_e c^2} \right] \left[ \frac{B}{B_Q} \right],$$

which immediately identifies the scale parameter  $\chi$  of QED:

$$\chi = \left[ \frac{h\nu}{m_e c^2} \right] \left[ \frac{B}{B_Q} \right] \quad (4.55)$$

Interestingly one can immediately guess that non-linear QED effect will be absent for photon propagating along the magnetic field, because in this case the Lorentz force on the virtual pair will be zero. Indeed this is the case even for a full QED derivation.

- For  $\chi \gg 1$  the pair separates more than  $\lambda_c$ , which implies that after a typical lifetime the wave-functions of the two virtual particles do not overlap and annihilation is suppressed.
- For  $\chi \ll 1$  the pair separates less than  $\lambda_c$ , which implies that after a typical lifetime the wave-functions of the two virtual particles still overlap and pair creation is suppressed. In particular, the probability to create a real pairs will be exponentially suppressed (pair creation is in this case a tunneling effect):  $P_{\text{creation}} \approx \text{Exp}[-1/\chi]$ . The correct QED solution is, in the limit  $\chi \ll 1$ ,  $P_{\text{creation}} = 0.5 \text{Exp}[-4/3\chi]$

For  $\chi \ll 1$  the pair never separates more than  $\lambda_c$ , so one can think of  $\lambda_c$  as the transverse dimension of the photon. This is the regime of interest for a PSR, so we will limit our discussion to this case.

We can define the *attenuation length*,  $L_a$  as the mean free path of a photon for pair creation. The pair creation process can be seen as an interaction of the photon with the magnetic field. In the same way as the photon field is quantized, also the magnetic field is quantized. More precisely the magnetic flux is quantized, and the magnetic flux quantum is given by the flux through a surface corresponding to the lowest Landau level:  $\Phi_B = \hbar c/e$ .

The number of magnetic flux quanta intercepted by a photon as it propagates a distance  $L$  is:  $n_B \approx L\lambda_c B/\Phi_B$ . The probability of a pair creation will be given by the number of magnetic flux quanta intercepted, times the coupling constant of QED (the fine structure constant  $\alpha$ ) times the probability of pair creation for single event:

$$\approx n_B \alpha e^{-4/3\chi} = \frac{L\lambda_c B \alpha}{\Phi_B} e^{-4/3\chi} \quad (4.56)$$

Setting this quantity equal to unity, gives the the attenuation length:

$$\begin{aligned} L_a^{-1} &\approx \frac{\lambda_c B_Q \alpha}{\Phi_B} \left( \frac{B}{B_Q} \right) e^{-4/3\chi} = \frac{\hbar}{mc} \frac{e}{\hbar c} \frac{m_e^2 c^3}{e\hbar} \alpha \left( \frac{B}{B_Q} \right) e^{-4/3\chi} = \frac{m_e c}{\hbar} \alpha \left( \frac{B}{B_Q} \right) e^{-4/3\chi} \\ &\approx \frac{\alpha}{\lambda_c} \left( \frac{B}{B_Q} \right) e^{-4/3\chi} \end{aligned} \quad (4.57)$$

where more generally  $B$  is the perpendicular magnetic field or  $L_a$  is the attenuation length in the transverse direction to the magnetic field.

## 4.6 Pair Creation in the Polar Cap

We saw in section 4.3 that, if a vacuum forms outside the surface of the NS, a strong parallel electric field arises that can extract and accelerate particles to replenish the magnetosphere. In particular, this process is going to be relevant in the open field line region. Let us investigate what happens to particles extracted in the polar cap. These particles will be rapidly accelerated to ultrarelativistic speeds over a distance  $l \ll R_{\text{NS}}$ . In the strong magnetic field of PSRs these particles will simply follow the magnetic field lines. Any amount of energy in the transverse direction will be rapidly lost due to synchrotron emission. The synchrotron power for an electron gyrating in a magnetic field  $B$ , and its typical lifetime  $\tau_{\text{syn}}$  are:

$$P_{\text{syn}} = \frac{2}{3} \frac{e^4}{m_e^2 c^3} \gamma^2 B^2 \quad \rightarrow \quad \tau_{\text{syn}} = \frac{\gamma m_e c^2}{P_{\text{syn}}} \simeq \frac{m_e^3 c^5}{e^4} \gamma^{-1} B^{-2} = 3 \times 10^{-16} \gamma^{-1} \left( \frac{B}{10^{12} \text{ G}} \right)^{-2} \text{ s} \quad (4.58)$$

indicating that any energy in transverse motion will be rapidly lost over distances  $\ll 1 \text{ cm}$ .

In the polar cap, particles (say electrons) can be accelerated to high Lorentz factor over very short distances. Moving along curved field lines they will emit curvature radiation. If the Lorentz factor is high enough, the energy of the emitted photon can be above the kinematic threshold for pair production ( $h\nu > 2m_e c^2 = 1 \text{ MeV}$ ). This photon can then interact with the magnetic field, and produce a new pair. The new pair will be then accelerated and the process can repeat, giving rise to a *pair creation cascade*. It is this process that provides the required charges to fill the magnetosphere and ultimately shorten the parallel electric field.

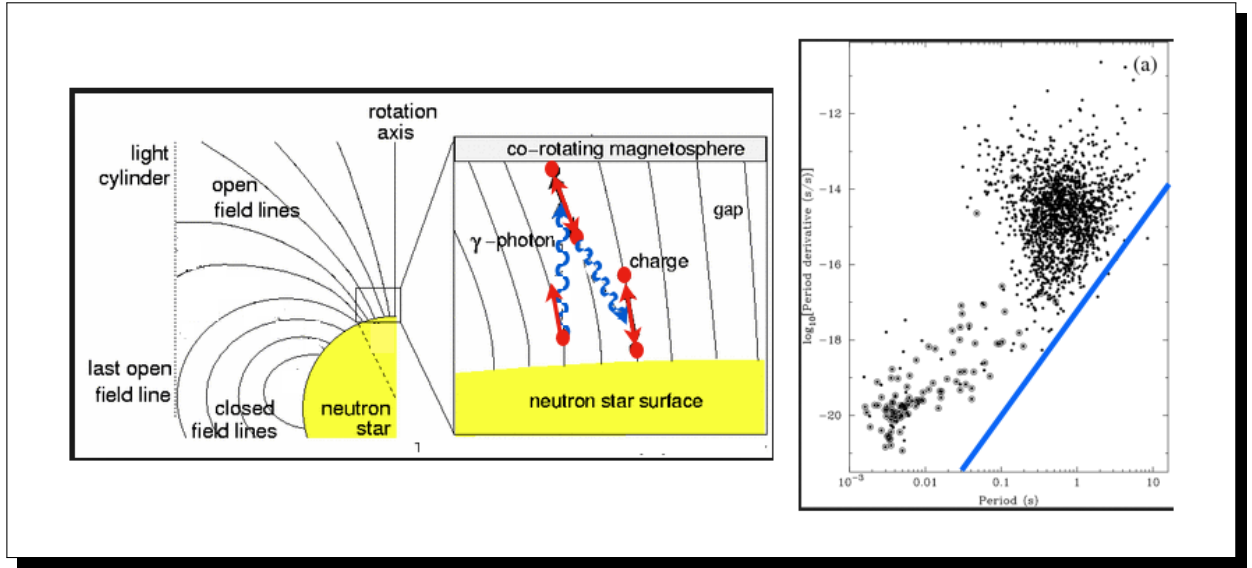


**Figure 4.9:** Left part: scheme of the pair production in a polar cap. Right part:  $P$ - $\dot{P}$  diagram and the location of the death line.

Three requirements must be satisfied for the pair cascade to work:

- particles must be accelerated to Lorentz factors high enough such that the curvature photons they produce are above the kinematic threshold. The energy of a curvature photon, emitted by an electron with Lorentz factor  $\gamma$  is  $h\nu = h\gamma^3 c/R_c$ , where  $R_c \approx R_{\text{NS}}$  is the radius of curvature of the magnetic field line. Given that the Lorentz factor depends on the accelerating distance  $l$  according to Eq. 4.26, the above condition reduces to a condition on  $l$  itself:

$$l > 2 \left[ \frac{m_e^4 c^{13}}{B^3 e^3 \Omega^6 h R_{\text{NS}}} \right]^{1/3} \approx 10^3 \left[ \frac{B}{10^{12} \text{ G}} \right]^{-1} \left[ \frac{\Omega}{30 \text{ s}^{-1}} \right]^{-2} \text{ cm} \quad \ll R_{\text{NS}} \ll R_{\text{LC}} \quad (4.59)$$

- the accelerated particle must be able to emit at least one of these high energy photons. This again can be translated into a condition on how far the particle should move along a field line, based on the power of curvature radiation:

$$P_{\text{curv}} = \frac{2}{3} \frac{e^2}{c^3} \gamma^4 \left( \frac{c^2}{R_c} \right)^2 \quad (4.60)$$

the number of photons  $n_\gamma$  of energy  $h\nu \simeq 2m_e c^2$  produced by the particle in the time it travels a distance  $l$  is:

$$n_\gamma = \frac{P_{\text{curv}} l}{h\nu c} = \frac{P_{\text{curv}}}{2m_e c^3} l > 1 \quad (4.61)$$

$$\rightarrow l > \left[ \frac{c^5 \hbar m_e}{e^3 B \Omega^2 R_{\text{NS}}} \right]^{\frac{1}{2}} \approx 5 \times 10^2 \left[ \frac{B}{10^{12} \text{ G}} \right]^{-\frac{1}{2}} \left[ \frac{\Omega}{30 \text{ s}^{-1}} \right]^{-1} \text{ cm} \ll R_{\text{NS}} \ll R_{\text{LC}} \quad (4.62)$$

- the emitted photon must pair create in the external magnetic field. This implies a condition on the distance  $l$  travelled by the photon that must be equal to the attenuation length. Recalling that it is the transverse component of the magnetic field that matters,  $B_\perp = Bl/R_c$ , and that the relevant quantity to compare with the attenuation length is the transverse direction  $l^2/R_c$ , the condition is:

$$\frac{l^2}{R_c} > \frac{\lambda_c}{\alpha} \left( \frac{B}{B_Q} \right) \text{Exp} \left[ \frac{4}{3} \frac{m_e c^2}{h\nu} \frac{B_Q}{B_\perp} \right] \quad (4.63)$$

For typical PSR parameters  $B = 10^{12} \text{ G}$ ,  $\Omega = 30 \text{ s}^{-1}$ , with  $R_c = R_{\text{NS}}$ , one gets  $l > 10^4 \text{ cm} \ll R_{\text{NS}} \ll R_{\text{LC}}$ . Such value is not much sensitive to the PSR parameters.

It is evident that the particles accelerated by the parallel electric field over the polar cap, will be able to produce a pair cascade over distances of a few hundreds of meters above the NS surface. Ultimately the charges that are created will shorten the electric field and a situation will arise where the parallel component of the electric field is negligible. The numbers of pair produced per every primary particle extracted by the PSR is known as *pair multiplicity* and for the Crab Pulsar is estimated to be  $\sim 10^5$ .

From the first condition on the energy of the emitted photon one can derive the so called *death condition* for PSRs, the condition for which pair creation ceases to operate and the PSR does not emit any longer. Recalling that the dipole magnetic field can be defined in terms of the period and its period derivative as:

$$B = 3 \times 10^{19} \sqrt{P\dot{P}} \text{ G} \quad (4.64)$$

and assuming that the limit for pair creation is  $l < R_{\text{NS}}$  one gets that the pair creation condition can be written as:

$$\left[ \frac{B}{10^{12} \text{ G}} \right] \left[ \frac{\Omega}{30 \text{ s}^{-1}} \right]^2 \approx 10^6 \sqrt{P\dot{P}} \left( \frac{P}{1 \text{ s}} \right)^{-2} > 10^{-3} \rightarrow \dot{P} > 10^{-18} \left( \frac{P}{1 \text{ s}} \right)^3 \quad (4.65)$$

This relation define the so called *death line* in the  $P-\dot{P}$  diagram. The region below it is called *the graveyard*.

## 4.7 The Force Free Pulsar Equation

The end result of the pair creation process is that in the PSR magnetosphere a sufficient charge density develops to shorten the parallel electric field. A situation will arise where the net EM force acting on a charged plasma will be zero:

$$\rho_e \mathbf{E} + \frac{\mathbf{J}}{c} \wedge \mathbf{B} = 0 \quad (4.66)$$

where  $\rho_e$  is the charge density and  $\mathbf{J}$  is the current density. This condition is known as *force-free condition*, and implies that the parallel electric field vanishes  $\mathbf{E} \cdot \mathbf{B} = 0$ .

Let us consider the simplest geometry of an aligned rotator, Fig.4.10. For this problem we will consider a cylindrical reference frame  $R, z, \phi$ , with the  $z$ -axis coincident with the rotation axis and the symmetry axis of the problem.

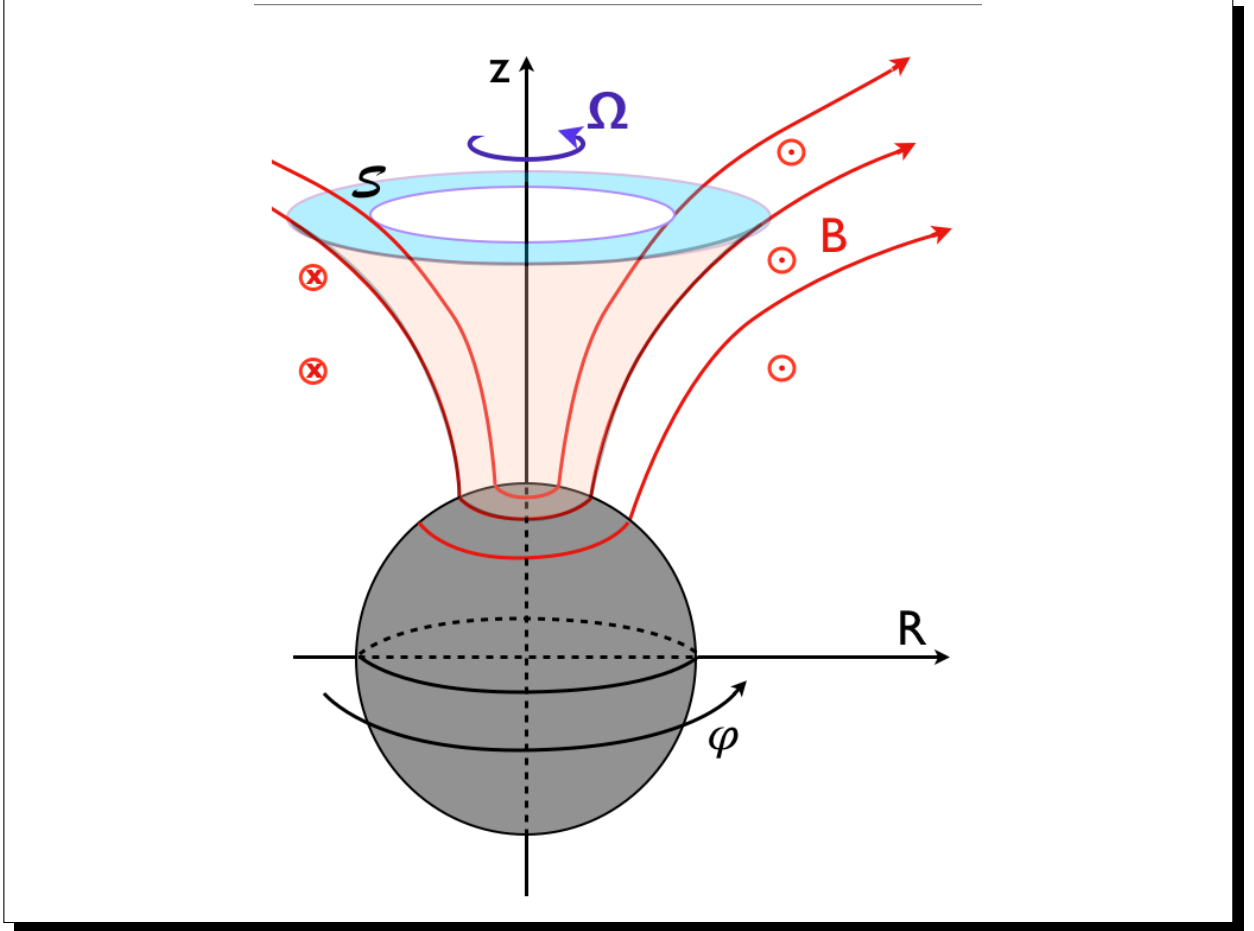


**Figure 4.10:** Scheme of the geometry of the Force Free PSR magnetosphere

The symmetry of the problem is such that the solution will be independent on the azimuthal angle  $\phi$ ,  $\partial_\phi = 0$ , and stationary in time  $\partial_t = 0$ . Let us begin by showing that in this case the azimuthal component of the electric field  $E_\phi$  vanishes. Axisymmetry implies  $\partial_\phi E_\phi = 0 \rightarrow E_\phi = E_\phi(R, z_o)$ , while stationarity implies:

$$\nabla \wedge \mathbf{E} = \frac{1}{c} \frac{\partial \mathbf{B}}{\partial t} = 0 \quad (4.67)$$

Let us apply this relation to a circular surface  $S$ , coaxial with the  $z$ -axis, with border  $\partial S$  at a vertical coordinate  $z_o$ . Using the circulation theorem:

$$\int_S \frac{1}{c} \frac{\partial \mathbf{B}}{\partial t} \cdot d\mathbf{s} = \int_S \nabla \wedge \mathbf{E} \cdot d\mathbf{s} = \int_{\partial S} \mathbf{E} \cdot d\mathbf{l} = \int_0^{2\pi} E_\phi(R, z_o) R d\phi = 0 \rightarrow E_\phi = 0 \quad (4.68)$$

for all  $R$  and  $z_o$ .

This result together with the force free condition implies that  $\mathbf{E} \perp \mathbf{e}_\phi$  and  $\mathbf{E} \perp \mathbf{B}$ . One can thus write it in the form:

$$\mathbf{E} = \frac{\omega(R, z)R}{c} \mathbf{B} \wedge \mathbf{e}_\phi \quad (4.69)$$

where  $\omega(R, z)$  is a generic function of position. Substituting this expression in the force free condition Eq. 4.66, one can find a relation between the current density and the magnetic field:

$$\rho_e \mathbf{E} + \frac{\mathbf{J}}{c} \wedge \mathbf{B} = \left( \frac{\mathbf{J}}{c} - \frac{\rho_e \omega(R, z) R}{c} \mathbf{e}_\phi \right) \wedge \mathbf{B} = 0 \quad \rightarrow \quad \mathbf{J} = \rho_e \omega(R, z) R \mathbf{e}_\phi + k \mathbf{B} \quad (4.70)$$

where  $k$  is a function to be determined. This relation implies that the current has a component aligned with the magnetic field, and another component that is purely toroidal.

Let us now turn to the magnetic field. The solenoidal condition for an axisymmetric field can be written as:

$$\nabla \cdot \mathbf{B} = \frac{1}{R} \frac{\partial(RB_R)}{\partial R} + \frac{\partial B_z}{\partial z} + \frac{1}{R} \frac{\partial B_\phi}{\partial \phi} = \frac{1}{R} \frac{\partial B_R}{\partial R} + \frac{\partial B_z}{\partial z} = \nabla \cdot \mathbf{B}_p = 0 \quad (4.71)$$

where  $\mathbf{B}_p = B_R \mathbf{e}_R + B_z \mathbf{e}_z$  is the poloidal component of the magnetic field. This implies that the poloidal magnetic field can be written as the curl of a toroidal vector potential, function of  $R$  and  $z$ :

$$\mathbf{B}_p = \frac{\nabla \Psi}{R} \wedge \mathbf{e}_\phi = -\frac{1}{R} \frac{\partial \Psi}{\partial z} \mathbf{e}_R + \frac{1}{R} \frac{\partial \Psi}{\partial R} \mathbf{e}_z \quad \rightarrow \quad \nabla \cdot \mathbf{B}_p = 0 \quad (4.72)$$

The scalar function  $\Psi$  is known as *Euler potential* or *magnetic flux function*. It allows one to reduce the problem of the poloidal field from two variables  $B_R$  and  $B_z$  to just one. Moreover it is evident that  $\mathbf{B}_p \cdot \nabla \Psi = 0$ , the poloidal magnetic field lines are orthogonal to the gradient of  $\Psi$ . This means that the surfaces  $\Psi = \text{const}$  represent the *magnetic surfaces* defined by the rotation of the poloidal field lines around the symmetry axis. Magnetic field lines lay on these surfaces. The various field lines on the same magnetic surface are all identified by the same value of  $\Psi$ .

Let us now go back to the electric field. We will derive here the value of the free function  $\omega(R, z)$ . Recalling that  $\mathbf{e}_\phi \wedge B_\phi \mathbf{e}_\phi = 0$ , and using Eq. 4.69 and Eq. 4.72, we get:

$$\mathbf{E} = \frac{\omega(R, z) R}{c} \mathbf{B} \wedge \mathbf{e}_\phi = \frac{\omega(R, z) R}{c} \left( \frac{\nabla \Psi}{R} \wedge \mathbf{e}_\phi \right) \wedge \mathbf{e}_\phi = -\frac{\omega(R, z)}{c} \nabla \Psi \quad (4.73)$$

where we have used the triple vector product rule,  $(\nabla \Psi \wedge \mathbf{e}_\phi) \wedge \mathbf{e}_\phi = (\mathbf{e}_\phi \cdot \nabla \Psi) \mathbf{e}_\phi - (\mathbf{e}_\phi \cdot \mathbf{e}_\phi) \nabla \Psi$ , and the axisymmetric assumption,  $(\mathbf{e}_\phi \cdot \nabla \Psi) = \partial_\phi \Psi = 0$ .

Stationarity implies:

$$\frac{1}{c} \frac{\partial \mathbf{B}}{\partial t} = 0 = \nabla \wedge \mathbf{E} = -\frac{1}{c} \nabla \wedge (\omega \nabla \Psi) = -\frac{1}{c} (\nabla \omega \wedge \nabla \Psi + \omega \nabla \wedge \nabla \Psi) = -\frac{1}{c} \nabla \omega \wedge \nabla \Psi = 0 \quad (4.74)$$

where we dropped the explicit  $R, z$  dependence of  $\omega$ . This states that  $\nabla \omega$  is parallel to  $\nabla \Psi$ , meaning that  $\omega$  is constant on magnetic surfaces  $\Psi = \text{const}$  ( $\omega$  is constant along a magnetic field line), and one can write  $\omega(R, z) = \omega(\Psi)$ . At the surface of the NS, assuming corotation of the plasma,  $\mathbf{v} = \Omega R \mathbf{e}_\phi$ , from the Ideal MHD condition one gets:

$$\mathbf{E} = -\frac{1}{c} \mathbf{v} \wedge \mathbf{B} = \frac{\Omega R}{c} \mathbf{B} \wedge \mathbf{e}_\phi = -\frac{\Omega}{c} \nabla \Psi \quad \rightarrow \quad \omega = \Omega \quad (4.75)$$

In case of rigid rotation  $\Omega = \text{const}$ , one finds that the Euler potential is equal to the electrostatic potential times the rotation rate.

At this point we can derive the charge density and current density for the plasma in the magnetosphere:

$$\rho_e = \frac{\nabla \cdot \mathbf{E}}{4\pi} = -\frac{\Omega}{4\pi c} \nabla^2 \Psi = -\frac{\Omega}{4\pi c} \left( \frac{\partial^2 \Psi}{\partial R^2} + \frac{1}{R} \frac{\partial \Psi}{\partial R} + \frac{\partial^2 \Psi}{\partial z^2} \right) \quad (4.76)$$

while using Eq. 4.70, and recalling that for a steady state  $4\pi \mathbf{J}/c = \nabla \wedge \mathbf{B}$ , we get:

$$\begin{aligned} J_\phi &= \frac{c}{4\pi} (\nabla \wedge \mathbf{B})_\phi = \frac{c}{4\pi} \left( \frac{\partial B_R}{\partial z} - \frac{\partial B_z}{\partial R} \right) = -\frac{c}{4\pi R} \left( \frac{\partial^2 \Psi}{\partial z^2} + \frac{\partial^2 \Psi}{\partial R^2} - \frac{1}{R} \frac{\partial \Psi}{\partial R} \right) = \\ &= -\frac{\Omega^2 R}{4\pi c} \left( \frac{\partial^2 \Psi}{\partial R^2} + \frac{1}{R} \frac{\partial \Psi}{\partial R} + \frac{\partial^2 \Psi}{\partial z^2} \right) + k B_\phi \end{aligned} \quad (4.77)$$

This equation can be rewritten as:

$$\begin{aligned}
\frac{4\pi k}{c} B_\phi &= \left( \frac{\partial^2 \Psi}{\partial R^2} + \frac{\partial^2 \Psi}{\partial z^2} \right) \left[ \frac{\Omega^2 R}{c^2} - \frac{1}{R} \right] + \frac{1}{R} \frac{\partial \Psi}{\partial R} \left[ \frac{\Omega^2 R}{c^2} + \frac{1}{R} \right] \\
&= \left( \frac{\partial^2 \Psi}{\partial R^2} + \frac{\partial^2 \Psi}{\partial z^2} \right) \left[ \frac{\Omega^2}{c^2} - \frac{1}{R^2} \right] R + \frac{1}{R} \frac{\partial \Psi}{\partial R} \left[ \frac{\Omega^2}{c^2} + \frac{1}{R^2} \right] R \\
&= \left( \frac{\partial^2 \Psi}{\partial R^2} + \frac{\partial^2 \Psi}{\partial z^2} \right) \left[ \frac{R^2 - R_{\text{LC}}^2}{R^2 R_{\text{LC}}^2} \right] R + \frac{1}{R} \frac{\partial \Psi}{\partial R} \left[ \frac{R^2 + R_{\text{LC}}^2}{R^2 R_{\text{LC}}^2} \right] R
\end{aligned} \tag{4.78}$$

where we have used  $R_{\text{LC}} = c/\Omega$ . From this, one gets:

$$-\frac{4\pi k}{c} \frac{R_{\text{LC}}^2 R}{R_{\text{LC}}^2 - R^2} B_\phi = \left( \frac{\partial^2 \Psi}{\partial R^2} + \frac{\partial^2 \Psi}{\partial z^2} \right) - \frac{1}{R} \left[ \frac{R_{\text{LC}}^2 + R^2}{R_{\text{LC}}^2 - R^2} \right] \frac{\partial \Psi}{\partial R} \tag{4.79}$$

In order to solve this equation, or at least to cast it in a closed form, one needs to find how  $B_\phi$  and  $k$  depend on  $\Psi$ .

Using Eq. 4.70, the condition of stationarity  $\partial_t = 0$ , and axisymmetry  $\partial_\phi = 0$ , one finds from the charge conservation law:

$$\nabla \cdot \mathbf{J} = 0 = \nabla \cdot (k\mathbf{B}) = \nabla k \cdot \mathbf{B} + k \nabla \cdot \mathbf{B} = \nabla k \cdot \mathbf{B}_p = (\nabla k \wedge \nabla \Psi) \cdot \frac{\mathbf{e}_\phi}{R} = 0. \tag{4.80}$$

This is a relation similar to the one we found for  $\omega$ . It states that  $\nabla k$  is parallel to  $\nabla \Psi$ , implying the  $k$  is constant on the surfaces  $\Psi = \text{const}$  (i.e. along magnetic field lines), and one can write  $k = k(\Psi)$ .

At this point we can compute the total current flux through a circular surface  $\mathcal{S}$ , coaxial with the  $z$ -axis, with border  $\partial\mathcal{S}$  at a vertical coordinate  $z_o$ :

$$I = \int_{\mathcal{S}} \mathbf{J} \cdot d\mathbf{A} = 2\pi \int_0^R J_z R dR = 2\pi \int_0^R k B_z R dR = 2\pi \int_0^R k \frac{\partial \Psi}{\partial R} dR \tag{4.81}$$

which implies that the net current through a magnetic surface is just a function of  $\Psi$ :  $I(\Psi)$ . From this we have:

$$\frac{\partial I}{\partial R} = 2\pi k \frac{\partial \Psi}{\partial R} \quad \rightarrow \quad k = \frac{1}{2\pi} \frac{\partial I}{\partial \Psi} \tag{4.82}$$

We have also from the circulation theorem:

$$I = \int_{\mathcal{S}} \mathbf{J} \cdot d\mathbf{A} = \frac{c}{4\pi} \int_{\mathcal{S}} \nabla \wedge \mathbf{B} \cdot d\mathbf{A} = \frac{c}{4\pi} \int_{\partial\mathcal{S}} \mathbf{B} \cdot d\mathbf{l} = \frac{c}{4\pi} \int_0^{2\pi} B_\phi R d\phi = \frac{c}{2} R B_\phi(R, z_o) \tag{4.83}$$

Finally, using the same approach, let us compute the total magnetic flux through a circular surface  $\mathcal{S}$ , coaxial with the  $z$ -axis, with border  $\partial\mathcal{S}$  at a vertical coordinate  $z_o$ :

$$\Phi_B = \int_{\mathcal{S}} \mathbf{B} \cdot d\mathbf{A} = 2\pi \int_0^R B_z R dR = 2\pi \int_0^R \frac{\partial \Psi}{\partial R} dR = 2\pi \Psi(R, z_o) \tag{4.84}$$

whence we see that  $\Psi$  represents the total magnetic flux within the magnetic surface it labels.

Putting together Eq. 4.79 with Eq. 4.82 and Eq. 4.83, we find:

$$\left( \frac{\partial^2 \Psi}{\partial R^2} + \frac{\partial^2 \Psi}{\partial z^2} \right) - \frac{1}{R} \left[ \frac{R_{\text{LC}}^2 + R^2}{R_{\text{LC}}^2 - R^2} \right] \frac{\partial \Psi}{\partial R} = -\frac{4}{c^2} \frac{R_{\text{LC}}^2}{R_{\text{LC}}^2 - R^2} I(\Psi) \frac{\partial I(\Psi)}{\partial \Psi} \tag{4.85}$$

which is known as *pulsar equation*

This is an elliptical equation that must be solved using the appropriate boundary conditions. The boundary conditions on  $\Psi$  should be set at the surface of the star, depending on the local geometry of the poloidal component of the magnetic field. The function  $I$  is in general arbitrary. One could naively think that it is set by the value of the azimuthal magnetic field at the surface  $B_\phi(r = R_{\text{NS}})$ . However the function  $I$  cannot be fixed this way but must be chosen such that Eq. 4.85 is regular in  $R = R_{\text{LC}}$ . It is evident that at the Light Cylinder the denominators vanish in Eq. 4.85. Regularity requires:

$$\frac{\partial \Psi}{\partial R} = \frac{2R_{\text{LC}}}{c^2} I(\Psi) \frac{\partial I(\Psi)}{\partial \Psi} \quad (4.86)$$

It is this regularity condition that fixes the possible choices of  $I$ . The azimuthal magnetic field at the surface  $B_\phi$  is just the outcome. Physically the regularity condition at the Light Cylinder determines the structure of the magnetic field at the surface, and not the other way around.

## 4.8 The Split Monopole Solution

Despite its simplicity the pulsar equation has proved quite challenging to solve. It took more than 30 years to find a realistic dipolar solution, and only with the use of multidimensional numerical tools.

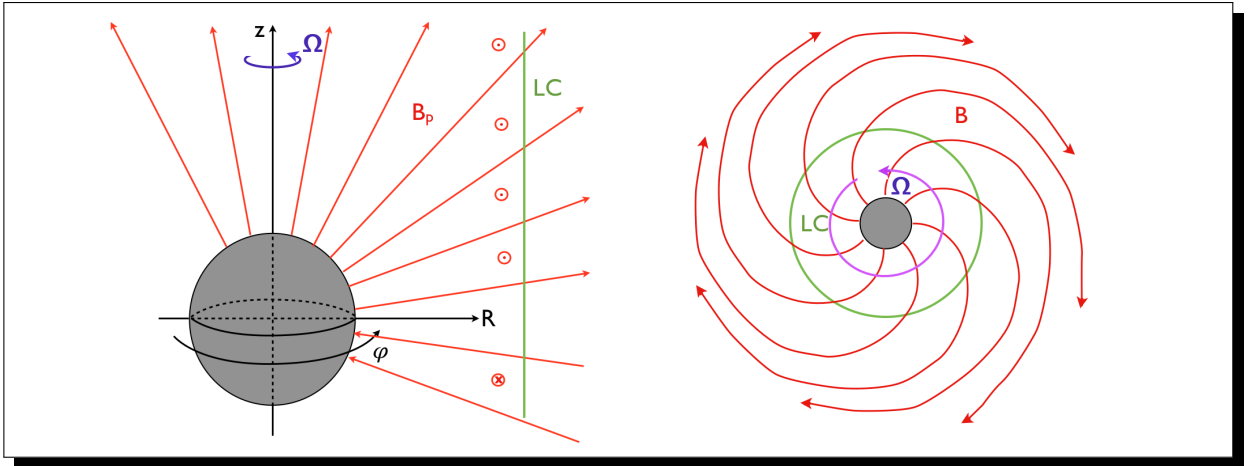


**Figure 4.11:** Geometry of the split monopole. Left part: side view. Right: top view.

There is however a very simple solution of the equation, that is fully analytic and that encapsulates the main properties of more complex results. Such solution is known as the *split monopole*. It corresponds to a magnetic configuration, where the magnetic field is purely radial  $B_\theta = 0$  and is uniform at the surface  $B_r(r = R_{\text{NS}}) = \pm B_o$ , where the sign changes between the north and south hemisphere in order to preserve  $\nabla \cdot \mathbf{B} = 0$  across any surface, even one containing the origin.

The first step is to write down the pulsar equation in terms of the adimensional coordinates  $\tilde{R} = R/R_{\text{LC}}$  and  $\tilde{z} = z/R_{\text{LC}}$ :

$$\left( \frac{\partial^2 \Psi}{\partial \tilde{R}^2} + \frac{\partial^2 \Psi}{\partial \tilde{z}^2} \right) - \frac{1}{\tilde{R}} \left[ \frac{1 + \tilde{R}^2}{1 - \tilde{R}^2} \right] \frac{\partial \Psi}{\partial \tilde{R}} = -\frac{4R_{\text{LC}}^2}{c^2} \frac{1}{1 - \tilde{R}^2} I(\Psi) \frac{\partial I(\Psi)}{\partial \Psi} \quad (4.87)$$

A radial uniform magnetic field, given the solenoidal condition  $\nabla \cdot \mathbf{B} = \partial_r(r^2 B_r)/r^2 = 0$ , can be written using spherical coordinates  $(r, \theta, \phi)$ , in terms of its value at the radius of the Light Cylinder  $B(r = R_{\text{LC}}) = \tilde{B}_o$  as:

$$\mathbf{B}_p = \begin{cases} +\tilde{B}_o/\tilde{r}^2 \mathbf{e}_r & \text{if } \theta < \pi/2 \\ -\tilde{B}_o/\tilde{r}^2 \mathbf{e}_r & \text{if } \theta > \pi/2 \end{cases} \quad (4.88)$$

where again  $\tilde{r} = r/R_{\text{LC}}$ . leading to:

$$\mathbf{B}_p = \begin{cases} +\tilde{B}_o \sin \theta / \tilde{r}^2 \mathbf{e}_R + \tilde{B}_o \cos \theta / \tilde{r}^2 \mathbf{e}_z & \text{if } \theta < \pi/2 \\ -\tilde{B}_o \sin \theta / \tilde{r}^2 \mathbf{e}_R - \tilde{B}_o \cos \theta / \tilde{r}^2 \mathbf{e}_z & \text{if } \theta > \pi/2 \end{cases} \quad (4.89)$$

And back in the original cylindrical coordinates:

$$\mathbf{B}_p = \begin{cases} +\tilde{B}_o \tilde{R} (\tilde{R}^2 + \tilde{z}^2)^{-3/2} \mathbf{e}_R + \tilde{B}_o \tilde{z} (\tilde{R}^2 + \tilde{z}^2)^{-3/2} \mathbf{e}_z & \text{if } \theta < \pi/2 \\ -\tilde{B}_o \tilde{R} (\tilde{R}^2 + \tilde{z}^2)^{-3/2} \mathbf{e}_R - \tilde{B}_o \tilde{z} (\tilde{R}^2 + \tilde{z}^2)^{-3/2} \mathbf{e}_z & \text{if } \theta > \pi/2 \end{cases} \quad (4.90)$$

The Euler potential leading to this field by Eq.4.72, can be computed from the enclosed magnetic flux, and it is:

$$\Psi = \frac{1}{2\pi} \int_S \mathbf{B} \cdot d\mathbf{A} = \int_0^\theta B_r r^2 \sin \theta d\theta = \pm \tilde{B}_o R_{\text{LC}}^2 (1 - \cos \theta) = \pm \tilde{B}_o R_{\text{LC}}^2 \left( 1 - \frac{\tilde{z}}{(\tilde{z}^2 + \tilde{R}^2)^{1/2}} \right) \quad (4.91)$$

where the sign depends on the hemisphere, and the dimensionality is that of a magnetic flux as expected. Note that, in principle, the Euler potential is always defined minus a constant, which is fixed by requiring it to be coincident with the enclosed magnetic flux.

Substituting this potential into the adimensionalized PSR equation Eq.4.87, one gets:

$$\mp \frac{2\tilde{B}_o R_{\text{LC}}^2 \tilde{R}^2 \tilde{z}}{(\tilde{R}^2 + \tilde{z}^2)^{3/2}} = \frac{4R_{\text{LC}}^2}{c^2} I(\Psi) \frac{\partial I(\Psi)}{\partial \Psi} \rightarrow \mp \frac{2\tilde{B}_o \tilde{R}^2 \tilde{z}}{(\tilde{R}^2 + \tilde{z}^2)^{3/2}} = \frac{4}{c^2} I(\Psi) \frac{\partial I(\Psi)}{\partial \Psi} \quad (4.92)$$

which has the following solution:

$$I(\Psi) = \mp \frac{c}{2R_{\text{LC}}} \Psi \left( 2 - \frac{\Psi}{\tilde{B}_o R_{\text{LC}}^2} \right) = \mp \frac{R_{\text{LC}} c \tilde{B}_o}{2} (1 - \cos \theta)(1 + \cos \theta) = \mp \frac{R_{\text{LC}} c \tilde{B}_o}{2} \sin^2 \theta \quad (4.93)$$

and this gives the azimuthal component of the magnetic field:

$$B_\phi = \mp \frac{R_{\text{LC}} \tilde{B}_o}{R} \sin^2 \theta = \mp \frac{R_{\text{LC}} \tilde{B}_o}{r} \sin \theta = -B_r \frac{r \sin \theta}{R_{\text{LC}}} \quad (4.94)$$

which shows that on the Light Cylinder the azimuthal component is equal to the poloidal one.

This is a result that holds also for more complex magnetic geometries. Moreover one finds that  $B_\phi/B_r \propto r \sin \theta$ : outside the LC the field is progressively more and more toroidal. The magnetic field lines are spirals: the rotation drag forward the foot-point of the field line, that trails backward. Already at  $10R_{\text{LC}}$  the toroidal component is 10 times stronger than the poloidal one and 100 times more energetic. The solution of the pulsar equation is asymptotically dominated by the toroidal component. Far away from the LC one can safely assume  $\mathbf{B} \approx B_\phi \mathbf{e}_\phi$

#### 4.8.1 Torque and Energy Losses

The split-monopole solution we have just derived, allows us to compute easily the energy and angular momentum losses, associated to a rotating force free magnetosphere.

To begin with, we compute the electric field, in a spherical coordinate system:

$$\mathbf{E} = -\frac{\Omega}{c}\nabla\Psi = \mp\frac{\Omega}{c}\tilde{B}_o R_{LC}^2 \frac{\sin\theta}{r}\mathbf{e}_\theta \quad (4.95)$$

The energy losses can be easily computed from the Poynting flux  $\mathbf{S}$ :

$$\mathbf{S} = \frac{c}{4\pi}\mathbf{E} \times \mathbf{B} = \frac{c}{4\pi}(E_\theta B_\phi \mathbf{e}_r - E_\theta B_r \mathbf{e}_\phi) = \frac{\Omega}{4\pi}\tilde{B}_o^2 R_{LC}^4 \frac{\sin\theta}{r^3}\mathbf{e}_\phi + \frac{\Omega}{4\pi}\tilde{B}_o^2 R_{LC}^3 \frac{\sin^2\theta}{r^2}\mathbf{e}_r \quad (4.96)$$

which is the same in the north and south hemisphere. The energy losses are associated with the radial component of the Poynting flux vector. Note that the latitudinal dependence of the energy flux is  $\propto \sin^2\theta$ . The flux is concentrated on the equatorial plane and goes to zero at the pole. This is not a collimated outflow.

$$\dot{E} = \int_0^{2\pi} d\phi \int_0^\pi \frac{\Omega}{4\pi}\tilde{B}_o^2 R_{LC}^3 \frac{\sin^2\theta}{r^2} r^2 \sin\theta d\theta = \frac{1}{2c}\tilde{B}_o^2 R_{LC}^4 \Omega^2 \int_0^\pi \sin^3\theta d\theta = \frac{2}{3}\frac{\mathcal{H}^2\Omega^2}{c} \quad (4.97)$$

independent on the radius at which it is computed. It is also evident that the energy losses can be written in terms of the two general independent invariants of the problem: the rotation rate  $\Omega$  and the *net open magnetic flux*,

$$\mathcal{H} = \frac{1}{4\pi} \int_{\text{sphere}} |B_r| r^2 \sin\theta d\theta d\phi \quad (4.98)$$

not to be confused with the total magnetic flux, which is always zero by the solenoidal condition.

In the same way one can compute the angular momentum losses  $\dot{L}$  associated to the  $\phi$  component of the Poynting flux:

$$\dot{L} = \int_0^{2\pi} d\phi \int_0^\pi S_\phi r \sin\theta r^2 \sin\theta d\theta d\phi = \frac{1}{2c}\tilde{B}_o^2 R_{LC}^4 \Omega \int_0^\pi \sin^3\theta d\theta = \frac{2}{3}\frac{\mathcal{H}^2\Omega}{c} \quad (4.99)$$

which show that  $\dot{E} = \Omega\dot{L}$  as expected for rotational energy losses.

Interestingly, despite being axisymmetric, this system has energy losses. This seems to contradict the statement that axisymmetric solutions of Maxwell equations have no energy losses. The difference is that, in this case, we are not dealing with a vacuum but with a space filled with charges and currents.

Note that the relation that we have derived for the split-monopole does not have the same scaling in terms of  $\Omega$  as the dipole spin-down formula. It corresponds instead to a braking index  $n = 1$ . The reason for this is the fact that we have assumed a purely monopolar structure for the field. There is no closed field line region. This also suggest a possible interpretation for the braking index: a braking index less than 3 can be interpreted as a magnetic geometry half way between a dipole and a monopole.

## 4.9 From the monopole to the dipole

The fact that the energy losses can be defined in terms of general independent invariants (quantities that do not depend on each other or on the radius where they are computed) suggests a way to renormalize the split-monopole solution to account for the dipolar structure of the magnetosphere inside the Light Cylinder.

Let us consider a surface far away from the LC, and compute there the general invariants. The location of such

surface is irrelevant. The rotation rate  $\Omega$  is always well defined. The net open flux instead needs some attention. Field lines that close within the LC, do not contribute any flux at large distances. The only field lines that extend beyond the LC (and they cannot close beyond the LC), are those coming from the polar cap. So the net open flux at infinity will be just the flux across the polar caps:

$$\mathcal{H} = \int_0^{\theta_{\text{cap}}} B_o \cos \theta R_{\text{NS}}^2 \sin \theta d\theta \approx B_o R_{\text{NS}}^2 \theta_{\text{cap}}^2 = B_o R_{\text{NS}}^3 \frac{\Omega}{c} \quad (4.100)$$

where we have assumed a dipolar field at the surface.

Substituting this effective net open flux in the formula for the split-monopole we get:

$$\dot{E} = \frac{2}{3c^3} B_o^2 R_{\text{NS}}^6 \Omega^4 \quad (4.101)$$

exactly the same scaling as the dipole radiation. The correct numerical coefficient, derived from more accurate numerical simulations, is not  $2/3$  but  $\approx 1$ .

It might seem surprising at first, that a force free solution, with all its complex distribution of charges and currents, gives exactly the same scaling that was found for the vacuum case. The reason is that, in both cases there are independent invariant quantities, and that there is only one possible combination of them with the correct dimensionality of energy losses.

Let us start with the split monopole. The two independent invariants are the rotation rate  $\Omega$  with dimensions  $[T^{-1}]$  and the net open flux  $\mathcal{H}$  with dimension  $[M^{1/2}L^{3/2}T^{-1}]$ . There is only one possible combination of them and the speed of light  $c$  with the dimensions of  $\dot{E}$  (i.e.  $[ML^2T^{-3}]$ ), and it is  $\mathcal{H}^2\Omega^2/c$ .

For the dipole, the net magnetic flux is not an invariant, because it depends on the size of the polar cap which is a function of the rotation rate. The invariant in this case is  $\mathcal{D} = \mathcal{H}/\Omega$ , as can be seen from Eq. 4.100. This is nothing else than the magnetic dipole moment. There is only one possible combination of the invariants  $\Omega$ ,  $\mathcal{D} = \mathcal{H}/\Omega$ , and  $c$  with the correct dimension for energy losses, and this is  $\mathcal{D}^2\Omega^4/c^3$ .

# CHAPTER 5

---

## PULSAR NEBULAE

---

### 5.1 Observations

A pulsar wind nebula (PWN, also known as "plerion", derived from a Greek word meaning "full") is a nebula powered by the pulsar wind of a pulsar. As we saw in the previous Chapter 4 and Sec. 4.7, a young pulsar, which is rapidly rotating, will lose its rotational energy via a relativistic wind. At the early stages (first few thousands of years) of their evolution, PWNe are often found inside the shells of the parent supernova remnants (SNR).

The first evidence that the pulsar transfer energy to the surrounding medium came from the Crab Nebula. The Crab Nebula is the remnant of a SN explosion that took place in 1054 AD. Its morphological aspect can be described as a combination of two distinct regions (see Fig. 5.1). The outer part shows a filamentary network, observed mostly in optical thermal emission lines, with typical expansion speeds of the order of  $1000 \text{ km s}^{-1}$ , corresponding to an expansion age of  $\sim 1000 \text{ yr}$ . The central region instead is filled with a uniform emission, characterized by a broadband non-thermal spectrum, extending from radio to X-ray and TeV energies, and a high degree of linear polarization. The Radio spectrum is well fitted by a power-law, and the same holds for the X-ray part, which however has a much steeper spectrum.

These characteristics are common to the class of PWNe: a flat spectral index in the radio band,  $\sim 0 - 0.3$  which steepens in the X-ray to  $2.3 - 3.3$ ; a highly linearly polarized flux; an increasing brightness towards the center.

Interestingly the typical X-ray luminosity of the Crab Nebula is about 10% of the spin-down luminosity of the pulsar, suggesting that it is indeed the pulsar itself to power the continuous emission from these objects.

Several PWNe are known today in different stages of evolution. They have also been found around older pulsars whose supernova remnants have disappeared, including millisecond radio pulsars. There are also systems where the pulsar, due to the kick velocity received at birth, has emerged from the SNR and is interacting directly with the ISM, giving rise to cometary shaped nebulae.

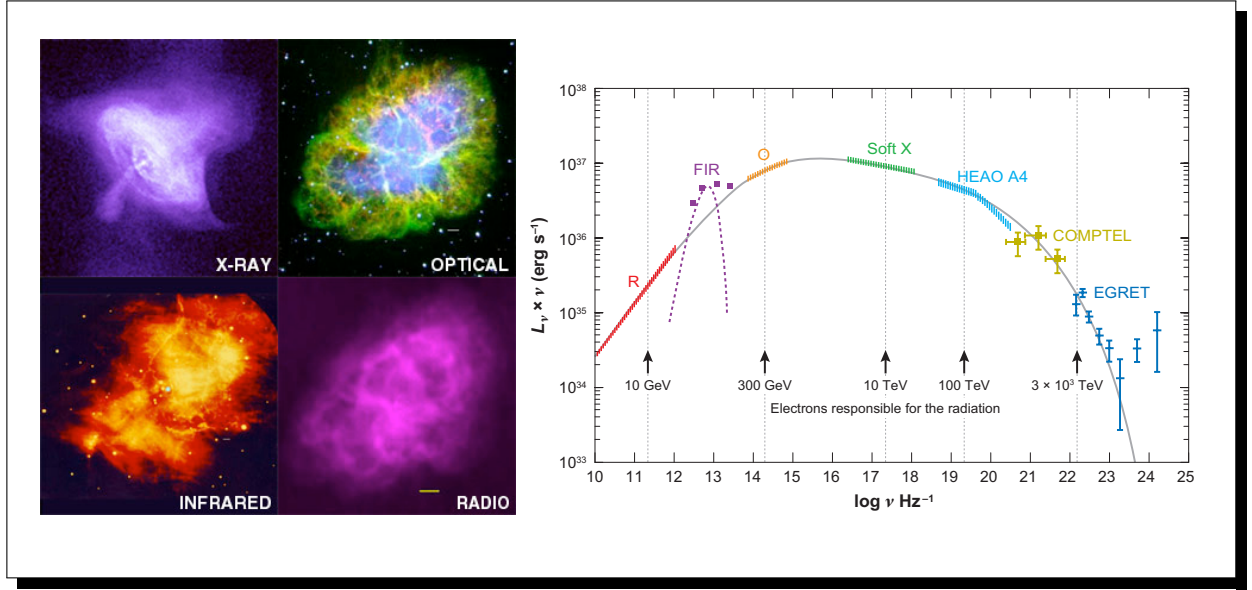


**Figure 5.1:** Left panel: images of the Crab Nebula in different bands. In optical the green filaments are a thermal lime emission, while the light blue is non-thermal synchrotron. Right panel: spectrum of the Crab Nebula from Radio to MeV.

## 5.2 PWNe Models

As we saw in Chapter 4 and Sec. 4.7 the pulsar wind is highly relativistic, while the typical expansion speeds of SNRs, are of the order of a few thousands  $\text{km s}^{-1}$ . Even if a PSR was to transfer all of its rotational energy to the SNR ejecta, the expansion speed  $V_{\text{pwn}}$  would be:

$$M_{\text{ej}} V_{\text{pwn}}^2 \simeq E_{\text{rot}} = \frac{I_{\text{NS}} \Omega_o^2}{2} \quad (5.1)$$

where  $M_{\text{ej}}$  is the ejecta mass,  $I_{\text{NS}}$  the NS moment of inertia and  $\Omega_o$  the spin-frequency at birth. For a typical PSR with  $I_{\text{NS}} \simeq 10^{45} \text{ g cm}^2$ , born with a period of  $\sim 0.01 \text{ s} \Rightarrow \Omega_o \simeq 600 \text{ s}^{-1}$ , inside a SNR with  $\sim 10 M_{\odot}$  of ejecta, one has:

$$V_{\text{pwn}} \simeq 10^8 \left( \frac{10 M_{\odot}}{M_{\text{ej}}} \right)^{1/2} \left( \frac{\Omega_o}{600} \right) \quad (5.2)$$

much smaller than the speed of light, and slightly smaller than typical SNR expansion speeds. This implies that the pulsar wind cannot force the surrounding medium to expand at the speed of light. Instead it will be the surrounding medium to force the pulsar wind to slow down. This interaction leads to the formation of a shock known as *termination shock* (TS). The PWN is the subsonic bubble formed by the wind downstream of the termination shock. A simple estimate for the location of the termination shock can be obtained by equating the pressure inside the PWN to the ram pressure of the wind. Neglecting the wind anisotropy, one has:

$$\frac{\dot{E}}{4\pi c R_{\text{TS}}^2} \approx P_{\text{pwn}} \approx \frac{E_{\text{pwn}}}{R_{\text{pwn}}^3} \approx \frac{\dot{E} t_{\text{pwn}}}{R_{\text{pwn}}^3} \Rightarrow R_{\text{TS}} \approx R_{\text{pwn}} \sqrt{\frac{V_{\text{pwn}}}{c}} \quad (5.3)$$

where  $E_{\text{pwn}}$  is the total energy in the nebula (for a relativistic subsonic fluid  $P_{\text{pwn}} = E_{\text{pwn}}/3$ ),  $t_{\text{pwn}}$  is the age of the nebula,  $R_{\text{pwn}}$  is its radius and we have assumed that the expansion speed is  $V_{\text{pwn}} \approx R_{\text{pwn}}/t_{\text{pwn}}$ . Given the typical expansion speeds derived above, one has that  $R_{\text{TS}} \approx R_{\text{pwn}}/20$ . Note also that the TS will expand outward at a speed comparable to the expansion speed of the nebula. In the Crab Nebula we observe in X-ray a dark central region, which obviously does not contain emitting material, and which is thought to represent the internal cavity occupied by the relativistic wind upstream of the TS.

To model the flow properties downstream of the TS one needs to solve first the shock jump conditions. The typical radius of the TS is much larger than the Light Cylinder (LC), and one can assume that the magnetic field is purely toroidal, and perpendicular to the wind flow velocity. Let us assume for simplicity a spherical TS (this is not strictly correct because of the energy flux anisotropy in the PSR wind). The wind will impact the shock perpendicularly to the shock surface.

Given its large radius, in comparison to the LC the shock can be treated as plane parallel, while given its slow speed with respect to the speed of light, it can be treated as stationary.

### 5.2.1 Shock Jump Conditions

At a stationary plane parallel shock, the relativistic conservation laws for the mass, momentum, energy, and magnetic field flux are:

$$\gamma_u \rho_u c = \gamma_d \rho_d v_d \quad (5.4)$$

$$(\rho_u c^2 + b_u^2) \gamma_u^2 c^2 + p_u + b_u^2/2 = (\rho_d c^2 + 4p_d + b_d^2) \gamma_d^2 v_d^2 + p_d + b_d^2/2 \quad (5.5)$$

$$(\rho_u c^2 + b_u^2) \gamma_u^2 c = (\rho_d c^2 + 4p_d + b_d^2) \gamma_d^2 v_d \quad (5.6)$$

$$b_u \gamma_u c = b_d \gamma_d v_d \quad (5.7)$$

where  $\rho$ ,  $p$  and  $b$  are the density, pressure and magnetic field in the comoving frame respectively,  $\gamma$  and  $v$  are the flow Lorentz factor and velocity measured in the shock frame (which given the small shock speed is equivalent to the PSR and lab frame), and the subscripts  $_u$  and  $_d$  refer to the upstream and downstream sides. We have moreover assumed that the upstream speed is  $c$ , the wind is cold  $p_u \ll \rho_u$ , and the adiabatic index downstream of the TS is  $4/3$ , appropriate for a relativistic fluid with  $p = e/3$ .

Let us introduce the following substitutions:

$$\rho_d \rightarrow c_1 \rho_u \gamma_u \quad p_d \rightarrow c_2 \rho_u \gamma_u^2 c^2 \quad b_d \rightarrow c_3 b_u \gamma_u \quad v_d \rightarrow \beta_d c \quad (5.8)$$

Then the equations for the jump become:

$$\gamma_u \rho_u (1 - c_1 \gamma_d \beta_d) = 0 \quad (5.9)$$

$$\frac{\gamma_u}{2} [(2 - c_3^2) b_u \gamma_u + 2(1 - c_2) \gamma_u \rho_u c^2 - 2\gamma_d^2 (c_3^2 b_u^2 \gamma_u + (c_1 + 4c_2 \gamma_u) \rho_u c^2) v_d^2] = 0 \quad (5.10)$$

$$\gamma_u^2 (\rho_u c^2 + b_u^2) - \gamma_u [\rho_u (c_1 + 4c_2 \gamma_u) c^2 + b_u^2 c_3^2 \gamma_u] \gamma_d^2 \beta_d = 0 \quad (5.11)$$

$$b_u \gamma_u (1 - c_3 \gamma_d \beta_d) = 0 \quad (5.12)$$

The first and the last have solution:

$$c_1 = c_3 = \frac{1}{\gamma_d \beta_d} \quad (5.13)$$

Defining a magnetization parameter of the upstream flow as  $\sigma = b_u^2 / \rho_u c^2$ , which is just the ratio of Poyting flux to kinetic energy flux, and using the solutions Eq. 5.13, then Eq. 5.11 has solution:

$$c_2 = \frac{2\gamma_d^2 \beta_d^2 (1 - \gamma_d \beta_d / \gamma_u) - \sigma}{2\gamma_d^2 \beta_d^2 (1 + 4\gamma_d^2 \beta_d^2)} \rightarrow \frac{2 - \sigma / \gamma_d^2 \beta_d^2}{2 + 8\gamma_d^2 \beta_d^2} \quad \text{in the limit } \gamma_u \rightarrow \infty \quad (5.14)$$

Substituting the solutions for  $c_1$ ,  $c_2$  and  $c_3$  in Eq. 5.10 one finds:

$$\frac{1}{1 + 4\gamma_d^2\beta_d^2}\gamma_u\rho_u[-\gamma_d\beta_d + \gamma_u(\beta_d(1 + 4\gamma_d^2(-1 + \beta_d)\beta_d) + \sigma(1 + \beta_d - 4\gamma_d^2\beta_d^2 + 4\gamma_d^2\beta_d^3))] = 0 \quad (5.15)$$

which in the limit  $\gamma_u \rightarrow \infty$  reduces to

$$\beta_d(1 + 4\gamma_d^2(-1 + \beta_d)\beta_d) + \sigma(1 + \beta_d - 4\gamma_d^2\beta_d^2 + 4\gamma_d^2\beta_d^3) = \frac{\sigma + \beta_d + 2\sigma\beta_d - 3\beta_d^2 - 3\sigma\beta_d^2}{1 + \beta_d} = 0 \quad (5.16)$$

where we have used the fact that  $1 - \beta_d^2 = \gamma_d^{-2}$ . The solution is:

$$\beta_d = \frac{1 + 2\sigma + \sqrt{1 + 16\sigma + 16\sigma^2}}{6(1 + \sigma)} \quad (5.17)$$

In Fig. 5.2 we show the post shock quantities as a function of the magnetization. In the limit of small magnetizations  $v_d \rightarrow c/3$ , while in the limit of high  $\sigma$  one has  $\gamma_d \rightarrow \sigma$ . Note that downstream of the shock both  $p_d$  and  $b_d^2$  are much larger than  $\rho_d c^2$ .

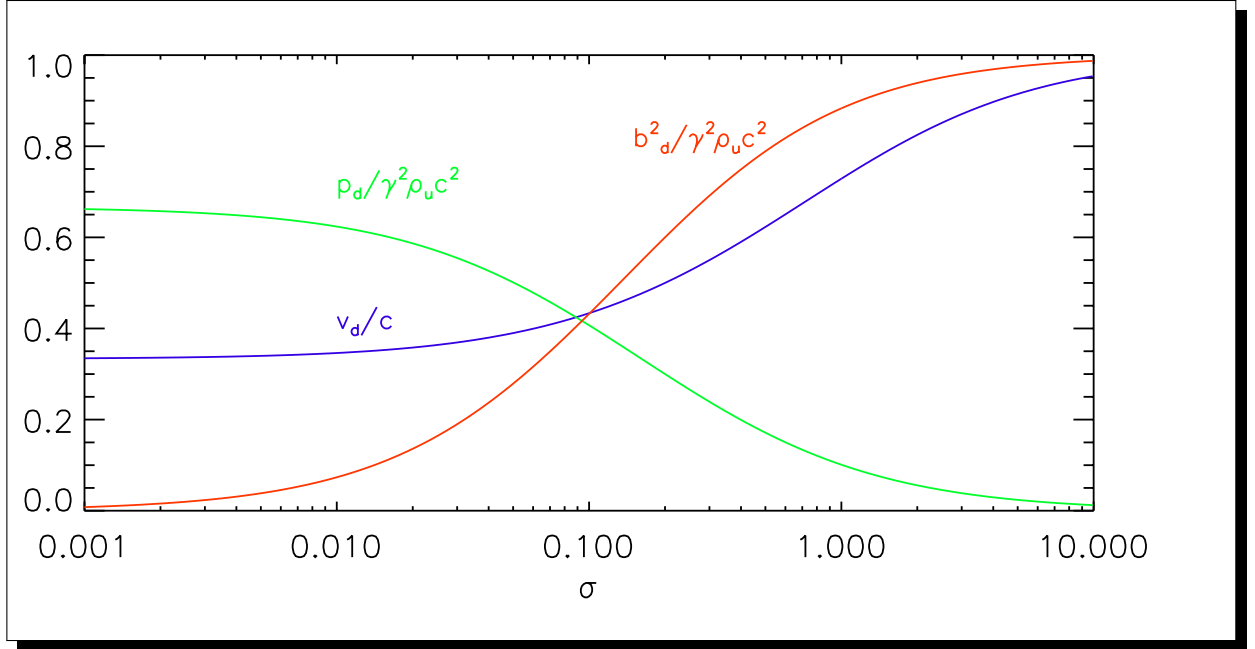


**Figure 5.2:** Jump conditions at the Termination Shock. Downstream value of the velocity (blue line) normalized to the speed of light, pressure (green line), and magnetic energy density (red line) normalized to the upstream wind ram pressure, as a function of the magnetization parameter.

## 5.2.2 Nebular Flow

It is evident that if the wind is still strongly magnetized upstream of the shock, the shock is weak and it is not efficient in slowing down the flow. This is known as *sigma paradox*. As we saw in Chapter 2.8 of the RMHD Notes the pulsar outflows is expected to be still magnetically dominated at large radii, in ideal MHD. However, the confinement by the SNR requires a small velocity achievable only with a small magnetization. Several solutions have been proposed, ranging from dissipation of the excess magnetic field in the wind, in the nebula or at the shock itself.

Let us assume that a shock forms. The downstream flow will be subsonic, and such that the rest mass density plays a negligible role in the flow dynamics. The typical timescale over which the pulsar wind evolves is of the order of the spin-down timescale, thousands of years, while the typical sound crossing time in the PWN, given the relativistic regime, is of the order of a light travel time, a few years. On the other hand the sound crossing time is much longer than the pulsar spin- period. This implies that the nebula will relax instantaneously to secular variations of the wind properties, and will be insensitive to variations at the magnetospheric pulsar timescale. Then it is reasonable to assume that the PWN is in a steady state equilibrium with the injection condition at the TS. If one assumes the flow to be purely radial, the equation for the conservation of the particles numbers (the rest mass) reads:

$$\gamma\rho v_r r^2 = \gamma_d \rho_d v_d R_{TS}^2 \quad (5.18)$$

The radial momentum conservation reads:

$$c^2 \partial_r (p + b^2/2) + b^2/r = \frac{1}{r^2} \partial_r [\gamma^2 (\rho c^2 + 4p + b^2) v_r v_r r^2] \simeq \frac{1}{r^2} \partial_r [\gamma^2 (4p + b^2) v_r v_r r^2] \quad (5.19)$$

The total energy conservation reads:

$$\gamma^2 (\rho c^2 + 4p + b^2) v_r r^2 \simeq \gamma^2 (4p + b^2) v_r r^2 = \gamma_d^2 (4p_d + b_d^2) v_d R_{TS}^2 \quad (5.20)$$

And the magnetic flux conservation is:

$$\gamma b v_r r = \gamma_d b_d v_d R_{TS} \quad (5.21)$$

For  $\sigma \gg 1$  the downstream flow will be magnetically dominated,  $b^2 \gg p$ , so that we can neglect in the momentum-energy conservation laws the pressure. Then Eq. 5.21 and Eq. 5.20 simplify to:

$$\gamma b v_r r = \text{const} \quad \gamma^2 b^2 v_r r^2 = \text{const} \quad (5.22)$$

with solutions  $b \propto r^{-1}$ , and  $v_r = \text{const}$ . One can show that this solutions also satisfy the momentum conservation law, while the mass conservation gives  $\rho \propto r^{-2}$  and the entropy conservation for a relativistic fluid gives  $p \propto \rho^{4/3} \propto r^{-8/3}$ . We see that for large  $\sigma$  the post shock flow does not slow down.

For  $\sigma \ll 0.1$  the downstream flow will be pressure dominated  $p \gg b^2$ , so that we can neglect in the momentum-energy conservation laws the magnetic field energy. Looking at the momentum conservation law Eq. 5.19 we see that the left side is of the order of  $c^2 p/r$  while the right side is of the order of  $v_r^2 p/r$ , much smaller. So to an approximation of the order  $v_r^2/c^2$ , the momentum conservation implies  $p = \text{const}$ . This, by entropy conservation, leads to  $\rho = \text{const}$ . Substituted in the mass conservation law this gives  $v_r \propto r^{-2}$ , assuming  $\gamma \simeq \gamma_d \simeq 1$ . And by magnetic flux conservation  $b \propto r$ . This means that the magnetic energy will rise as  $r^2$ , so that there will be a radius where the flow becomes magnetically dominated. As we have seen previously when this happens the flow stops to slow down and  $v_r$  saturates at a finite value. One can then think a PWN as formed by two regions: an internal one which is pressure dominated, and where the outflow slows down, and an outer one magnetically dominated, with a constant radial expansion speed.

One can estimate the radius  $r_{eq}$  at which this transition takes place and the value of the asymptotic speed. In the internal region one has:

$$\frac{b^2}{p} \approx \frac{r^2}{R_{TS}^2} \frac{B_d^2}{p_d} \approx \sigma \frac{r^2}{R_{TS}^2} \rightarrow r_{eq} = R_{TS} \sqrt{\sigma^{-1}} \quad (5.23)$$

while the asymptotic speed will be:

$$v_{asy} \approx v_d \frac{R_{TS}^2}{r_{eq}^2} \approx \sigma \frac{c}{3} \quad (5.24)$$

The requirement that the nebular outflow matches at the boundary the expansion speed of the PWN inside the SNR, can be translated into an upper limit to the allowed value of wind magnetization:  $\sigma < 3V_{pwn}/c \sim 0.001$ . So the wind must be weakly magnetized. taking the upper limit of  $\sigma$  into Eq. 5.23, one finds that  $r_{eq} \simeq R_{pwn}$ . Equipartition is reached in the outer part of the PWN.

### 5.3 PWNe Evolution

In this section we will develop a simplified model for the evolution of a PWN inside its parent SNR. A young SNR can be described as a radially expanding sphere of ejecta (Fig. 5.3). As the ejecta expand following the SN explosion, their density will scale as  $r^{-3}$ . On the other hand for a non relativistic fluid  $p \propto \rho^{5/3}$  so that  $p/\rho \propto r^{-2}$ . It is reasonable to assume at the ejecta are cold, and to neglect their pressure. We have seen in the previous section, that a PWN can be modelled as a subsonic bubble, of relativistic plasma with  $p \gg \rho c^2$ . We have also seen that the confinement inside the SNR can only be achieved if the PWN is pressure dominated (reaching magnetic equipartition only at the edge). This implies that the nebular pressure is almost constant inside. We will then assume that inside the PWN the pressure is constant and neglect the magnetic field.

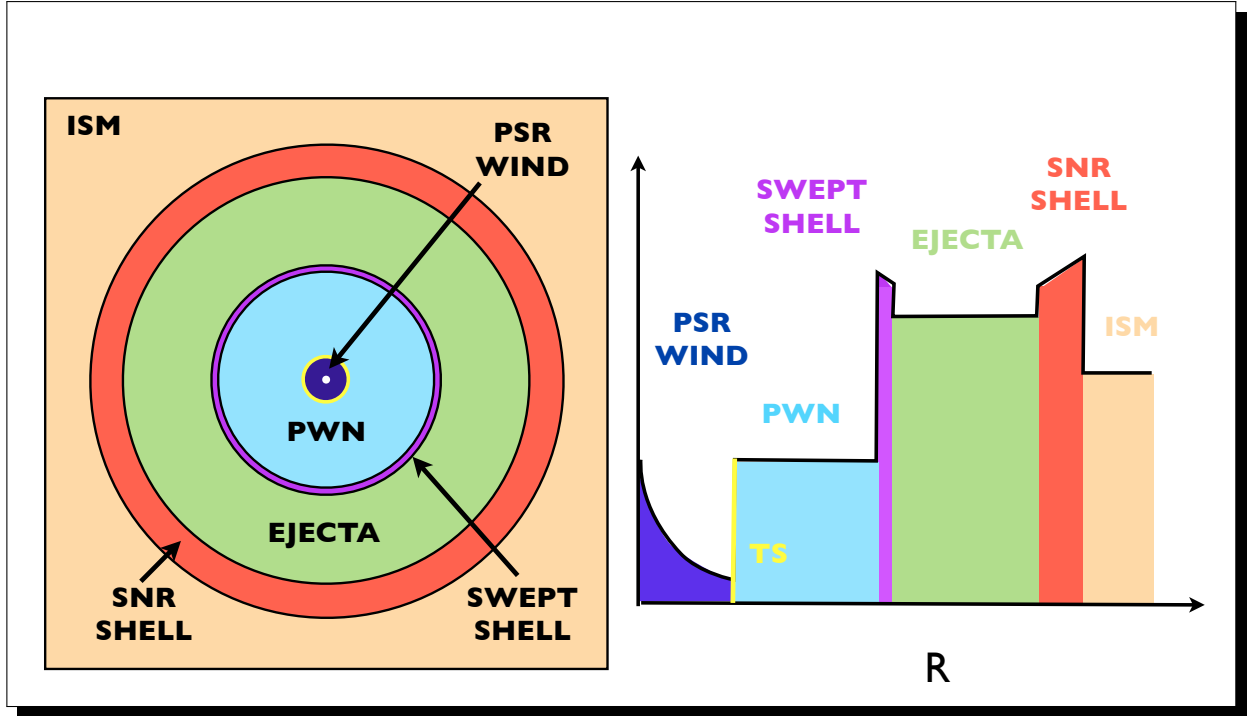


**Figure 5.3:** Left panel: schematic representation of a PWN-SNR system in the early stages of evolution, when the PWN expands inside the cold SNR ejecta. Right panel: same as left panel but now we show the typical density structure. Various regions are shown in different colors. The yellow boundary marked as TS is the termination shock.

**5.3.0.1 The SN Ejecta** We begin by modeling the structure of the density of the ejecta, as a function of the radial coordinate  $r$  and the time  $t$ . For simplicity let us look for a self-similar solution of the form  $\rho_{ej} \propto t^{-\alpha} r^\beta$ , with  $\alpha < 3$  for the total ejecta mass to be finite. On the other hand we search a solution for the ejecta velocity as  $v_{ej} \propto r^\gamma t^{-\delta}$ . The mass conservation and the momentum conservation equations for a non relativistic fluid reads:

$$\frac{\partial \rho_{ej}}{\partial t} + \frac{1}{r^2} \frac{\partial}{\partial r} (\rho_{ej} r^2 v_{ej}) = -\alpha \frac{\rho_{ej}}{t} + (2 + \beta + \gamma) \frac{\rho_{ej} v_{ej}}{r} = 0 \quad (5.25)$$

$$\frac{\partial \rho_{ej} v_{ej}}{\partial t} + \frac{1}{r^2} \frac{\partial}{\partial r} (\rho_{ej} r^2 v_{ej}^2) = \frac{\partial v_{ej}}{\partial t} + v_{ej} \frac{\partial}{\partial r} (v_{ej}) = -\delta \frac{v_{ej}}{t} + \gamma \frac{v_{ej}^2}{r} = \gamma \frac{v_{ej}}{r} - \frac{\delta}{t} = 0 \quad (5.26)$$

$$(5.27)$$

The solution of these equations requires:

$$\gamma = 1 \quad \delta = 1 \quad \beta = \alpha - 3 \quad (5.28)$$

If the ejecta density are assumed to be constant in radius  $\alpha = 0$  then one can write:

$$\rho_{ej} \propto t^{-3} \quad v_{ej} = \frac{r}{t} = V_o \frac{r}{R_{ej}} \quad (5.29)$$

where  $R_{ej} = V_o t$  is the outer radius of the ejecta. The value of the density and of the velocity are fixed once the total ejecta mass and ejecta energy, which is just the SN explosion energy  $E_{sn}$ , are known:

$$M_{ej} = 4\pi \int_0^{R_{ej}} \rho_{ej} r^2 dr \quad E_{sn} = 4\pi \int_0^{R_{ej}} \frac{1}{2} v_{ej}^2 \rho_{ej} r^2 dr \quad (5.30)$$

$$\rho_{ej} = \frac{3M_{ej}}{4\pi R_{ej}^3} \quad V_o = \sqrt{\frac{10}{3} \frac{E_{sn}}{M_{ej}}} \quad (5.31)$$

where the integral is truncated at the outer radius of the ejecta,  $R_{ej}$ .

### 5.3.1 The PWN

Let us call  $R_{pwn}$  the radius of the PWN as it expands inside the SNR ejecta. The only source of energy is the PSR spin-down  $\dot{E}$ , and if we neglect radiative losses, energy conservation reads:

$$\dot{E}(t) = \frac{dE_{pwn}}{dt} + P_{pwn} \frac{dV_{pwn}}{dt} = \frac{d}{dt} (4\pi R_{pwn}^3 P_{pwn}) + P_{pwn} 4\pi R_{pwn}^2 \frac{dR_{pwn}}{dt} = \frac{1}{R_{pwn}} \frac{d}{dt} (4\pi R_{pwn}^4 P_{pwn}) \Rightarrow P_{pwn} = \frac{1}{4\pi R_{pwn}^4} \int_0^t R_{pwn} \dot{E} dt \quad (5.32)$$

$$E_{pwn} = \frac{4\pi R_{pwn}^3}{3} \frac{3}{4\pi R_{pwn}^4} \int_0^t R_{pwn} \dot{E} dt = \frac{1}{R_{pwn}} \int_0^t R_{pwn} \dot{E} dt \quad (5.33)$$

where, for a relativistic gas, we have assumed that the energy density is three times the pressure. Eq.s 5.32-5.33 relate the evolution of the pressure and energy of the PWN to the evolution of the radius and the PSR luminosity, all of which are time dependent.

### 5.3.2 The Swept-up Shell

As the PWN expands it will push against the ejecta (themselves expanding) and will create a swept-up shell, of shocked ejecta matter. Given that the pressure in the ejecta is negligible, the shock will be strong, and the compression ratio is 4. The thickness  $\Delta$  of the shell can be estimated assuming that the density of shocked ejecta inside the shell is four times the density of the unshocked ones, as it is expected for a strong shock. The total mass in the swept-up shell  $M_{sh}$  is just the mass originally contained by the ejecta inside the shell radius  $R_{sh}$ :

$$M_{sh} = \frac{4\pi}{3} \rho_{ej} R_{sh}^3 = 4\pi (4\rho_{ej}) R_{sh}^2 \Delta \Rightarrow \Delta = \frac{1}{12} R_{sh} \quad (5.34)$$

The shell thickness is small and we can assume  $R_{sh} = R_{pwn}$ . This is known as *thin shell approximation*. All the swept-up ejecta mass is confined within a thin shell with the radius equal to the one of the PWN.

The total energy of the shell is:

$$E_{sh} = \frac{1}{2} M_{sh} \dot{R}_{sh}^2 = \frac{1}{2} M_{sh} \dot{R}_{pwn}^2 = \frac{4\pi}{6} \rho_{ej} R_{pwn}^3 \dot{R}_{pwn}^2 = \frac{M_{ej}}{2} \frac{1}{V_o^3 t^3} R_{pwn}^3 \dot{R}_{pwn}^2 \quad (5.35)$$

The evolution of this mass of swept-up material is just given by the balance of the PWN pressure from the interior and the ram pressure of the ejecta into which it is expanding.

$$M_{sh}\ddot{R}_{pwn} = 4\pi R_{pwn}^2 [P_{pwn} - \rho_{ej} V_{rel}^2] \quad \text{with} \quad V_{rel} = \dot{R}_{pwn} - \frac{R_{pwn}}{t} \quad (5.36)$$

where the velocity of the ejecta just upstream of the shell is  $R_{pwn}/t$  according to Eq. 5.29.

### 5.3.3 Self-Similar Solution

Given that the typical spin-down timescales for young PSR are of the order of a few thousands of years, it is reasonable to assume that for young PWNe the pulsar spin-down luminosity is constant. Then conservation of energy for the entire system of the PWN plus the swept-up shell can be written as:

$$\dot{E}t + E_{ini} = E_{pwn} + E_{sh} \quad (5.37)$$

where  $E_{ini}$  is the energy already contained in the swept-up ejecta;

$$E_{ini} = 2\pi \int_0^{R_{pwn}} \rho_{ej} v_{ej}^2 r^2 dr = \frac{3M_{ej}}{2V_o^3 t^3} \int_0^{R_{pwn}} \frac{r^2}{t^2} r^2 dr = \frac{3M_{ej} V_o^2}{10} \left( \frac{R_{pwn}}{V_o t} \right)^5 = E_{sn} \left( \frac{R_{pwn}}{V_o t} \right)^5 \quad (5.38)$$

If we assume a powerlaw expansion for the PWN radius  $R_{pwn} = Ct^\xi$  then, recalling Eq. 5.33 and 5.35, Eq. 5.37 can be rewritten as:

$$\dot{E}t + E_{sn} \left( \frac{C}{V_o} \right)^5 t^{5\xi-5} = \frac{\dot{E}t}{\xi+1} + \frac{M_{ej}}{2V_o^3} C^5 \xi^2 t^{5\xi-5} \quad (5.39)$$

$$\frac{\xi}{\xi+1} \dot{E}t = C^5 \frac{2\xi^2}{3} \frac{E_{sn}}{V_o^5} t^{5\xi-5} \quad (5.40)$$

The solution is:

$$\xi = 6/5 \quad C \simeq 0.9 \quad \Rightarrow \quad R_{pwn} = 0.9 \left( \frac{\dot{E}t}{E_{sn}} \right)^{1/5} V_o t \propto t^{6/5} \quad (5.41)$$

### 5.3.4 Interaction with the SNR

Eq. 5.41 shows that the PWN has a slightly accelerated expansion inside the ejecta. On the other hand the SNR shell that forms at the outer edge of the SNR due to the interaction with the ISM has a decelerated expansion described by the Sedov law:

$$R_{snr} \simeq \left( \frac{E_{sn}}{\rho_{ism}} \right)^{1/5} t^{2/5} \quad (5.42)$$

The free expansion inside the cold ejecta will then terminate once the PWN reaches the SNR shell:

$$\left( \frac{\dot{E}t}{E_{sn}} \right)^{1/5} V_o t \simeq R_{pwn} = R_{snr} \simeq \left( \frac{E_{sn}}{\rho_{ism}} \right)^{1/5} t^{2/5} \quad (5.43)$$

$$t_r \approx \frac{M_{ej}^{5/8}}{E_{sn}^{1/8} \dot{E}^{1/4} \rho_{ism}^{1/4}} \approx 10^4 \text{yr} \left( \frac{M_{ej}}{10M_\odot} \right)^{5/8} \left( \frac{E_{sn}}{10^{51} \text{erg}} \right)^{-1/8} \left( \frac{\dot{E}}{10^{38} \text{erg s}^{-1}} \right)^{-1/4} \left( \frac{n_{ism}}{1 \text{cm}^{-3}} \right)^{1/4} \quad (5.44)$$

The free expansion inside the cold ejecta will terminate after a few thousands of years. So the starting assumption of an almost constant PSR spin down luminosity is consistent.

### 5.3.5 Late Time Evolution

The interaction of the PWN with the SNR shell can be quite complex in its initial phases. It is possible however to derive how the PWN will evolve inside the parent SNR at late time, once the SNR-PWN system is completely relaxed into its asymptotic state. This happens after a few  $t_r$ . At this point the PSR spin down luminosity can be quite weak, and to a first approximation one can assume that its contribution to the PWN energy is negligible. In this case the relativistic PWN will evolve adiabatically with  $P_{pwn} \propto R_{pwn}^{-4}$ . On the other hand the SNR will be fully relaxed to the self similar Sedov solution, with the interior pressure  $P_{snr} \simeq \rho_{ism} \dot{R}_{snr}^2 \propto t^{-6/5}$ . Assuming pressure equilibrium between the PWN and the interior of the SNR one has:  $R_{pwn} \propto t^{3/10}$ .

PSR are known to have high kick velocity, due most likely to anisotropies in the SN explosion whence they originate. Typical speeds are  $V_{psr} \sim 200 \text{ km s}^{-1}$ . One can expect such PSRs to emerge from their parent SNR at a typical time:

$$\begin{aligned} t_{esc} V_{psr} &= R_{snr} = \left( \frac{E_{sn}}{\rho_{ism}} \right)^{1/5} t_{esc}^{2/5} \\ \Rightarrow t_{esc} &\approx \left( \frac{E_{sn}}{\rho_{ism}} \right)^{1/3} \left( \frac{1}{V_{psr}} \right)^{5/3} \approx 2 \times 10^5 \text{ yr} \left( \frac{E_{sn}}{10^{51} \text{ erg}} \right)^{1/3} \left( \frac{V_{psr}}{200 \text{ km s}^{-1}} \right)^{5/3} \left( \frac{n_{ism}}{1 \text{ cm}^{-3}} \right)^{-1/3} \end{aligned} \quad (5.45)$$

## 5.4 PWNe Emission

Let us assume for simplicity that the PWN expands at a constant rate  $\dot{R}$  such that  $R = \dot{R}t \propto t$  instead of  $R \propto t^{6/5}$  as we found in Sec. 5.3, and that the pulsar spin-down luminosity  $\dot{E}$  is constant. These are minor simplifications for a young PWN, and yet they afford a substantial simplification in the following analysis. The total energy in the nebula can be evaluated using Eq. 5.33, and assuming the magnetic energy is a constant fraction  $\eta$  of the total nebular energy one has:

$$E_{pwn} = \frac{\dot{E}t}{2} \quad \frac{B^2}{8\pi} = \eta \frac{\dot{E}t}{2} \frac{3}{4\pi R^3} \quad \Rightarrow \quad B^2 = \eta \frac{3\dot{E}t}{R^3} = \eta \frac{3\dot{E}}{\dot{R}^3 t^2} \quad (5.46)$$

The strength of the magnetic field drops linearly in time.

### 5.4.1 Particles Losses

For a system composed of particles with energy  $E$ , subject to adiabatic losses in an expanding sphere of volume  $V$  and radius  $R$ , one finds:

$$d(NE) = -PdV = -\frac{(EN)}{3V}dV \quad \Rightarrow \quad dE = -\frac{E}{3} \frac{dV}{V} = -E \frac{dR}{R} \quad \Rightarrow \quad \frac{dE}{dt} = -E \frac{\dot{R}}{R} \quad (5.47)$$

where  $N = \text{const}$  is the total particle number, and we have assumed relativistic particles for which  $P = EN/3V$ . The energy losses in this case are usually referred as *adiabatic losses*.

A particle of energy  $E$  in a magnetic field of strength  $B$  will also loose energy because of *synchrotron losses* according to:

$$\frac{dE}{dt} = -\frac{4}{9} \frac{e^4}{m^4 c^7} B^2 E^2 = -c_1 B^2 E^2 \quad \text{with} \quad c_1 = \frac{4}{9} \frac{e^4}{m^4 c^7} \quad (5.48)$$

where  $m$  is the particle mass (in our case electrons/positrons) and  $e$  its charge, while the factor  $4/9$  comes from averaging over pitch angle, in the particle distribution function.

The time evolution of a particle energy is determined by the combination of adiabatic losses due to the nebular expansion and of synchrotron losses in the nebular magnetic field:

$$\frac{dE}{dt} = -E \frac{\dot{R}}{R} - c_1 B^2 E^2 \quad \Rightarrow \quad \frac{1}{RE^2} \frac{dE}{dt} = -\frac{1}{RE} \frac{\dot{R}}{R} - c_1 \frac{B^2}{R} \quad \Rightarrow \quad \frac{d}{dt} \left( \frac{1}{ER} \right) = c_1 \frac{B^2}{R} \quad (5.49)$$

which trivially integrates between a reference initial time  $t_i$  (for example the time the particle was injected) and a final time  $t$  as:

$$\frac{1}{ERt} - \frac{1}{E_i R t_i} = \int_{t_i}^t c_1 \eta \frac{3\dot{E}}{R^4 t^3} dt = c_1 \eta \frac{3\dot{E}}{2R^4} \left[ \frac{1}{t_i^2} - \frac{1}{t^2} \right] \quad \Rightarrow \quad \frac{1}{Et} - \frac{1}{E_i t_i} = c_1 \eta \frac{3\dot{E}}{2R^3} \left[ \frac{1}{t_i^2} - \frac{1}{t^2} \right] \quad (5.50)$$

Looking at eq. 5.49 one sees that for particles with:

$$E \frac{\dot{R}}{R} \ll c_1 B^2 E^2 \quad \Rightarrow \quad E \gg \frac{\dot{R}^3}{3c_1 \eta \dot{E}} t \quad (5.51)$$

synchrotron losses dominate over adiabatic losses and viceversa at lower energies. While from Eq. 5.50 one finds that particles injected at time  $t_i$  with infinite energy  $E_i \rightarrow \infty$  will have at time  $t$  an energy:

$$E(t) = \frac{2\dot{R}^3 t_i^2}{3c_1 \eta \dot{E} t} \quad (5.52)$$

Consider now particles which were injected at energies such that:

$$E_i \ll \frac{2\dot{R}^3}{3c_1 \eta \dot{E}} t_i \quad (5.53)$$

then one has

$$\frac{1}{Et} = \frac{1}{E_i t_i} + c_1 \eta \frac{3\dot{E}}{2R^3} \left[ \frac{1}{t_i^2} - \frac{1}{t^2} \right] \gg +c_1 \eta \frac{3\dot{E}}{2R^3} \left[ \frac{2}{t_i^2} - \frac{1}{t^2} \right] > +c_1 \eta \frac{3\dot{E}}{2R^3} \left[ \frac{1}{t^2} \right] \Rightarrow E \ll \frac{2\dot{R}^3}{3c_1 \eta \dot{E}} t \quad (5.54)$$

so these particles will always (at any time  $t > t_i$ ) loose energy in the adiabatic dominated regime. In this case neglecting the synchrotron term in Eq. 5.50 one can recast the condition of Eq. 5.53 into a condition on the energy  $E$  at time  $t$ , and the injection time:

$$E \ll \frac{2\dot{R}^3}{3c_1 \eta \dot{E}} t_i^2 \quad (5.55)$$

Consider instead particles with an energy such that:

$$E \gg \frac{2\dot{R}^3}{3c_1 \eta \dot{E}} t \quad (5.56)$$

In this case one finds:

$$\frac{1}{E_i t_i} = \frac{1}{E t} - c_1 \eta \frac{3\dot{R}}{2\dot{R}^3} \left[ \frac{1}{t_i^2} - \frac{1}{t^2} \right] \ll +c_1 \eta \frac{3\dot{R}}{2\dot{R}^3} \left[ \frac{2}{t^2} - \frac{1}{t_i^2} \right] < +c_1 \eta \frac{3\dot{R}}{2\dot{R}^3} \left[ \frac{1}{t_i^2} \right] \Rightarrow E_i \gg \frac{2\dot{R}^3}{3c_1 \eta \dot{E}} t_i \quad (5.57)$$

so these particles have always (at any time  $t_i < t$ ) lost their energy mostly due to synchrotron.

There is also range of particles with energy such that:

$$E < \frac{2\dot{R}^3}{3c_1 \eta \dot{E}} t \quad E_i > \frac{2\dot{R}^3}{3c_1 \eta \dot{E}} t_i \Rightarrow E > \frac{2\dot{R}^3}{3c_1 \eta \dot{E}} t_i^2 \quad (5.58)$$

which are now losing their energy mostly by adiabatic losses, but in the past have been losing their energy mostly via synchrotron.

## 5.4.2 Particles Distribution

Let us name  $\dot{N}(E, t)$  the number of particles injected into the nebula per unit time per unit energy interval. Such number is normalized according to:

$$(1 - \eta) \dot{E} = \int_0^{E_{max}} \dot{N}(E, t) E dt \quad (5.59)$$

where  $E_{max}$  is the maximum energy at injection. We shall assume that injection obeys a simple power-law  $\dot{N}(E) = K E^{-\gamma}$ , constant in time. For  $\gamma > 2$  the value of  $E_{max}$  can be set to infinity. For  $\gamma < 2$  injection must have a cutoff at finite energy to satisfy Eq. 5.59. One can use Eq. 5.50 to relate the energy of a particle at a given time  $t$  to the energy it had at a previous time  $t_i$ , or equivalently to relate the time of injection  $t_i$  to the injection energy  $E_i$  and final energy  $E$  at time  $t$ ,  $t_i = t_i(E, t, E_i)$ . Then one has :

$$dN(E, t, E_i) dE = \dot{N}(E_i, t_i(E, t, E_i)) dt_i dE_i \quad (5.60)$$

where  $dN(E, t, E_i) dE$  is the number of particles with energy between  $E$  and  $E + dE$  at time  $t$ , which were injected with initial energy  $E_i$ , between time  $t_i(E, t, E_i)$  and  $t_i(E, t, E_i) + dt_i$ .  $dE_i$  is the initial energy range ending into  $dE$  at time  $t$ . The total number is found integrating over all energies  $E_i > E$  (there are only losses):

$$N(E, t) = \int_E^\infty \dot{N}(E_i, t_i(E, t, E_i)) \frac{\partial t_i}{\partial E} dE_i \quad (5.61)$$

where  $N(E, t)$  is the total number of particles with energy between  $E$  and  $E + dE$  at time  $t$ .

Let assume that the injection process begins at a time  $t_o$ . One can divide the energy into three intervals:

- Range A :

$$0 < E < \frac{2\dot{R}^3}{3c_1 \eta \dot{E}} t_o^2 < \frac{2\dot{R}^3}{3c_1 \eta \dot{E}} t_i^2 \quad \text{for any } t_i > t_o \quad (5.62)$$

Particles in this range come from particles which were injected with an initial energy so small to be subject solely to adiabatic losses, as Eq. 5.55.

- Range B :

$$\frac{2\dot{R}^3}{3c_1\eta\dot{E}}t < E \quad (5.63)$$

Particles in this range come from particles which were injected with an initial energy so high to be subject solely to synchrotron losses, as Eq. 5.56.

- Range C :

$$\frac{2\dot{R}^3}{3c_1\eta\dot{E}}t_o^2 < E < \frac{2\dot{R}^3}{3c_1\eta\dot{E}}t \quad (5.64)$$

Particles in this range come both from particles which were injected at time  $t_i > \sqrt{(3c_1\eta\dot{E}Et)/(2\dot{R}^3)}$  (as Eq. 5.55) and so have only suffered adiabatic losses ad those injected at time  $t_o < t_i < \sqrt{(3c_1\eta\dot{E}Et)/(2\dot{R}^3)}$  which where injected with an initial energy so high to be subject initially to synchrotron losses as Eq. 5.56.

For particles in Range A, that lost their energy always in the adiabatic dominated regime, neglecting the synchrotron term in Eq. 5.50 one has:

$$t_i = t \frac{E}{E_i} \Rightarrow E_i = E \frac{t}{t_i} \quad \frac{\partial t_i}{\partial E} = \frac{t}{E_i} \quad E_i < \frac{2\dot{R}^3}{3c_1\eta\dot{E}} \frac{E}{E_i} t \Rightarrow E_i^2 < \frac{2\dot{R}^3}{3c_1\eta\dot{E}} Et \quad (5.65)$$

then substituting into Eq. 5.61 one finds:

$$\begin{aligned} N(E, t) &= \int_E^{Et/t_i} K E_i^{-\gamma} \frac{t}{E_i} dE_i = \int_E^{Et/t_i} K E_i^{-\gamma-1} t dE_i = -\frac{Kt}{\gamma} E^{-\gamma} \Big|_E^{Et/t_i} \\ &\Rightarrow \frac{Kt}{\gamma} E^{-\gamma} \quad \text{for } \gamma > 0, t_i \ll t \end{aligned} \quad (5.66)$$

The particle spectrum is a powerlaw with the same index as the injection spectrum and a normalization that rises linearly in time.

For particles in Range B, that lost their energy always in the synchrotron dominated regime, neglecting the adiabatic term in Eq. 5.50, and imposing condition Eq. 5.56 one has:

$$Et = \frac{2\dot{R}^3}{3c_1\eta\dot{E}} \frac{t_i^2 t^2}{t^2 - t_i^2} \gg \frac{2\dot{R}^3}{3c_1\eta\dot{E}} t^2 \Rightarrow t_i \simeq t \quad (5.67)$$

$$\frac{\partial E}{\partial t} = -c_1 B^2 E^2 \Rightarrow \frac{\partial t_i}{\partial E} = -\frac{\partial t_i}{\partial t} \frac{\partial t}{\partial E} = -\frac{\dot{R}^3}{3c_1\eta\dot{E}} \frac{t^2}{E^2} \quad (5.68)$$

Then substituting into Eq. 5.61 one finds:

$$\begin{aligned} N(E, t) &= -\int_E^{E_{max}} K E_i^{-\gamma} \frac{\dot{R}^3}{3c_1\eta\dot{E}} \frac{t^2}{E^2} dE_i = -\int_E^{E_{max}} K E_i^{-\gamma} \frac{\dot{R}^3 t^2}{3c_1 E^2 \eta \dot{E}} dE_i = \\ &= \frac{K \dot{R}^3 t^2}{3c_1 E^2 \eta \dot{E} (\gamma - 1)} E^{1-\gamma} \Big|_E^{E_{max}} \Rightarrow \frac{K \dot{R}^3 t^2}{3c_1 \eta \dot{E} (\gamma - 1)} E^{-\gamma-1} \quad \text{for } \gamma > 0, E_{max} \gg E \end{aligned} \quad (5.69)$$

The particle spectrum is again a powerlaw but now the index is reduced by unity with respect to the injection, and the normalization rises quadratically in time.

Finally one can consider particles in Range C, where there is mixed contribution. The particles injected at  $t_i > \sqrt{(3c_1\eta\dot{E}Et)/(2\dot{R}^3)}$  have injection energy below the threshold energy  $E_{ref}$  set by the second relation in Eq. 5.65, and so follow a purely adiabatic evolution. The particles injected at  $t_i < \sqrt{(3c_1\eta\dot{E}Et)/(2\dot{R}^3)}$  have injection energy above the threshold energy  $E_{ref}$ . Given that the synchrotron dominated phase has  $t \simeq t_i$ , synchrotron losses are almost instantaneous such that particles injected above  $E_{ref}$ , immediately go to  $E_{ref}$ , after which they evolve adiabatically. Then one has:

$$E_{ref}^2 = \frac{2\dot{R}^3}{3c_1\eta\dot{E}}Et \quad t_i = t\frac{E}{E_i} \simeq t\frac{E}{E_{ref}} = \sqrt{\frac{3c_1\eta\dot{E}}{2\dot{R}}Et} \Rightarrow \frac{\partial t_i}{\partial E} = \sqrt{\frac{3c_1\eta\dot{E}}{8\dot{R}}\frac{t}{E}} \quad (5.70)$$

Then substituting into Eq. 5.61 one finds:

$$N(E, t) = \int_E^{E_{ref}} \frac{t}{E_i} K E_i^\gamma dE_i + \int_{E_{ref}}^{E_{max}} K E_i^{-\gamma} \left( \frac{\dot{R}^3 t^2}{3c_1\eta\dot{E}E} \right)^{1/2} dE_i \quad (5.71)$$

Where the first integral takes the contribution from those particles which were subject only to adiabatic losses, while the second, takes all particles injected at  $E_i > E_{ref}$ , and evolve them as if they were all injected at  $E_{ref}$  and subject just to the remaining adiabatic losses, as discusses above. It is evident that for  $\gamma > 1$  it is always the lower extreme of the first integral that dominates, so that even in Range C:

$$N(E, t) = \frac{Kt}{\gamma} E^{-\gamma} \quad (5.72)$$

So the total particle spectrum will be given by a broken powerlaw, with low energy index  $-\gamma$ , a high energy index  $-\gamma - 1$ , and a break energy  $E_b$  that corresponds to the energy of particles whose synchrotron lifetime is equal to the age of the nebula:

$$E_b = \frac{2\dot{R}^3}{3c_1\eta\dot{E}}t \Rightarrow c_1 B^2 E_b^2 = \frac{3c_1\eta\dot{E}}{\dot{R}^3 t^2} E_b^2 \simeq \frac{E_b}{t} \quad (5.73)$$

The break energy gets larger in time with  $N(E_b, t) \propto t^{1-\gamma}$ , while the overall normalization rises. An example of how the spectrum evolves, is shown in Fig. 5.4.

### 5.4.3 Synchrotron Spectrum

Once the particle energy distribution is known one can easily derive the spectrum. The radiation mechanism is synchrotron from the particles gyrating in the nebular magnetic field.

A particle with energy  $E$  in a magnetic field of strength  $B$  radiates most of its energy around a critical frequency:

$$\nu_c = \frac{e}{m^3 c^5} B E^2 = c_2 B E^2 \quad (5.74)$$

Under the *monochromatic approximation* we will assume that all the energy is radiates at the frequency  $\nu = \nu_c$ . Then, using eq. 5.48, one can write for the energy emitted per unit time per unit frequency, the so called *spectral density*:

$$\begin{aligned} S(\nu) &= - \left( \frac{dE}{dt} \right)_{syn} N(E) \frac{dE}{d\nu} = c_1 B^2 E^2 N(E) \frac{1}{2c_2 E B} = \frac{c_1}{c_2} \frac{B E}{2} N(E) = \\ &= \frac{c_1}{2} B \left( \frac{B \nu}{c_2^3} \right)^{1/2} N \left( \left( \frac{B \nu}{c_2^3} \right)^{1/2} \right) \end{aligned} \quad (5.75)$$

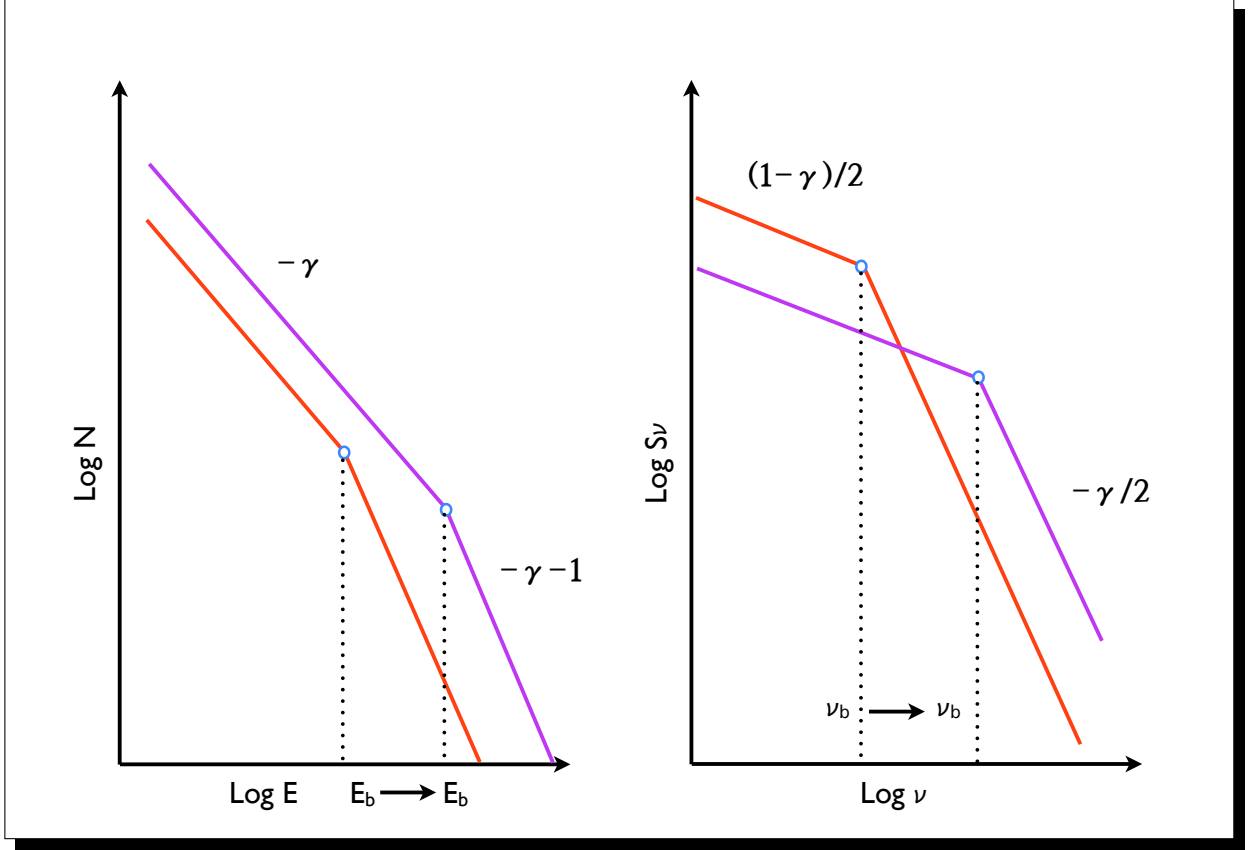


**Figure 5.4:** Left panel: evolution of the particle distribution as a function of energy inside a PWN (from the red curve at earlier times to the purple curve at later times), for a single power-law injection. Right panel: evolution of the spectral density as a function of frequency (for  $\gamma < 2$ ).

where  $B$  and  $N$  are also time dependent.

It is evident that the existence of a break in the particle spectrum causes a break also in the spectral density. Recalling that the break energy is given by Eq. 5.73, and that the magnetic field evolves according to Eq. 5.46, the break frequency is:

$$\nu_b \simeq 4t \left( \frac{\dot{R}^3}{3c_1 \eta \dot{E}} \right)^{3/2} \quad (5.76)$$

which moves to higher energy in time.

Recalling that the particle spectrum is given by Eq. 5.72 at energy below  $E_b$  and by Eq. 5.69 above  $E_b$ , the spectral density will be:

$$S(\nu) = \frac{Kc_2}{2\gamma} \left( \frac{3\eta\dot{E}}{\dot{R}^3} \right)^{(\gamma+1)/4} c_2^{(\gamma-3)/2} t^{(1-\gamma)/2} \nu^{(1-\gamma)/2} \quad \text{for } \nu < \nu_b \quad (5.77)$$

$$S(\nu) = \frac{Kc_2}{2\gamma-2} \left( \frac{3\eta\dot{E}}{\dot{R}^3} \right)^{(\gamma-2)/4} c_2^{(\gamma-2)/2} t^{1-\gamma/2} \nu^{-\gamma/2} \quad \text{for } \nu > \nu_b \quad (5.78)$$

The spectrum is also a broken power-law and the spectral index is directly related to the index of the particle distribution. Note that for  $1 < \gamma < 2$ , the spectral density below  $E_b$  drops in time while above  $E_b$  it rises. For  $\gamma > 2$  it drops in both ranges.

One can also compute the total synchrotron luminosity of the nebula:

$$L_{syn} = \int_0^{\nu_{max}} S(\nu) d\nu = \frac{Kc_2}{2\gamma} \left( \frac{3\eta\dot{E}}{\dot{R}^3} \right)^{(\gamma+1)/4} c_2^{(\gamma-3)/2} t^{(1-\gamma)/2} \int_0^{\nu_b} \nu^{(1-\gamma)/2} d\nu + \frac{Kc_2}{2\gamma-2} \left( \frac{3\eta\dot{E}}{\dot{R}^3} \right)^{(\gamma-2)/4} c_2^{(\gamma-2)/2} t^{1-\gamma/2} \int_{\nu_b}^{\nu_{max}} \nu^{-\gamma/2} d\nu \quad (5.79)$$

where  $\nu_{max}$  is the frequency corresponding to  $E_{max}$ . For  $\gamma < 2$  the luminosity is mostly (logarithmically) due to the highest energy photons at  $\nu_{max}$ . For  $\gamma > 3$  the luminosity is due to the lowest energy photons. For  $2 < \gamma < 3$ , assuming  $E_{max} \gg E_b$  the integral is:

$$L_{syn} = \frac{Kc_2}{2\gamma} \left( \frac{3\eta\dot{E}}{\dot{R}^3} \right)^{(\gamma+1)/4} \frac{c_2^{(\gamma-3)/2} 2\nu_b^{(3-\gamma)/2}}{t^{(\gamma-1)/2} 3-\gamma} + \frac{Kc_2}{2\gamma-2} \left( \frac{3\eta\dot{E}}{\dot{R}^3} \right)^{(\gamma-2)/4} \frac{c_2^{(\gamma-2)/2} 2\nu_b^{(2-\gamma)/2}}{t^{\gamma/2-1} \gamma-2} \quad (5.80)$$

$$\propto t^{2-\gamma} \quad (5.81)$$

The luminosity is dominated by photons emitted around  $\nu_b$  and drops in time less than linearly (for  $\gamma$  close to 2 the luminosity remains almost constant).

#### 5.4.4 IC Emission

PWNe are known to emit also at TeV energies. Such emission cannot be due to synchrotron. The maximum synchrotron frequency emittable by a particle, corresponds to a particle energy for which the synchrotron cooling time  $\tau_s$  equals the gyration time  $\tau_g$ . At higher energy a particle will loose all of its energy before completing an orbit, and emitting a synchrotron photon. This condition is:

$$\tau_g = \frac{E}{eBc} = \frac{E}{c_1 E^2 B^2} = \tau_s \Rightarrow E^2 = \frac{ec}{c_1 B} \Rightarrow \nu = \frac{c_2 ec}{c_1} \quad h\nu = \frac{hc}{e^2} m_e c^2 \simeq 100 \text{ MeV} \quad (5.82)$$

The TeV emission is due to IC scattering of a background photon field. The usual photon fields for PWNe are: the CMB which is well known; the Galactic background whose local value is known within a factor a few (it is strongly influenced by the presence of nearby sources); the synchrotron field from the PWN itself (important only for young bright objects i.e. just the Crab Nebula).

The CMB photons have typical energy  $\sim 3 \times 10^{-4}$  eV, so IC on the CMB will happen in the Thompson regime for:

$$10^{-4} \frac{E}{m_e c^2} < 0.1 \text{ MeV} \Rightarrow E < 10^9 m_e c^2 \quad (5.83)$$

higher than the maximum energy achievable using the full potential drop of the PSR, which constitute the acceleration limit for a PSR powered system. So IC-CMB is always in the Thompson regime.

The Galactic background photons have typical energy  $\sim 0.01 - 0.1$  eV, so IC on the CMB will happen in the Thomson regime for  $E < 10^6 - 10^7 m_e c^2$ . This exclude most of the particles, except perhaps the highest energy.

In the Thomson regime the IC luminosity from a particle with energy  $E$  in a photon field of energy density  $U$  is:

$$\left(\frac{dE}{dt}\right)_{IC} = 8\pi c_1 U E^2 = c_3 U E^2 \quad \text{at} \quad \nu = \nu_{ph} \frac{4}{3} \left(\frac{E}{m_e c^2}\right)^2 \simeq \nu_{ph} \left(\frac{E}{m_e c^2}\right)^2 \quad (5.84)$$

where  $\nu_{ph}$  is the typical photon frequency of the background, and the  $4/3$  comes from averaging over an isotropic photon background. For a black body (as the case for CMB) this is related to the energy density of the photon field by:

$$\nu_{ph} \simeq 3 \frac{k_b T}{h} \simeq \frac{k_b}{h} \left(\frac{U}{a}\right)^{1/4} \Rightarrow \nu = c_4 U^{1/4} E^2 \quad (5.85)$$

where  $k_b$  is the Boltzmann constant,  $T$  the temperature, and  $a$  the black body constant.

By comparison to Eq. 5.48 one sees immediately that the IC spectral density in the Thomson regime will have similar trends as for synchrotron. There is an energy break:

$$\nu_s = c_4 (aT)^{1/4} \left(\frac{2\dot{R}}{3c_1 \eta \dot{E}}\right)^2 t^2 \propto t^2 \quad (5.86)$$

And the spectrum will be:

$$\begin{aligned} S(\nu) &= - \left(\frac{dE}{dt}\right)_{IC} N(E) \frac{dE}{d\nu} = c_3 U E^2 N(E) \frac{1}{2c_4 E U^{1/4}} = \frac{c_3}{2} \frac{E U^{3/4}}{c_4} N(E) = \\ &= \frac{c_3}{2} \left(\frac{\nu U^{5/8}}{c_4^3}\right)^{1/2} N\left(\left(\frac{\nu}{c_4 U^{1/4}}\right)^{1/2}\right) \end{aligned} \quad (5.87)$$

That gives:

$$S(\nu) = \frac{K c_3}{2\gamma} c_4^{(\gamma-3)/2} a^{(5+\gamma)/8} T^{(5+\gamma)/2} t \nu^{(1-\gamma)/2} \quad \text{for} \quad \nu < \nu_s \quad (5.88)$$

$$S(\nu) = \frac{K c_3}{2\gamma - 2} \frac{\dot{R}^3}{3c_1 \eta \dot{E}} c_4^{(\gamma-2)/2} a^{(6+\gamma)/8} T^{(6+\gamma)/2} t^2 \nu^{-\gamma/2} \quad \text{for} \quad \nu > \nu_s \quad (5.89)$$

$$(5.90)$$

a broken power-law with the same spectral index as for the synchrotron. Unlike synchrotron however, the CMB and Galactic background do not change in time as the magnetic field does, so the temporal dependence is different. The break frequency has also a different temporal behavior.

Again for  $2 < \gamma < 3$ , the IC luminosity is dominated by photons with a frequency  $\nu = \nu_s = \nu_{ph} E_b^2 / m_e^2 c^4$ . The IC spectrum reproduces at higher energy the synchrotron spectrum. Given the different temporal dependence, the IC luminosity grows in time as  $t^{4-\gamma}$ . The ratio of IC luminosity to synchrotron luminosity, is nothing else than the ratio of the magnetic field energy density to the photon field energy density, and can be used to estimate the magnetic field in the nebula, once the photon field is known (as for CMB):

$$\frac{L_{syn}}{L_{IC}} = \frac{B^2}{8\pi U} \propto t^{-2} \quad (5.91)$$

## 5.5 Cooling

Let us consider a system in an initial state  $|i\rangle$  decaying into a final state  $|f\rangle$ , fully characterized by all its quantum numbers. The decay rate for the transition is:

$$R = \frac{2\pi}{\hbar} |\langle f|H|i\rangle|^2 = \frac{2\pi}{\hbar} |H_{i\rightarrow f}|^2 \quad (5.92)$$

where  $H$  is the Hamiltonian of the decay. If the system, from the initial state  $|i\rangle$ , can decay into  $m$  final states  $|f_j\rangle$ , then the total decay rate of the state  $|i\rangle$  is:

$$R = \frac{2\pi}{\hbar} \sum_{j=1}^m |\langle f_j|H|i\rangle|^2 = \frac{2\pi}{\hbar} \sum_{j=1}^m |H_{i\rightarrow f_j}|^2 \quad (5.93)$$

If  $|H_{i\rightarrow f_j}|$  is the same for all  $f_j$  (i.e. if  $|f_j\rangle$  are degenerate for the Hamiltonian  $H$ ), then one has:

$$R = \frac{2\pi}{\hbar} m |H_{i\rightarrow f}|^2 \quad (5.94)$$

where we set  $|H_{i\rightarrow f_j}| = |H_{i\rightarrow f}|$ . More generally if the final state  $|f\rangle$  has a degeneracy  $g$  (density of final states around available final state energy) then:

$$R = \frac{2\pi}{\hbar} g |H_{i\rightarrow f}|^2 \quad (5.95)$$

which is just the Fermi Golden Rule.

Let us consider the  $\beta$ -decay reaction for a free neutron into a proton, and electron and a neutrino:

$$n \rightarrow p + e + \bar{\nu} \quad (5.96)$$

assuming for simplicity that the decay is due to a ‘‘contact interaction’’ of strength  $G$  (Fermi constant) among the particles involved (the neutron will decay into a proton at its same exact position). This mean that Hamiltonian of the interaction can be describes as a Dirac delta in space, over the position  $\mathbf{x}'$  of the neutron  $H = G\delta(\mathbf{x} - \mathbf{x}')$ :

$$|H_{i\rightarrow f}| = \langle p e \bar{\nu} | H | n \rangle = G \int (\psi_{\bar{\nu}}^* \psi_e^* \psi_p^*) \psi_n d^3 \mathbf{x} \quad (5.97)$$

where  $\psi$  are the various wave functions.

Given that the mass difference between the neutron and the proton  $E \sim 8$  MeV is much smaller that the mass of the proton, but much larger that that either the mass of the electron or the anti-neutrino, the proton will be almost at rest. On the other hand the typical wavelength of the leptons will be  $\sim \hbar/p \sim \hbar c/E \gg 10^{-13}$  cm, the typical sizes of the proton and neutron. Neclecting Coulomb corrections for the electron due to the proton, and given that leptons do not feel the strong force, one can assume both leptons to be described by plane waves:

$$\psi_{\bar{\nu}} = e^{-i\mathbf{q}\cdot\mathbf{x}/\hbar} \quad \text{and} \quad \psi_e = e^{-i\mathbf{p}\cdot\mathbf{x}/\hbar} \quad (5.98)$$

where  $\mathbf{q}$  and  $\mathbf{p}$  are the omentum of the anti-neutrino and electron respectively, and we have assume unitary volume for simplicity. Then

$$|H_{i\rightarrow f}| = G \int \psi_p^* \psi_n e^{i(\mathbf{p}+\mathbf{q})\cdot\mathbf{x}/\hbar} d^3 \mathbf{x} \quad (5.99)$$

$$= G \int \psi_p^* \psi_n d^3 \mathbf{x} + iG \int \psi_p^* \psi_n \frac{(\mathbf{p} + \mathbf{q}) \cdot \mathbf{x}}{\hbar} d^3 \mathbf{x} \quad (5.100)$$

And assume that the  $\beta$ -decay is mediated by

Given that the neutron to proton mass difference, i.e. the energy released in the decay, is small compare to the mass of the proton, one can use the Fermi Golden rule:

$$R = \frac{2\pi}{\hbar} \left( \frac{1}{2} \sum_{\text{spins}} |H_{fi}| \right) \frac{d^3 p_e}{(2\pi\hbar)^3} \frac{d^3 p_{\bar{\nu}}}{(2\pi\hbar)^3} \quad (5.101)$$

let us consider the following reaction involving  $n$  initial particles  $X_1, \dots, X_n$  and leading to  $m$  final particles  $Y_1, \dots, Y_m$ , mediated by an interaction Hamiltonian  $H$ :

$$X_1 + X_2 + \dots + X_n \rightarrow Y_1 + Y_2 + \dots + Y_m \quad (5.102)$$

then the rate of transition from an initial state  $|1, 2, \dots, n\rangle$  to a final state  $|1', 2', \dots, m'\rangle$  is:

$$R = \frac{2\pi}{\hbar} |\langle 1', 2', \dots, m' | H | 1, 2, \dots, n \rangle|^2 \quad (5.103)$$

where we have assumed the states to be fully characterized (no degeneracy).

If we wish to know the differential rate of transitions of a system having  $f_1(e_1)$  particles  $X_1$  in the energy range  $[e_1, e_1 + de_1]$ ,  $f_2(e_2)$  particles  $X_2$  in the energy range  $[e_2, e_2 + de_2]$ , ...,  $f_n(e_n)$  particles  $X_n$  in the energy range  $[e_n, e_n + de_n]$ , and leading to particles  $Y_1$  with energy in the range  $[e'_1, e'_1 + de'_1]$ ,  $Y_2$  with energy in the range  $[e'_2, e'_2 + de'_2]$ , ...,  $Y_m$  with energy in the range  $[e'_m, e'_m + de'_m]$  then we have:

$$dR = \frac{2\pi}{\hbar} |\langle 1', 2', \dots, m' | H | 1, 2, \dots, n \rangle|^2 \quad (5.104)$$